Computer Simulation of Solar Combisystem Based on the Second Law Analysis

Xiao-Nan Wen

A Thesis

in

The Department

of

Building, Civil and Environmental Engineering

Presented in Partial Fulfillment of the Requirements

for the Degree of Master of Applied Science (Building Engineering) at

Concordia University

Montréal, Québec, Canada

December 2013

CONCORDIA UNIVERSTIY

School of Graduate Studies

This is to certify that the thesis prepared

By: Xiao-Nan Wen

Entitled: Computer Simulation of Solar Combisystem Based on the Second Law Analysis

and submitted in partial fulfillment of requirements for the degree of

Master of Applied Science (Building Engineering)

complies with the regulations of the University and meets the accepted standards with respect to originality and quality.

Signed by the final examining committee:

_____ Chair
Dr. Fariborz Haghighat

_____ Examiner
Dr. Marius Paraschivoiu

_____ Examiner
Dr. Fariborz Haghighat

_____ Examiner
Dr. S. Samuel Li

_____ Supervisor
Dr. Radu G. Zmeureanu

Approved by _____
Dr. Tarek Zayed, GPD
Department of Building, Civil and Environment Engineering

_____
Dr. Christopher W. Trueman, Interim Dean
Faculty of Engineering and Computer Science

Date _____

Abstract

Computer Simulation of Solar Combisystem Based on the Second Law Analysis

Xiao-Nan Wen

This thesis presents the development of a Second Law model of a solar combisystem for residential applications. The work presented in the thesis includes: 1) A methodology for the development of a combisystem computer model; 2) The mathematical models of a solar combisystem components; 3) The features of an EES-based computer model of a solar combisystem being developed; 4) The simulated operation of a solar combisystem; and 5) The analysis of the performance of a simulated solar combisystem based on the Second Law of thermodynamics.

The solar combisystem had an annual system Coefficient of Performance (COP) of 3.98, an annual system exergetic COP of 0.17, an annual system energy efficiency of 42.0%, an annual system exergy efficiency of 40.7%, an annual overall solar energy contribution of 89.5%, an annual overall solar exergy contribution of 88.8%, an annual input solar energy contribution of 82.7%, and an annual input solar exergy contribution of 26.5%. Compared to an electric heating system, the solar combisystem had an annual solar energy fraction of 1.3 and an annual solar exergy fraction of 0.1.

Acknowledgements

I am grateful to many people who encouraged and inspired me during the graduate study.

First of all, I thank my teachers: Dr. Andreas K. Athienitis, Dr. Theodore Stathopoulos, Dr. Ramani Ramakrishnan (Ryerson University, Toronto), Dr. Hashem Akbari, Dr. Radu G. Zmeureanu, Dr. Paul P. Fazio, Dr. Fariborz Haghighat, and Dr. Mohammed Zaheeruddin. Their course lectures were enlightening.

I benefited greatly from peer discussion with my fellow graduate students on technical topics. Their various strengths directly or indirectly contributed to my study. Thanks to: Justin Tamasauskas on ice storage; Dr. Ahmed El Shenawy on research methodology; Jun Liu on system control; Laurent Magnier on transport phenomena; Véronique Tremblay on uncertainty; Eric McDonald on substance property; Nicholas Zibin on calibration; Liya Luo on verification.

The completion of my thesis project would not be possible without the resources provided by our group. Thanks to: Jason Ng Cheng Hin for extracting data from TRNSYS and models by Mitchell Leckner and Alexandre Hugo; Justin Tamasauskas for sharing data, and Dr. Danielle Monfet for EnergyPlus references. I also thank the support and friendship of Marie-Claude Hamelin, Andreea Mihai, and Mathieu Le Cam.

I owe very special thanks to my thesis supervisor Dr. Radu G. Zmeureanu for laying the foundation and taking me on this journey of research. I have been fortunate to sit in his class and join in his research student group. During this thesis project, his constant challenges motivated me to deepen my understanding of the studied topic. He taught me focus and determination. I am truly grateful for his guidance.

I would also like to thank Ms. Jenny Drapeau my Graduate Programs Advisor and Ms. Olga Soares my Department Administrator for their support.

The research was funded by the financial support of the Natural Sciences and Engineering Research Council of Canada and the Faculty of Engineering and Computer Science of Concordia University.

At last, I thank my parents who have been supportive with open minds, and my sister and her husband who have been with me every step of the way.

In Memory Of

My Grandmother, Shu-Kui Wang

Table of Contents

List of Figures

List of Tables

Nomenclature

Symbols	Descriptions	Units
A	Area	m^2
a_0	Coefficient, as in η^{Coll} solar collector thermal efficiency	dimensionless
a_1	Coefficient, as in η^{Coll} solar collector thermal efficiency	$W/(m^2 \cdot ^\circ C)$
a_2	Coefficient, as in η^{Coll} solar collector thermal efficiency	$W/(m^2 \cdot ^\circ C^2)$
$b_0, b_1, \ldots\ b_4$	Coefficients, as in $\dot{W}^{HP}$ heat pump electric power input	dimensionless
$c_0, c_1, \ldots\ c_8$	Coefficients, as in $\dot{W}^{Pump}$ circulating pump power input	dimensionless
c_p	Constant pressure specific heat	$J/(kg \cdot ^\circ C)$
D	Diameter	m
$d_0, d_1, \ldots\ d_4$	Coefficients, as in $\dot{Q}^{Cond}$ heat pump heating capacity	dimensionless
E	Energy	J
$\dot{E}$	Energy change rate	W
e	Coefficient, as in T_w^{Main} city main water temperature	°C
F	Flow fraction of circulating pump	dimensionless
$f_1, f_2, \ldots\ f_{17}$	Coefficients, as in T_w^{Main} city main water temperature	°C
G	Insolation	J
$\dot{G}$	Insolation rate on tilted surface	W
Gr	Grashof number	dimensionless
g	Gravity acceleration	m/s^2
$g_1, g_2, \ldots\ g_{17}$	Coefficients, as in T_w^{Main} city main water temperature	°C
H	Height	m
h	Specific enthalpy	J/kg
k	Thermal conductivity	$W/(m \cdot ^\circ C)$
L	Length; latent heat of fusion	m; J/kg
m	Mass	kg
$\dot{m}$	Mass flow rate	kg/s
N	Day of the year	dimensionless
n	Numbers	dimensionless
Nu	Nusselt number	dimensionless
P	Pressure	Pa
Pr	Prandtl number	dimensionless
Q	Heat	J
$\dot{Q}$	Heat transfer rate	W
R	Surface film resistance of heat transfer	$(m^2 \cdot ^\circ C)/W$
Ra	Rayleigh number	dimensionless
Run	Number of simulation runs	dimensionless
s	Specific entropy	$J/(kg \cdot ^\circ C)$

T	Temperature	℃
TK	Thermodynamic temperature	K
t	Time	s
$Time$	Simulation time	s
U	Thermal transmittance	W/(m^2·℃)
u	Specific internal energy	J/kg
$\dot{V}$	Volume flow rate	m^3/s
W	Work	J
$\dot{W}$	Electrical power input rate	W
X	Exergy	J
$\dot{X}$	Exergy transfer rate	W

Greek Letters	**Descriptions**	**Units**
α	Node exchange contribution	dimensionless
β	Volume expansion coefficient	1/℃
γ	Mass fraction of ice in storage tank	dimensionless
Δ	Difference	-
Δt	Time step	s
ε	Cooling effect of ice-layer in storage tank	dimensionless
η	Energetic efficiency	dimensionless
η_{II}	Exergetic efficiency	dimensionless
θ	Open/close signal of flow control valve	dimensionless
μ	Viscosity	kg/(m·s)
ν	Specific volume	m^3/kg
ξ	Mass fraction of ice at evaporator outlet	dimensionless
ρ	Density	kg/m^3
σ	Energy/exergy ratio	dimensionless
τ	Exergetic quality factor	dimensionless
φ	specific non-flow exergy	J/kg
χ	Quality of saturated refrigerant	dimensionless
ψ	specific flow exergy	J/kg
ω	Coefficients, as in T_w^{Main} city main water temperature	dimensionless

Superscripts	**Descriptions**
Aux	Auxiliary heater
$Coll$	Solar collector
$Coll4IT$	Circulation loop connecting solar collector to ice storage tank
$Coll4WT$	Circulation loop connecting solar collector to water storage tank
$CollP$	Circulating pump of collector loop
$Comp$	Compressor
$Cond$	Condenser
$CondP$	Circulating pump of condenser loop
DHW	Domestic hot water
$Evap$	Evaporator
$EvapP$	Circulating pump of evaporator loop
HP	Heat pump
$HP4RF$	Circulation loop connecting heat pump to radiant floor
$HP4WT$	Circulation loop connecting heat pump to water storage tank
I	Ice-layer in ice storage tank
$I2W$	From ice-layer to water-layer in ice storage tank
IT	Ice storage tank
ITL	Ice storage tank heating load
ITS	Ice storage tank heating source
$Main$	City main
N	Water-node in water storage tank
Ni	Water-node i
$Pump$	Circulation pump
RF	Radiant floor
RFL	Radiant floor heating load
RFS	Radiant floor heating source
SH	Space heating
Sun	Sun
Sys	System
$Valv$	Expansion valve
W	Water-layer in ice storage tank
$W2I$	From water-layer to ice-layer in ice storage tank
WT	Water storage tank
WTL	Water storage tank heating load
WTS	Water storage tank heating source
$WT4RF$	Circulation loop connecting water storage tank to radiant floor
$\bar{}$ (over bar)	Quantity mean
$\dot{}$ (over dot)	Quantity per unit time

Subscripts	Descriptions
air	Air
avg	Average
c	Condensation
b	Base
$base$	Baseline condition
cnt	Contact
com	Thermal comfort
$demd$	Demands
$dest$	Destruction
$down$	Downward
E	Energetic
e	Vaporization
ele	Electricity
$estm$	Estimated value
ext	External surface
f	Flow in storage tanks
hs	Horizontal surface
H	High-temperature reservoir
HX	Heat exchanger
ia	Indoor air
ice	Ice
in	Inlet
$insu$	Thermal insulation
int	Internal surface
$isen$	Isentropic
L	Low-temperature reservoir
$load$	Heating load
$loss$	loss
max	Maximum
$mean$	Mean
min	Minimum
oa	Outdoor air
out	Outlet
$overall$	Overall
$panel$	Solar collector panel
r	Refrigerant
ref	Reference system
set	Set point
$shell$	Tank shell
$slurry$	Ice slurry

sol	Solar
sto	Storage
$supp$	Supply
$suprh$	Superheating
$unit$	Unit area
up	Upward
var	Variation
vs	Vertical surface
w	Water
wf	Liquid water
wi	Solid water (ice)
X	Exergetic
0	Reference state
$1, 2, \ldots 8$	State of refrigerant

Abbreviation	**Descriptions**
ASHRAE	American Society of Heating, Refrigerating and Air-Conditioning Engineers
BLAST	Building Loads Analysis and System
COP	Coefficient of Performance
EBC, ECBCS	Energy Conservation in Buildings and Community Systems
EES	Engineering Equation Solver
HVAC	Heating, Ventilating, and Air-Conditioning
HVACSIM+	HVAC Simulation Plus
IEA	International Energy Agency
MATLAB	MaTrix LaBoratory
NIST	National Institute of Standards and Technology
REFPROP	Reference Fluid Thermodynamic and Transport Properties Database
SC	Solar contribution
SF	Solar fraction
SPARK	Simulation Problem Analysis Research Kernel
TRNSYS	Transient System Simulation Tool
VAV	Variable Air Volume

1. Introduction

1.1. Background

Computer simulation is the prominent practice to aid looking into some physical process. Through modeling physical process of a mechanical device, we can better understand the device behavior. Mankind's deep dependency of mechanical device arouses the eternal pursue for effectiveness improvement of energy use. Strengthening energy security, nowadays, is not the matter of one nation, but worldwide. The pressing challenges on expanding energy needs and non-stopping emissions of greenhouse gas urge actions. The latest report issued by the U.N. climate panel assessed that at least 95% of the climate change are human-caused (IPCC WGI 2013). Promoting the effectiveness of energy use is one solution to reduce the negative impact on the globe. Fig. 1.1 plots the energy efficiency effect of Canadian residential energy end-use over the past two decades up to 2009. Without the energy efficiency effect, the energy end-use would rise dramatically from the past level of 1990. The most ineffectiveness of energy use occurred in the thermodynamic processes can be identified with the Second Law of thermodynamics. Through exploring the quality of energy, the method of Second Law analysis facilitates the leverage of potential measures for energy conservation and efficiency improvement.

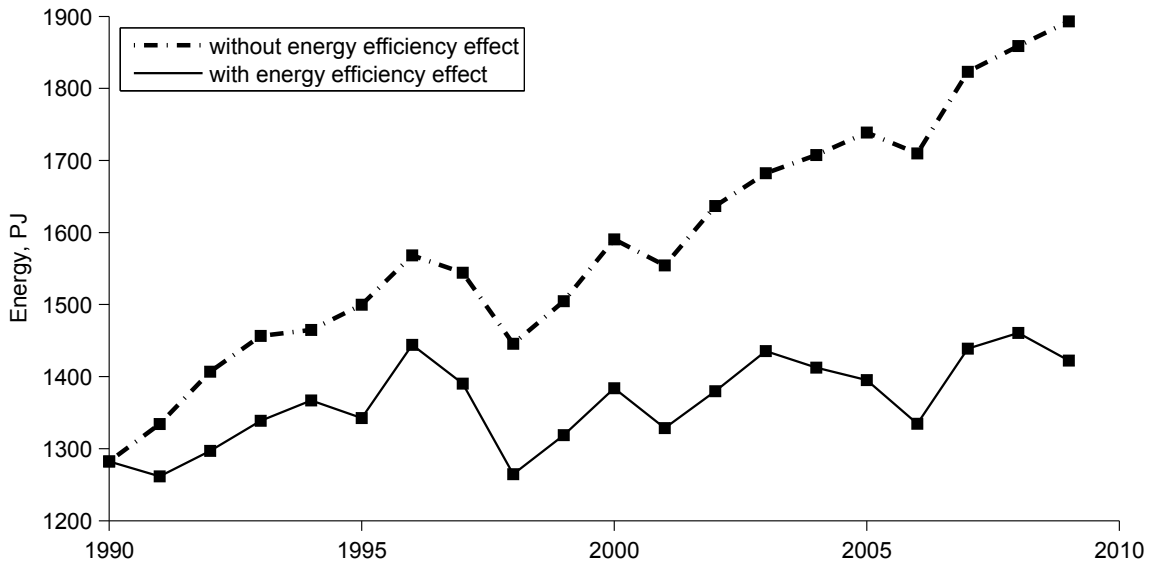

Fig. 1.1 Energy efficiency effect on energy end-use in residential sector of Canada

Data source: NRCan-OEE (2012)

We embraced the technology that uses energy efficiently. We also embraced the technology (such as solar technology) that promotes the environmental sustainability because we agree on taking the renewable energies into our energy scheme for good. Metz (1977) reviewed the earlier studies and reported the most economic high-temperature solar systems serves several purposes in a complementary fashion. The author also forecasted that the medium-temperature solar systems will have a great potential by 2000. Coming to present days, solar systems have been seen applied widely. Particularly, the applications of solar technology do present the complementary fashion of serving multiple purposes. And the low-temperature solar thermal systems have taken over the majority of solar thermal collectors produced into this century.

Solar combisystem is one class of low-temperature solar thermal system that uses solar thermal energy, together with electricity, to work on the dual heating missions in a residential house: to heat the domestic water and to heat the indoor space.

The extensive practices and the active signs in the market, especially in Europe (Ellehauge 2003, Papillon et al. 2010), have confirmed the vitality of solar combisystem. In various configurations, solar combisystems share a typical feature component, the water storage tank. Because the availability of solar energy varies with time (Laughlin 2011), the storage scheme provides the solar energy some degree of continuity.

The heat pump is one of the energy conservative solutions that uses less of the primary energy than the conventional heating systems (IEA HPC 2012). Harris (1957) counted the combination advantage of "solar heater" with "thermal pump". Anon (1977) reported the revival of heat pumps while the energy cost was soaring; in particular, the heat pumps were coupled with the "heat-reclaim" and solar systems. Stepping into the current decade, the combination of solar technologies with heat pump has redrawn research attention (IEA-SHC T44/A38 2011). Upgraded from the American Society of Heating, Refrigerating and Air-Conditioning Engineers (ASHRAE) Technical Group 1 Exergy in summer of 2012, the ASHRAE Technical Committee 7.4 Exergy Analysis for Sustainable Buildings addressed that the application of solar collector and heat pump is preferred and more sustainable, versus fossil fuel (ASHRAE TC7.4 2013).

What the operating conditions would be with the solar collector and heat pump combined in a combisystem? How is the operation performance? Insights from the point of view of the Second Law of thermodynamics are worth for an investigation.

1.2. Research objectives

This research aims to use computer simulation technique to examine the energy use of a solar combisystem coupled with storage tanks and a heat pump. Our research group has accumulated substantial experience in a specialized area documented by Wu (2004), Zheng (2006), Wei (2006), Zmeureanu & Wu (2007), Zmeureanu & Zheng (2008), Leckner (2008), Hugo (2008), Wei & Zmeureanu (2009), Hugo et al. (2010), Leckner & Zmeureanu (2011), Ng Cheng Hin (2013), and Ng Cheng Hin et al. (2013). This research is proposed as a contribution to the employment of the Second Law analysis for the investigation of HVAC systems by means of computer modeling.

The research objectives are:

- Formulate mathematical models of a solar combisystem components;
- Develop a solar combisystem mathematical model based on the Second Law of thermodynamics;
- Implement the solar combisystem computer model;
- Analyze the performance of a simulated solar combisystem.

2. Literature review

2.1. Computer modeling of HVAC systems

The computer-based simulation of Heating, Ventilating, and Air-Conditioning (HVAC) systems is performed on HVAC system computer models, which are composed of modular elements representing the HVAC component equipment and the control system (ASHRAE 2009a). Such modular type of HVAC models have been included in simulation packages and software, such as, ASHRAE HVAC1 Toolkit (ASHRAE 1994), ASHRAE HVAC2 Toolkit (Brandemeuhl 1993, Brandemuehl & Gabel 1994), TRNSYS (Klein 2006), EnergyPlus (Building Technologies Office 2013, Crawley et al. 2001), etc. Computer modeling strategies of HVAC and building systems have emerged with three typical schemes (ASHRAE 2009a): system-based, component-based, and equation-based.

In a system-based scheme, calculations are performed for the building zone loads, secondary HVAC systems, and central plant together at each time step, e.g. eQuest (JJH/LBNL 2013), or calculations are processed in sequence, from the building zone loads to the secondary HVAC systems, then from the central plant to the economic aspect, e.g. EnergyPlus (Building Technologies Office 2013).

In a component-based scheme, calculations are performed at the component level, and a complete system is a flexible integration of the components. Simulation programs with a component-based scheme are, for example, HVAC Simulation Plus

(HVACSIM+) (Park et al. 1985) and Transient System Simulation Tool (TRNSYS) (Klein 2006).

The equation-based scheme enables a user to write the mathematical formulations of every single component and specify the inputs and outputs. The equation-based scheme has been used by, for instance, the Simulation Problem Analysis Research Kernel (SPARK) (Buhl et al. 1993, Sowell & Moshier 1995) and the Engineering Equation Solver (EES) (F-Chart Software, 1989 as cited in Panek & Johnson 1994, Klein and Alvarado, 1991 as cited in Myers 1992, Staus 1997).

2.2. Solar combisystem

Solar combisystems, being mostly used in residential applications, can be classified to: solar combisystem, solar combi-plus system, and high solar combi-plus system (Balaras et al. 2010).

A typical installation of a solar combisystem combines the production of domestic hot water and the space heating (Papillon et al. 2010). The initially developed solar combisystem was studied by the International Energy Agency (IEA) under the task 26 Solar Combisystems (SHC T26 2012). The task gave one of the conclusions that the solar combisystem has a main drawback of oversizing. Sized based on the higher thermal demands in winter, the solar combisystem is, therefore, oversized for the lower

thermal demands in summer. The task report concluded that the cases with long heating seasons are more promising.

Due to the drawback of oversizing, the development of solar combi-plus system was motivated to connect the solar thermal collector with the thermal driven cooling device (IEE SolarCombi+ 2010). Combing solar space heating and cooling with the domestic hot water production, a solar combi-plus system may avoid the drawback of oversizing.

The operation of a high solar combi-plus system is same as of a solar combi-plus system, however, the solar fraction is higher (EU HighCombi 2011). For instance, the improvement may lie in an integration of solar heat storage. The system performance was expected to improve during the spring and the autumn when the heating loads are moderate.

The IEA project Solar Combisystems, in active from 1998 through 2002, assessed twenty-one configurations of solar combisystems. For one-family house application, the solar combisystems had solar thermal collectors of 10 to 30 m^2 and a water storage tank of 0.3 to 3 m^3. Lund (2005) analyzed the sizing of solar combisystems, in terms of the area of solar thermal collector and the volume of short-term heat storage. The use of heat output of larger area of solar thermal collector was better in the case of supplying both domestic hot water and space heating than in the case only producing domestic hot water. Enlarging the area of solar thermal collector increased the solar fraction of a complete system, but reduced the heat output of collector within unit area of collector

panel. The study concluded that there were only marginal effects onto the heat output of collector from the increase of the size of heat storage. Furbo, Vejen, et al. (2005) reported a large scale installation of a solar combisystem in Denmark. With the solar thermal collector of 336 m^2 and hot water storage tank of 10 m^3, the system supplied the district heating network and the hot water use. Raffenel et al. (2009) studied the sizing of solar combisystems. Two objective functions, the annual fractional energy savings and the mean annual efficiency, were developed as function of the area of solar thermal collector and the volume of heat storage. The sizing decision was made by trading off between the two functions.

Among various configurations of solar combisystem, those include a heat pump are also belong to a type of solar and heat pump system (SHC T44A38 2011). In terms of coupling solar thermal collectors with heat pump, the combination can be generally classified as parallel system, series system, or hybrid system. In a series system, solar heat is transferred to a heat pump (through a thermal storage tank) for heating (Freeman et al. 1979). Chandrashekar et al. (1982) estimated the conditions of Canada by simulation. They concluded that higher energy savings could be obtained by the combination, compared to a resistance heating system and a conventional air-to-air heat pump system. The study also examined the 20-year life cycle cost. But the results differed among the single, multiplex dwellings at different locations.

The operation control of a solar heat pump combination is complex. The operation control should try to maximize the delivery of the non-purchased solar energy.

From this perspective, giving priority to use the solar source seems easier to be realized in a paralleled system. However, Day & Karayiannis (1994) concluded that performance improvement of parallel system was not as expected. In the review conducted by Freeman et al. (1979), a parallel system was the most practical configuration. The series system is complex in the control of bypassing a heat pump and directly using the storage tank to supply, when the sole solar operation is sufficient. Bong (1983) pointed out, bypass temperatures are not subject to a unified decision, but depend on the prevailing building load. The operation of a heat pump is subjecte to the capacity of solar heat collection, or the area of solar collector had to be large enough taking into account the heat needs of operating a heat pump.

The operation of a solar heat pump system involves the balance of using the solar source and/or the heat pump. Kush (1980) indicated that the thermal efficiency of solar thermal collector is more important than the COP of heat pump. Karagiorgas et al. (2010) used a “change-over curve”, as a function of the outdoor temperature and the solar radiation on collectors, to decide the operation switch between a direct mode and an indirect mode. In the direct mode, distributed air was heated using solar air collectors; in the indirect mode, a heat pump was used to reheat the air before being distributed. The switch of operation reflected the needs for operating a heat pump when the heat collection of solar thermal collector is insufficient.

The operation performance of solar heat pump system installations was reported. Kugle et al. (1984) reported the solar heat pump operation for a single-family

house could be free from using electrical heating elements. A solar only mode had the system COP up to 35. Stojanović & Akander (2010) tested the performance of a full-scale solar-assisted heat pump system for the residential heating in Sweden. In the heating season, a ground-coupled heat pump used solar heat being stored during the months of late spring, summer and early autumn. The heat pump had a seasonal COP of 2.85, and the system had a seasonal COP of 2.09. Bakirci & Yuksel (2011) monitored a solar source heat pump system installed in a building in Turkey. The system consisted of flat-plate solar collectors and a heat pump using a sensible storage tank as the heat source. The average COP was 3.8 for the heat pump and 2.9 for the system. Moreno-Rodríguez et al. (2012) studied a direct-expansion solar assisted heat pump and found the strong dependence of the heat pump COP with the outdoor conditions, especially the solar radiation. The simulated COP ranged from 1.85 to 3.1, whereas the calculated using experiment results ranged from 1.7 to 2.9.

2.3. Stratified water storage tank

Water storage tank is a most common type of sensible thermal energy storage (ASHRAE 2009b). Various aspects of thermal energy storage systems were addressed in (Dincer & Rosen 2011). Thermal energy storage improve the integration of system (Baker 2008) and create the potential of economic saving (Ehyaei et al. 2010). Thermal stratification is a phenomenon featured by a positive temperature gradient along the vertical direction in fluids (Turner 1973). The maintenance of stratification in a thermal

storage tank enhances the operation performance of a system (Nelson et al. 1998, Duffie & Beckman 2006). Attentions were paid to stratified storage tanks in studies. Various indicators regarding stratification have appeared to address the performance of thermal storage tank (Panthalookaran et al. 2007): the stability index and the entropy generation number from the 70's; the stratification coefficient, stratification factor, stratification parameters, figure of merit, and the overall second law efficiency from the 80's; the MIX number and the equivalent temperature from the 90's. The emerge of new indicators continued, such as, the equivalent lost tank height by Bahnfleth & Song (2005), the energy response factor and the entropy generation ratio by Panthalookaran et al. (2007). Some studies traced the variation of thermocline to comprehend the thermal state in storage tanks (Behschnitt 1996, Nelson et al. 1998, Hasnain 1998, Rosen et al. 2004, Shin et al. 2004).

Thermal stratification can be damaged in various ways, including the turbulence of jet flow, buoyancy effect, and the heat conduction along the walls of storage tank. The jet flow is referred to the flow channeled by tank ports from the inlets to the outlets. The jet flow disturbs water body in the storage tank causing mixing. The turbulence of jet flow, i.e. jet mixing, was described in the studies of Visser & Van Dijk (1991), Haller et al. (2008), and Haller et al. (2009). Turner (1973) gave an account of flow motions driven or influenced by the buoyancy force in a stratified fluid: Along the vertical direction in fluids, the existence of negative temperature gradient or positive density gradient would overturn the local stability by moving thermals, intending to uniform the local density and smooth the temperature gradient. Fan & Furbo (2012a) and Fan & Furbo

(2012b) showed the magnitude of velocity of a downward flow in a water storage tank under a standby operation. The flow was caused by the loss of heat from the storage tank to the surroundings, which led the downward flow along the tank side walls and the upward flow around the vertical axial of storage tank. The heat retained within storage tank walls would conduct downward (Oppel et al. 1986) causing the degradation of thermal stratification (Nelson et al. 1999a). Cruickshank & Harrison (2010) reported a modeling study with the heat conduction taking place not only across the common boundary of stratified nodes but also through the tank walls.

Reverse stratification exists in operated water storage tank. Rhee et al. (2010) conducted an experimental study on a hot water storage tank with a double chimney device. The device has two nozzle stubs to route the buoyancy driven flow through. The experiment showed the reverse stratification taking place during the heating period of the storage tank. This suggested that relatively stable stratification needs time to be developed in an operated storage tank. Cruickshank & Harrison (2011) reported thermal response to the charge of heat in the studied multi-tanks. Stratification in a series-connected thermal storage disappeared while the flow rate in a heat charge-loop increased.

Different approaches were employed in the computer modeling of stratified storage tank for the purpose of eliminating the reverse stratification. For instance, a reversion elimination algorithm was implemented in the model 4PORT by Visser & Van Dijk (1991). The model forces stratified node in higher temperature to stay at higher

position in each time step. Within a time step, whenever a maximum temperature does not belong to a top node, averaged temperature would be reassigned to the nodes, from the bottom one to the one with the maximum temperature. The average calculation and the reassignment of temperature would repeat till the distribution of the temperatures demonstrating thermal stratification, the simulation of next time step then starts. With this algorithm, a stably stratified store is achieved always. Allard et al. (2011) compared five electrical water heaters models implemented in the TRNSYS software. The study concluded that the model TYPE 534 represented the best trade-off because the user can have cold water entering different nodes (under a fractional inlet mode) and/or use several heating elements (under a virtual heating mode).

Both the buoyancy effect and the turbulence of jet flow cause water mixing in a storage tank. This should be reflected in certain ways in the modeling of stratified storage tank. When stably stratified natural bodies of fluid are disturbed in any way, internal waves are generated (Turner 1973). Visser & Van Dijk (1991) realized that taking into account only the inter-nodal heat conduction resulted unreasonable temperature distribution; they chose to employ a reversion elimination algorithm to present stratification. Ismail et al. (1997) studied a stratified hot thermal storage in an experimental setup. They concluded that the use of sole conduction in modeling was unsatisfying. Modeling the mixing was included in Loehrke et al. (1978), Oppel et al. (1986), Al-Najem & El-Refaee (1997), and Nelson et al. (1999b), however these studies did not reach an agreed solution yet.

Kleinbach et al. (1993) validated a one-dimensional multi-node model. Cruickshank & Harrison (2010) reported a one-dimensional stratified water storage tank model was acceptable for a cold-down test. Kleinbach (1990) concluded his model predictions differed more among the models with small (≤ 4) number of nodes than among the models with large (≥ 8) number of nodes. Visser & Van Dijk (1991) suggested use a large number of nodes, like 100 or even larger, like 500, to represent the contribution of actual turbulent mixing properly. Duffie & Beckman (2006) suggested that the use of three or four nodes may be suitable. The position and the design of tank ports affect the operation of stratified water storage tank (Jordan & Furbo 2005, Duffie & Beckman 2006). The energy performance of storage tank benefits from a cold water port at the tank bottom and a hot water port at the tank top (Spur et al. 2006, Ievers & Lin 2009). Keeping a distance between the inlet and outlet ports avoids the overlapping of mixing zones (Palacios et al. 2012). Furbo, Andersen, et al. (2005) reported the thermal performance of storage tank benefits from the multi-discharging of heat. The study concluded that increasing the frequency of heat charging-discharging was worth to do for making more use of the thermal storage and avoiding thermal stagnation. Glembin & Rockendorf (2012) reported a stratified charging device led higher utilization of solar energy in a thermal storage of a single family house.

2.4. Second law analysis

From the thermodynamic principle, the exergy indicates the extent of the energy parting from the theoretical maximum (Moran & Shapiro 1999), and the Second Law of thermodynamics needs to be considered (Rosen & Dincer 2001, Dincer & Rosen 2005, Dewulf et al. 2008, Rosen et al. 2008, and Ao et al. 2008). The exergy analysis has been fallen far behind the energy analysis in the studies regarding building energy systems. Torío et al. (2009) gave a critical review of exergy analysis studies conducted for systems that use the renewable energy. The programme Energy Conservation in Buildings and Community Systems (EBC, formerly ECBCS) carried out the research project Annex 37 Low Exergy Systems for Heating and Cooling, from 1999 to 2003, to promote the use of low valued and environmentally sustainable energy sources (ECBCS A37 2003). The ECBCS carried out another research project from 2006 to 2010, the Annex 49 Low Exergy Systems for High Performance Buildings and Communities, to promote the use of exergy analysis method as the basis practice for designers and decision makers to take energy/exergy and cost efficient measures (ECBCS A49 2010).

The state-of-art building energy analysis programs use only the energy balance to estimate the energy use in buildings (Rosen et al. 2001, Zmeureanu & Wu 2007). Itard (2005) implemented exergy calculations in the H.e.n.k. program (Itard 2003) for an early design to count the flows of exergy within a building. Based on the spreadsheet applications, e.g. Microsoft Excel (Microsoft 2013) and OpenOffice Calc (Apache Openoffice 2013), a few of exergy analysis tools for buildings and communities were developed. For instance, the Pre-Design Tool (Schmidt 2004, Torío 2010) for buildings,

the Cascadia (Church 2008) for neighborhood design, and the Software for Exergy Performance (SEPE) (Molinari 2011) for exergy demands of cooling and heating in buildings. These tools were developed for design, pre-design, or general assessment, performing the steady state exergy analysis. A quasi-steady state exergy analysis study was reported by Wu (2004) and Zmeureanu & Wu (2007). The EES program demonstrated to be an ideal environment in the exergy analysis study of residential heating systems. Wei (2006) used the EES program to simulate the Variable Air Volume (VAV) systems of an office building. Gaggioli (2010) recommended the adoption of the EES or a counterpart for thermodynamic problems. The routines of the MaTrix LaBoratory (MATLAB) program (Mathworks 2011) already can directly use the NIST Reference Fluid Thermodynamic and Transport Properties Database (REFPROP) (Lemmon et al. 2013). This provided an alternative programming environment to perform more detailed exergy analysis.

The exergy analysis was employed in HVAC system studies by Rosen et al. (1999), Badescu (2002), Rosen (2001a), Dincer (2002), Shah & Furbo (2003), Rosen et al. (2004), Singh et al. (2012), and Soni & Gupta (2012). Exergy analysis study of power plants were documented by Durmayaz & Yavuz (2001), Rosen (2001b), Verkhivker & Kosoy (2001), and Aljundi (2009). Results of energetic performance and exergetic performance are not unanimous, with great discrepancy under most of the cases. For instance, Bjurstrom & Carlsson B. (1985) yielded different results regarding the transition temperature in the latent heat storage operation from the energy and exergy analyses. Petela (2005) found the exergy efficiency of a solar cylindrical-parabolic cooker was around 1%, about 10

times smaller than the respective energy efficiency. Zmeureanu & Wu (2007) reported the heat recovery equipment increased the energy efficiency but decreased the exergy efficiency of the system.

The exergy analysis is appreciated for bringing extra perspective to the view of energy analysis. Alta et al. (2010) found that the increase of air flow rate of a solar heater improved the energy efficiency but reduced the exergy efficiency. Ezan et al. (2011) analyzed an ice-on-coil thermal energy storage. Using the energy analysis method, the storage capacity and the system efficiency increased with decreased inlet temperature of heat transfer fluid and increased length of tube. Using the exergy analysis method, the exergy efficiency was increased with increasing inlet temperature of heat transfer fluid and increasing length of tube. Koroneos & Tsarouhis (2012) studied a solar system applied to a residence in Northern Greece. Comparing a solar heating, a solar cooling, and a solar domestic water heating systems, the overall system exergy efficiency was the highest in the solar cooling system, the lowest in the solar heating system.

The industry of solar thermal collector employs energy performance to assess collector products (FSEC 2010 and SRCC 2013). In the research area, various indicators, from the energetic aspect, exergetic aspect, or economic aspect, were employed to evaluate the performance of various types of solar collector. Chow (2010) reviewed the indicators for the performance of photovoltaic/thermal hybrid solar technology, including the thermal efficiency, electrical efficiency, total efficiency, energy saving

efficiency, exergetic efficiency, cost payback time, energy payback time, and the greenhouse gas payback time. In terms of calculating the available solar exergy, the Carnot efficiency and the exergy/energy ratio of radiation were often being used, for example, by Alta et al. (2010), Akpinar & Koçyiğit (2010), and Akyuz et al. (2012).

Studies focusing on the exergetic performance of solar collector were documented since the late 80's. Bejan et al. (1981) analyzed the irreversibility associated with the collection-delivery process of solar collector. Suzuki (1988) presented the expression of exergy balance of solar thermal collector. The capacity of exergy gain of evacuated tubular collector was nearly equal to that of flat plate collector. The study also concluded that the loss during the absorption of solar heat took the largest proportion among the overall exergy loss, which included the optical loss, leakage loss, and the heat conduction loss as well. Petela (2005) concluded that the escaping of insolation and the heat loss to the environment decreased the efficiency of solar collection device from the exergetic viewpoint. In Akyuz et al. (2012), the exergy efficiency of solar photovoltaic panel was calculated with the exergy loss due to wind speed being taken into account.

The maximum exergy embodied in the radiative energy, especially the solar radiation, was concerned in studies, since the 60's to the 80's. Petela (1964) derived the exergy/energy ratio of radiation for the estimation of the theoretical maximum exergy embodied in the radiative heat. Parrott (1978) addressed the theoretical maximum exergy in solar radiation. Edgerton (1980) questioned the convertibility of solar radiation

to thermodynamic work. Jeter (1981) theoretically investigated the maximum conversion efficiency of direct solar energy utilization, which was as the Carnot efficiency. Petela (2010) and Agudelo & Cortés (2010) were the latest to review and summarize the studies regarding the exergy analysis of thermal radiation process.

2.5. Conclusions

Based on the literature review conducted for this research, four main issues got the attention: (i) The computer modeling of HVAC systems are popular among the applications in a system-based scheme or the applications in a component-based scheme. An equation-based modeling scheme is superior at allowing specifications of inputs and outputs. (ii) Solar combisystems have proofed the vitality, however, exergy analysis studies on solar combisystems are rare; (iii) The modeling of water storage tank is an indispensable aspect in the modeling of a solar combisystem. Research in the modeling of stratified storage tank should be conducted; and (iv) Including a heat pump as a component of a solar combisystem makes a challenging system configuration for investigation.

To address these issues, a model development study should be done, to use the EES program as the modeling platform developing a Second-Law model of a solar combisystem presenting the solar heat pump combination. Using the component approach, the solar combisystem model being developed is obtained by integrating the model components, which are to be developed at first. With the developed solar

combisystem computer model, the system operation can be simulated and performed with the Second-Law analyses.

3. Methodology

This chapter presents the methodology of the research presented in this thesis. This research investigated a solar combisystem in a specified configuration using computer simulation. The steps followed are:

- Choosing the modeling approach;
- Determining model inputs and outputs and performing case data collection;
- Establishing the control scheme and defining the controlled variables;
- Developing the solar combisystem mathematical model;
- Implementing the solar combisystem computer model in the EES program;
- Assigning the case study data and control settings;
- Model validation and verification;
- Simulating the solar combisystem model and performing results analysis;
- Drawing the conclusions based on the simulated solar combisystem operation and performance analysis.

Regarding the steps listed above, the followed sections will provide more details.

3.1. Quasi-equilibrium process

Many actual processes are approximated by the quasi-equilibrium processes with negligible error (Cengel & Boles 2002). In such a quasi-steady approach, the

combisystem mathematical model was formulated. The thermodynamic balance was written for rate of energy in W. The time increment of 15 minutes was used, which is also used by other modeling programs, for instance, the simulation program EnergyPlus (Building Technologies Office 2013) uses as default of simulation time step. In the development of IBLAST, a research version of simulation program Building Loads Analysis and System (BLAST), the value has been identified giving stable results without largely increase in computation time (BLAST Support Office 1991).

The modeling of the solar combisystem is in a dynamic modeling because of the thermal energy storage tanks being the combisystem components in connection with other component equipment. The modeling of thermal energy storage tank follows a dynamic approach, where the computation results of time-lagged variables from the previous time are processed as the initial values for calculating the time-lagged variables at the current time.

3.2. Input and output

The input and output of the solar combisystem computer model were identified at the beginning stage, before starting the mathematical model development. Data collection is part of the inputs identification because a computer modeling of HVAC system only represents the system operation scenario by cases, which is the same true for the development of a computer model. The collected data will be input to the model during the development for trial run.

The solar combisystem outputs were identified for the purpose of operation investigation, including the temperature of working fluid, heat transfer rate between components, auxiliary energy use, and performance indices. The model inputs identified can be grouped to input parameters and input variables. The input parameters are constants including the equipment dimensions and the operation constraints. The operation constraints are, such as, the operation temperature limits. The input variables have values varying time, including the heating requirements and the boundary conditions. The heating requirements are the space heating demand and the domestic hot water consumption. The boundary conditions are referred to the conditions of the environment of thermodynamic system, including the insolation, outdoor temperature, indoor temperature, and city main temperature.

The input equipment dimensions can be from the documents published by the manufacturers, which could be the installation, operation and maintenance manuals, specification catalogues, rating certifications, etc. However, to fix certain parameters one might need to specify the exact product model to set the capacity. The input variables can be from other studies or applications. For instance, the studied case used data from other studies for the heating demands, indoor temperature, and city main temperature; used weather data from TRNSYS simulation program for the climate conditions.

3.3. Control scheme

The control scheme presents the general thoughts about how to operate the control devices (e.g., valves, thermostats, etc.) to actuate the component in order to manipulate the solar combisystem operation. Bearing a control scheme in mind was one of the premises to formulate the mathematical model.

3.4. Mathematical model

The mathematical model of solar combisystem was developed using the component approach. In this approach, the whole combisystem model is composed of component models, including the solar thermal collector model, heat pump model, ice storage tank model, water storage tank model, circulating pump model, system model (to describe the operating conditions and to evaluate the operation performance at the system level), and control system model. By developing relations among the component models, the whole combisystem model was formed. The component mathematical models were formulated mainly in equations, some in conditions. The equations were to describe the thermodynamic process that each of the components undergoes. The conditions were for the decision algorithms of the control system model.

The presented models in this thesis, some parts of certain component models are new approaches or new algorithms being developed during this research. The other parts were adopted from existing models documented by other researchers, with or without modification.

3.5. Computer model

The solar combisystem computer model was obtained by implementing the developed component mathematical models in the EES program. Essentially, the program can solve coupled non-linear algebraic and differential equations. The program has the built-in functions calculating the thermodynamic and transport properties of substances. The program can check unit consistency, which may appear to be a minor feature, but is especially useful for complex models; the solar combisystem being studied in this research is one of those.

At this step, the interface for model inputs was created in the EES program. The equations and conditions were implemented as procedures. Main procedure was set up to compile the computation directives, functions, and procedures so for the execution in sequence. During implementing the procedures, efforts were made to prepare the component models ready for future reuse in different system configurations.

3.6. Testing and modifications

The computer model needed tests and verification before running the simulation for final results. The testing was performed by running the model and observing the model responds and model outputs to ensure if the observed are as being expected (Kennedy & O'Hagan 2001). The tests were performed for various simulation time spans,

for day, and for season (i.e., heating season and non-heating season), before performing on a complete simulation year.

Detailed outputs from the test simulations were examined. The error detection at this step was time consuming. The model was examined with energy balance, as well as with certain variables, such as temperatures, efficiencies, exergy destructions. For instance, the efficiency, exergy destruction, and dimensionless variables typically have values within certain range. Their outputs can expose problems or errors hiding in the model.

3.7. Simulation and results analysis

The developed computer model was run to simulate the solar combisystem annual operation. To eliminate the impact made by the initial values, the simulation of three continuous years was performed, and only the results for the third year were used for the analysis. The exported simulation results were vast sets of data requiring data treatment. The program MATLAB was used in this study as a post-processor for this purpose.

At the step of data treatment, an important aspect is to distinguish the *on*/*off* status of solar thermal collector, heat pump, and radiant floor, because a variable that belongs to the model of either one of them is a step function. When the operation is in *off* status, the variable does not have a value. However, a dummy value of 0 was

assigned out of the computation needs. When analyzing the data exported, the dummy value must be filtered out first due to the value does not represent any physical meaning. A variable that belongs to the water storage tank model or the ice storage tank model is not a step function. The controlled variables (Section 4.9.1) and the variables regarding the heating demands were used in filtering the dummy values. Any of them served as a classifying index to recognize dummy values for certain step function.

4. Development of mathematical model

4.1. Solar combisystem configuration

The solar combisystem consists of solar thermal collector, a water storage tank, a radiant floor, a heat pump, an ice storage tank, and three circulating pumps. The solar combisystem configuration is illustrated in Fig. 4.1. Three circulation loops ($L1, L2, L3$) make connections among the solar thermal collector, water storage tank, ice storage tank, heat pump, and radiant floor. The circulating pumps drive water, the heat transfer fluid, circulating along the loops to transfer heat among the connected equipment. The solar thermal collector traps solar heat input to the combisystem, and the heat is stored in the water storage tank and ice storage tank. By using solar thermal energy and electricity, the combisystem covers the needs for domestic hot water and residential space heating. Cold water from the city main is heated in the water storage tank. While preparing domestic hot water, the water storage tank also supplies heat being used for space heating. The space heating is provided by the radiant floor using heat supplied from the water storage tank, or by the heat pump. The heat pump extracts heat from the ice storage tank to supply, in a given sequence, the radiant floor, and the water storage tank as well.

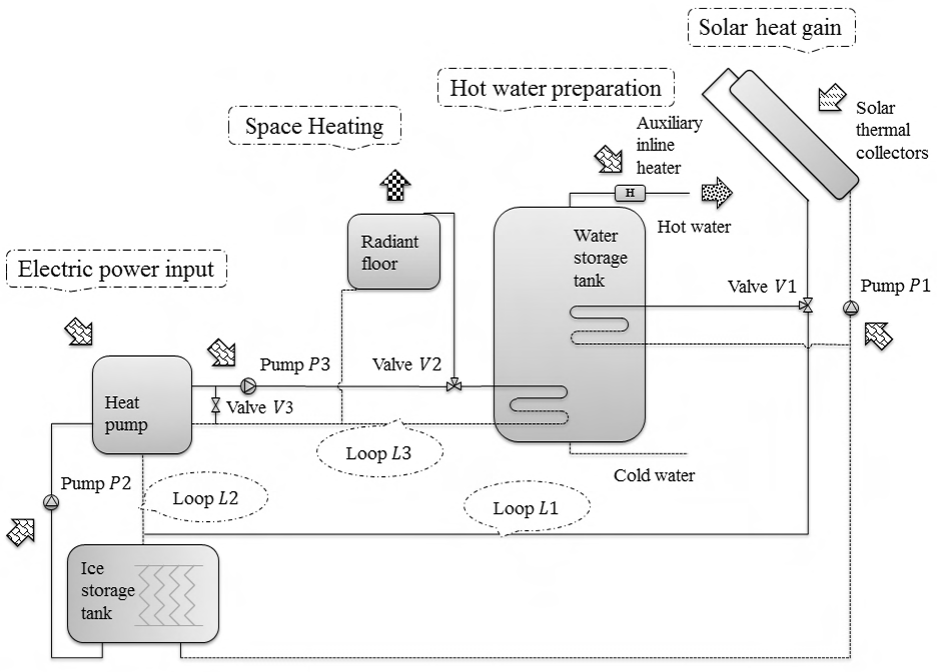

Fig. 4.1 Schematic of solar combisystem configuration

The modeling is based on the combisystem characteristics and residential design requirements. The combisystem characteristics include the insolation density, outdoor air dry bulb temperature, and main water temperature. The residential design requirements include the sensible heating load, design indoor temperature, and domestic hot water consumption. Assumptions being made for the modeling include,

- The pressure of water is assumed to be constant at the standard atmosphere pressure;
- Heat transfer to the heat transfer water due to electrical power input to circulating pumps is neglected;
- Heat transfer through the circulation loop pipes is neglected;

- Heat storage in pipe walls, device shell and attached insulations, floor material and surface attachment is neglected;
- Tank shell is assumed to be uniformly insulated; neglecting pipe entrance on tank shell as well as junctions of thermal or control instruments;
- The magnitude of immersion heat exchangers, mounted in the water storage tank, is neglected. Thus, the volume of immersion heat exchanger does not reduce the inside volume of water storage tank;
- The turbulence of jet flow (due to water drawn-off) in the water storage tank is neglected;
- Thermal transmittance of the pipe walls, device shell, and insulation material is constant. Film resistance on the exterior surface of storage tanks is constant.

This chapter presents the mathematical models of the solar combisystem components, and the integration of all models to comprise the combisystem computer model.

4.2. Mathematical model of solar thermal collector

The solar thermal collector (Fig. 4.2) absorbs solar radiation that is transferred to the heat sink through the circulation loop using water as the working fluid. The mathematical model calculates the heat transferred by the working fluid and the fluid leaving temperature.

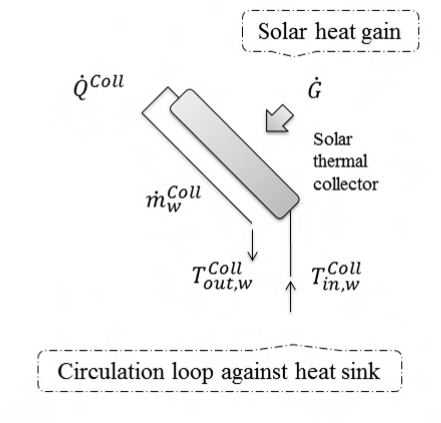

Fig. 4.2 Schematic of solar thermal collector model

4.2.1. Solar heat absorption and loss

The incident solar radiation on the solar thermal collector is calculated as:

$$\dot{Q}_{sol}^{Coll} = \dot{G} A_{panel}^{Coll} n^{Coll}, \tag{4.1}$$

where, $\dot{Q}_{sol}^{Coll}$ is the insolation rate upon tilted solar thermal collector when the solar thermal collector is operated; $\dot{G}$ is the power density of insolation upon tilted collector panel surface; A_{panel}^{Coll} is the gross area of single solar thermal collector panel; n^{Coll} is the number of solar thermal collector panel.

The absorbed solar energy is calculated as function of the thermal efficiency of solar thermal collector, η^{Coll}, and the incident insolation as:

$$\dot{Q}^{Coll} = \eta^{Coll} \dot{Q}_{sol}^{Coll}, \tag{4.2}$$

where,

$$\eta^{Coll} = a_0 + a_1 \frac{T_{in,w}^{Coll} - T_{oa}}{\dot{G}} + a_2 \frac{\left(T_{in,w}^{Coll} - T_{oa}\right)^2}{\dot{G}}, \tag{4.3}$$

$\dot{Q}^{Coll}$ is the solar heat absorption rate of solar thermal collector; $a_0 \ldots a_2$ are the coefficients of solar collector thermal efficiency; $T_{in,w}^{Coll}$ is the temperature of water entering the solar thermal collector; T_{oa} is the outdoor air temperature. For the calculations of solar collector thermal efficiency, two situations are excluded: (1) η^{Coll}< 0, and (2) η^{Coll}> 1. Constraints required to apply Eqn. (4.3) are presented in Appendix A.

The solar energy loss rate at the solar thermal collector, $\dot{E}_{loss}^{Coll}$, is calculated as:

$$\dot{E}_{loss}^{Coll} = \left(1 - \eta^{Coll}\right)\dot{Q}_{sol}^{Coll}. \quad (4.4)$$

The surface area A_{panel}^{Coll}, the number n^{Coll}, and the coefficients a_0, a_1, a_2, are input parameters. The Certification and Rating sheet of selected solar thermal collector product provides such information. For instance, the studied case simulated the Empire EC-24 glazed flat plate solar collector (SunEarth 2012) of 14 panels in parallel. Each panel has the area of 2.298 m^2. The coefficients are a_0= 0.728, a_1= -2.98830 W/(m^2·°C), a_2= -0.01930 W/(m^2·°C^2). The coefficient a_0 has positive value; the coefficients a_1, a_2 have negative values to take into account the decrease of efficiency due to heat loss.

The insolation $\dot{G}$ and the temperature T_{oa} are input variables. For instance, the case study was performed for Montreal. The insolation density on the tilted surface of 60° due south, and the local outdoor dry bulb temperature were used. These weather information were extracted from the weather data file TMY2 of TRNSYS 16 simulation environment (Klein 2006) at 15 minutes time step.

4.2.2. Entering temperature of heat transfer fluid

The entering temperature of heat transfer fluid is determined by the operation of other device connected to the solar thermal collector. The entering temperature is the input of the solar thermal collector model.

The water storage tank and ice storage tank are the heat sinks of solar thermal collector in the solar combisystem. Operating the solar thermal collector against one of the storage tanks at a time, the temperature of water in the storage tank is taken as the temperature of water entering the solar thermal collector,

$$T_{in,w}^{Coll} = \begin{cases} T_w^{N1}, & against\ water\ storage\ tank \\ T_w^{W}, & against\ ice\ storage\ tank \end{cases}, \tag{4.5}$$

where, T_w^{N1} is the temperature of the water-node $N1$ in the water storage tank (Section 4.5.1); T_w^{W} is the temperature of the water-layer in the ice storage tank (Section 4.4.1).

The heat transfer rate of solar thermal collector $\dot{Q}^{Coll}$ is noted as $\dot{Q}^{Coll4WT}$ for the transfer to the water storage tank and $\dot{Q}^{Coll4IT}$ for the transfer to the ice storage tank.

4.2.3. Leaving temperature of heat transfer fluid

The temperature of water leaving the solar thermal collector, $T_{out,w}^{Coll}$, is calculated as:

$$T_{out,w}^{Coll} = T_{in,w}^{Coll} + \frac{\dot{Q}^{Coll}}{\dot{m}_w^{Coll} C_{p_w}^{Coll}}, \tag{4.6}$$

and

$$\dot{m}_w^{Coll} = \rho_w^{Coll} \dot{V}_w^{Coll}, \quad (4.7)$$

$$\dot{V}_w^{Coll} = \dot{V}_{unit}^{Coll} A_{panel}^{Coll} n^{Coll}. \quad (4.8)$$

where, $\dot{m}_w^{Coll}$ is the mass flow rate of water; $\dot{V}_w^{Coll}$ is the volume flow rate of water, $\dot{V}_{unit}^{Coll}$ is the volume flow rate per unit collector area. The water properties, constant pressure specific heat $C_{p_w}^{Coll}$ and density ρ_w^{Coll}, are estimated at the average temperature of water through the solar thermal collector, $T_{avg,w}^{Coll}$, as:

$$T_{avg,w}^{Coll} = \frac{\left(T_{in,w}^{Coll} + T_{out,w}^{Coll}\right)}{2}. \quad (4.9)$$

The volume flow rate $\dot{V}_{unit}^{Coll}$ is the input parameter. For instance $\dot{V}_{unit}^{Coll}$= 20.1×10^{-6} m^3/(s·m^2) was used in this case study referring to Certification and Rating sheet of Empire EC-24 (SunEarth 2012).

4.2.4. Exergy analysis of solar thermal collector

This section presents the exergy analysis of the solar thermal collector operation by regarding the solar thermal collector as the thermodynamic open system. The exergy balance equation is established considering the absorption of solar radiation, the flow of water, and the exergy destroyed during the operation.

Specific exergy of fluids

The velocity of substance and the elevation of substance are neglected to calculate the specific exergy of the fluid. The specific exergy of the flow mass ψ, e.g. liquid water, is calculated as:

$$\psi = h - TK_0 s, \tag{4.10}$$

and the specific exergy of the non-flow mass φ, e.g. solid water (ice), is calculated as:

$$\varphi = u + P_0 v - TK_0 s, \tag{4.11}$$

where, h is the specific enthalpy; s is the specific entropy; u is the specific internal energy; v is the specific volume; P_0 is the pressure at the reference state; TK_0 is the absolute temperature at the reference state. Eqn. (4.10) and (4.11) are referred to Cengel & Boles (2002).

Solar exergy absorption

The solar exergy input rate, $\dot{X}_{sol}$, due to the absorbed solar enengy is calculated as:

$$\dot{X}_{sol} = \dot{Q}^{Coll} |\sigma_{sol}|, \tag{4.12}$$

where, σ_{sol} is the exergy/energy ratio of radiation with respect to the Sun's temperature (Petela 1964),

$$\sigma_{sol} = 1 - \frac{4}{3}\frac{TK_0}{TK_{sun}} + \frac{1}{3}\left(\frac{TK_0}{TK_{sun}}\right)^4, \tag{4.13}$$

TK_{sun} is the absolute temperature of the Sun, 5700 K (Petela 2010).

The solar exergy absorption is calculated with the associated solar energy absorption. The solar energy absorption is the net of the incident solar energy on the solar thermal collector panel surface and the loss of the incident occurred at the same time in various ways.

Exergy of water flow through solar thermal collector

The exergy transfer rate by water flow through the solar thermal collector, $\dot{X}^{Coll}$, is calculated as:

$$\dot{X}^{Coll} = \dot{m}_w^{Coll}\left(\psi_{out,w}^{Coll} - \psi_{in,w}^{Coll}\right), \tag{4.14}$$

where, $\psi_{out,w}^{Coll}$ is the specific exergy of water leaving the solar thermal collector; $\psi_{in,w}^{Coll}$ is the specific exergy of water entering the solar thermal collector.

The exergy transfer rate of solar thermal collector $\dot{X}^{Coll}$ is noted as $\dot{X}^{Coll4WT}$ for the transfer to the water storage tank, and $\dot{X}^{Coll4IT}$ for the transfer to the ice storage tank.

Exergy destruction and exergetic efficiency

The exergy destruction rate by the solar thermal collector operation, $\dot{X}_{dest}^{Coll}$, is obtained from the exergy balance equation:

$$\dot{X}_{dest}^{Coll} = \dot{X}_{sol} - \dot{X}^{Coll}, \tag{4.15}$$

The exergetic efficiency of the solar thermal collector operation, η_{II}^{Coll}, is calculated as:

$$\eta_{II}^{Coll} = 1 - \frac{\dot{X}_{dest}^{Coll}}{\dot{X}_{sol}}. \tag{4.16}$$

4.3. Mathematical model of water-to-water heat pump

The heat pump (Fig. 4.3) is operated under the vapor compression refrigeration cycle of the refrigerant. The heat pump evaporator is connected to the heat source by one circulation loop. The heat pump condenser is connected to the heat sink by another circulation loop. By operating the heat pump, heat is transferred from the heat source to the heat sink. The mathematical model calculates the electric power input to the water-to-water heat pump, the heat transferred by heat transfer fluids, and the fluid leaving temperatures.

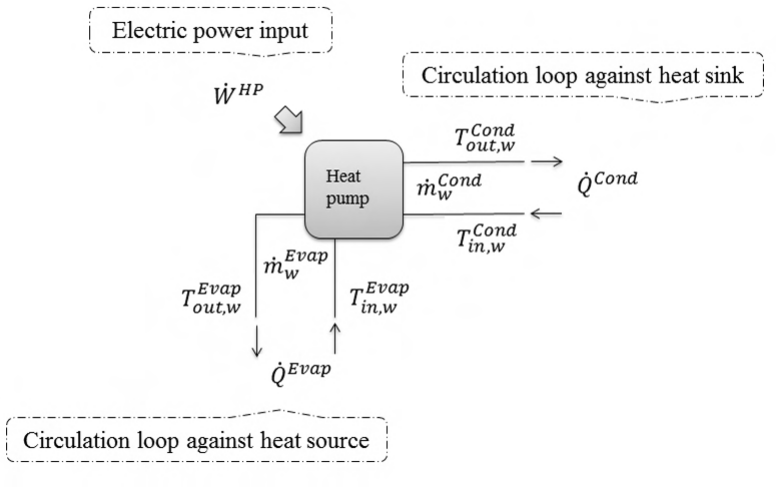

Fig. 4.3 Schematic of heat pump model

4.3.1. Electric power and heating capacity

The electric power, $\dot{W}^{HP}$, and the heat output rate at the condenser, $\dot{Q}^{Cond}$, are estimated for given inlet temperature and volume flow rate at both of condenser and evaporator using a regression model developed by Tang (2005):

$$\dot{W}^{HP} = \left(b_0 + b_1 \frac{TK_{in,w}^{Cond}}{283.15} + b_2 \frac{TK_{in,w}^{Evap}}{283.15} + b_3 \frac{\dot{V}_w^{Cond}}{\dot{V}_{base}^{Cond}} + b_4 \frac{\dot{V}_w^{Evap}}{\dot{V}_{base}^{Evap}} \right) \dot{W}_{base}^{HP}, \quad (4.17)$$

$$\dot{Q}^{Cond} = \left(d_0 + d_1 \frac{TK_{in,w}^{Cond}}{283.15} + d_2 \frac{TK_{in,w}^{Evap}}{283.15} + d_3 \frac{\dot{V}_w^{Cond}}{\dot{V}_{base}^{Cond}} + d_4 \frac{\dot{V}_w^{Evap}}{\dot{V}_{base}^{Evap}} \right) \dot{Q}_{base}^{Cond}, \quad (4.18)$$

where, $TK_{in,w}^{Cond}$ is the absolute temperature of water entering the condenser; $TK_{in,w}^{Evap}$ is the absolute temperature of water entering the evaporator; $\dot{V}_w^{Cond}$ is the volume flow rate of water through the condenser; $\dot{V}_w^{Evap}$ is the volume flow rate of water through the evaporator. The subscript $_{base}$ denotes the physical quantity at the *baseline condition*. The so-called *reference condition* in Tang (2005) is called *baseline condition* in this thesis to avoid the confusion with the reference state of the thermodynamic analysis.

The coefficients $b_0, b_1, \ldots b_4$ and $d_0, d_1, \ldots d_4$, and the quantities $\dot{W}_{base}^{HP}$, $\dot{Q}_{base}^{Cond}$, $\dot{V}_{base}^{Cond}$ and $\dot{V}_{base}^{Evap}$ are specific values assigned by the user for a specified heat pump. The ten coefficients and four quantities are identified as constants using regression technique. The absolute temperatures $TK_{in,w}^{Cond}$ and $TK_{in,w}^{Evap}$, and the volume flow rates $\dot{V}_w^{Cond}$ and $\dot{V}_w^{Evap}$ are dependent variables. Table 4.1 shows the coefficients and the baseline condition of the case heat pump used in this study prepared for a heat pump GeoSmart HS050 (GeoSmart 2012) using StatGraphics software (StatPoint 2012).

Table 4.1 Coefficients and baseline condition of case heat pump

Coefficients of electric power input, dimensionless	b_0	b_1	b_2	b_3	b_4
	-6.32321	0.498219	6.52788	0.0211943	-0.115108
Coefficients of heat output rate, dimensionless	d_0	d_1	d_2	d_3	d_4
	-2.36262	4.11641	-0.949693	0.0853777	-0.0135187
Baseline condition	$\dot{W}_{base}^{HP}$	$\dot{Q}_{base}^{Cond}$	$\dot{V}_{base}^{Cond}$	$\dot{V}_{base}^{Evap}$	
	3390 W	21072 W	9.46×10^{-3} m^3/s	9.46×10^{-3} m^3/s	

Eqns. (4.19) and (4.20) are used to calculate the power $\dot{W}^{HP}$ and heat output rate $\dot{Q}^{Cond}$ of the modeled case heat pump.

$$\dot{W}^{HP} = \left(-6.32321 + 0.498219\frac{TK_{in,w}^{Cond}}{283.15} + 6.52788\frac{TK_{in,w}^{Evap}}{283.15} + 0.0211943\frac{\dot{V}_w^{Cond}}{0.000946353} - 0.115108\frac{\dot{V}_w^{Evap}}{0.000946353}\right) \times 3390, \tag{4.19}$$

$$\dot{Q}^{Cond} = \left(-2.36262 + 4.11641\frac{TK_{in,w}^{Cond}}{283.15} - 0.949693\frac{TK_{in,w}^{Evap}}{283.15} + 0.0853777\frac{\dot{V}_w^{Cond}}{0.000946353} - 0.0135187\frac{\dot{V}_w^{Evap}}{0.000946353}\right) \times 21072. \tag{4.20}$$

In this study, the heat pump has equal flow rates at the condenser side and the evaporator side. The baseline condition was chosen with equal flow rates as well (Table 4.1). The Coefficient of Performance (COP) was calculated from Eqns. (4.19) and (4.20) and compared with the case heat pump performance data. The comparison is fairly good (see results). However, when the flow rates are unequal, the results are not in agreement with the manufacturer's data.

Shenoy (2004) indicated the use of computer model of the manufacturer to generate the technical data table with a few measured points obtained from the testing process. In preparing the case heat pump model, sample points were carefully chosen by examining the reversible cycle COP (Cengel & Boles 2002):

$$COP_{rev} = \frac{TK_H}{TK_H - TK_L}, \tag{4.21}$$

where, COP_{rev} is the reversible cycle COP; TK_H is the absolute temperature of the high-temperature reservoir; TK_L is the absolute temperature of the low-temperature reservoir. The high temperature corresponds to the entering temperature at the condenser, the low temperature to the entering temperature at the evaporator. Among the performance data of the case heat pump, the points corresponding to COP_{rev} in negative or at unreasonable high values (up to hundreds even thousands) were rejected.

With the electric power input and heat output rate, the COP of heat pump, COP^{HP}, is calculated as:

$$COP^{HP} = \frac{\dot{Q}^{Cond}}{\dot{W}^{HP}}. \tag{4.22}$$

4.3.2. Flow rates and entering temperatures of heat transfer fluids

The flow rates $\dot{V}_w^{Cond}$ and $\dot{V}_w^{Evap}$ are input parameters of the heat pump model. In this study, $\dot{V}_w^{Cond}$= $\dot{V}_w^{Evap}$= 9.46×10^{-3} m^3/s, referred to the case heat pump performance data.

The entering temperatures of heat transfer fluids are determined by the operation of other devices connected to the heat pump. The entering temperatures are the inputs of the heat pump model. At the heat pump evaporator side, the entering temperature is taken the temperature of the water-layer T_w^W in the ice storage tank (Section 4.4.1) as:

$$TK_{in,w}^{Evap} = 273.15 + T_w^W. \tag{4.23}$$

At the condenser side, the water storage tank and the radiant floor are the heat sinks. The temperature of water entering the condenser either is the temperature of water leaving the radiant floor $T_{out,w}^{RF}$ (Section 4.6.1), or the water-node temperature T_w^{N1} in the water storage tank (Section 4.5.1), or the mass-weighted average temperature of those two as:

$$TK_{in,w}^{Cond} = \begin{cases} 273.15 + T_{out,w}^{RF}, & against\ radiant\ floor \\ 273.15 + T_w^{N1}, & against\ water\ storage\ tank \\ 273.15 + \dfrac{\dot{m}_w^{RF} T_{out,w}^{RF} + (\dot{m}_w^{Cond} - \dot{m}_w^{RF}) T_w^{N1}}{\dot{m}_w^{Cond}}, & against\ both\ radiant\ floor\ and\ water\ storage\ tank \end{cases}, \tag{4.24}$$

where,

$$\dot{m}_w^{Cond} = \rho_{mean,w}^{Cond} \dot{V}_w^{Cond}, \tag{4.25}$$

$T_{out,w}^{RF}$ is the temperature of water leaving the radiant floor; T_w^{N1} is the temperature of the water-node $N1$ of the water storage tank; $\dot{m}_w^{RF}$ is the mass flow rate of water through the radiant floor; $\dot{m}_w^{Cond}$ is the mass flow rate of water through the heat pump condenser; $\rho_{mean,w}^{Cond}$ is the mean density of water through the condenser.

The density $\rho_{mean,w}^{Cond}$ is calculated at the mean water temperature over the certain period of time t_k (k= 1…k), as of

$$T_{mean,w}^{Cond} = \frac{\sum_{k=1}^{k} T_{avg,w}^{Cond}{}_{t_k}}{k}, \tag{4.26}$$

where,

$$T_{avg,w}^{Cond} = \frac{T_{in,w}^{Cond} + T_{out,w}^{Cond}}{2}. \tag{4.27}$$

The time interval t_k (k= 1…k) denotes the time interval when the heat pump is in operation; the temperature $T_{avg,w}^{Cond}$ is the average temperature of water through the condenser.

The average temperature $T_{avg,w}^{Cond}{}_{t_k}$ is step function. The mean temperature $T_{mean,w}^{Cond}$ therefore only corresponds to the time spans when the heat pump is turned on. In the model, the mean is the input parameter of the heat pump model. The input to the modeled case was based on the Eqns. (4.26) and (4.27). The studied case used $T_{mean,w}^{Cond}$= 44.1 ℃, which is the mean value during the heating season when the heat pump is on operation.

4.3.3. Energy balance and leaving temperatures of heat transfer fluids

The heat input rate at the evaporator, $\dot{Q}^{Evap}$, is derived from the heat pump energy balance equation as:

$$\dot{Q}^{Evap} = \dot{Q}^{Cond} - \dot{W}^{HP}. \tag{4.28}$$

The temperature of water leaving the condenser, $T_{out,w}^{Cond}$, is calculated as:

$$T_{out,w}^{Cond} = T_{in,w}^{Cond} + \frac{\dot{Q}^{Cond}}{\dot{m}_w^{Cond} C_{p_{mean,w}}^{Cond}}, \tag{4.29}$$

where, $\dot{m}_w^{Cond}$ is the mass flow rate of water through the condenser; the constant pressure specific heat $C_{p_{mean,w}}^{Cond}$ is calculated at the temperature $T_{mean,w}^{Cond}$.

The temperature of water leaving the evaporator, $T_{out,w}^{Evap}$, is calculated as:

$$T_{out,w}^{Evap} = T_{in,w}^{Evap} - \frac{\dot{Q}^{Evap}}{\dot{m}_w^{Evap} C_{p_{mean,w}}^{Evap}}, \tag{4.30}$$

where,

$$\dot{m}_w^{Evap} = \rho_{mean,w}^{Evap} \dot{V}_w^{Evap}, \tag{4.31}$$

$\dot{m}_w^{Evap}$ is the mass flow rate of water through the evaporator; $C_{p_{mean,w}}^{Evap}$ is the mean constant pressure specific heat of water through the evaporator; $\rho_{mean,w}^{Evap}$ is the mean density of water through the evaporator.

The water properties, the density $\rho_{mean,w}^{Evap}$ and constant pressure specific heat $C_{p_{mean,w}}^{Evap}$, are calculated as at the mean water temperature over the certain period of time t_k (k= 1…k), as of

$$T_{mean,w}^{Evap} = \frac{\sum_{k=1}^{k} T_{avg,w_{t_k}}^{Evap}}{k}, \tag{4.32}$$

where, the average temperature of water through the evaporator

$$T_{avg,w}^{Evap} = \frac{T_{in,w}^{Evap} + T_{out,w}^{Evap}}{2}. \quad (4.33)$$

The mean temperature $T_{mean,w}^{Evap}$ is the input parameter of the heat pump model. The studied case used $T_{mean,w}^{Evap}$= 3.9 ℃, which is the mean value during the heat season when the heat pump is turned on.

4.3.4. Ice mass fraction at evaporator outlet

Ice mass fraction, ξ, is the fractional mass flow rate of solid water (ice) in the water through the evaporator. The mass flow rate of solid water, liquid water, and the overall without distinguishing phases are subject to the following relations:

$$\dot{m}_{wi}^{Evap} = \xi \dot{m}_{w}^{Evap}, \quad (4.34)$$

$$\dot{m}_{wf}^{Evap} = (1 - \xi) \dot{m}_{w}^{Evap}, \quad (4.35)$$

where, $\dot{m}_{wi}^{Evap}$ is the mass flow rate of solid water (ice) leaving the evaporator; $\dot{m}_{wf}^{Evap}$ is the mass flow rate of liquid water leaving the evaporator.

The heat transfer rate at the evaporator can be formulated as:

$$\dot{Q}^{Evap} = \dot{m}_{wi}^{Evap} L_w + \dot{m}_{wf}^{Evap} C_{p}{}_{avg,w}^{Evap} \left(T_{in,w}^{Evap} - T_{out,wf}^{Evap}\right), \quad (4.36)$$

where, L_w is the specific enthalpy of fusion of water, 333606 J/kg. The constant pressure specific heat $C_{p}{}_{avg,w}^{Evap}$ is calculated at the average temperature of water at the evaporator,

$$T_{avg,w}^{Evap} = \frac{T_{in,w}^{Evap} + T_{out,wf}^{Evap}}{2}, \tag{4.37}$$

where, $T_{out,wf}^{Evap}$ is the temperature of liquid water leaving the evaporator. When solidification occurs, the liquid water temperature is noted by $T_{out,wf}^{Evap}$, while the solid water temperature is noted by $T_{out,wi}^{Evap}$. The liquid water temperature is estimated as 0.01 ℃. The solid water temperature is estimated as 0 ℃ regardless of sub-cooling (Tamasauskas et al. 2012).

By substituting Eqns. (4.34) and (4.35) onto Eqn. (4.36), the mass fraction is derived as:

$$\xi = \frac{\frac{\dot{Q}^{Evap}}{\dot{m}_w^{Evap}} - C_{p_{avg,w}}^{Evap}\left(T_{in,w}^{Evap} - T_{out,wf}^{Evap}\right)}{L_w - C_{p_{avg,w}}^{Evap}\left(T_{in,w}^{Evap} - T_{out,wf}^{Evap}\right)}. \tag{4.38}$$

4.3.5. Isentropic efficiency of compressor

The isentropic efficiency of compressor is a measure of the deviation of the compressor operation from the corresponding ideal process. The compressor isentropic efficiency, η_{isen}^{Comp}, is calculated as:

$$\eta_{isen}^{Comp} = \frac{\dot{W}_{isen}^{HP}}{\dot{W}^{HP}}, \tag{4.39}$$

where, $\dot{W}_{isen}^{HP}$ is the isentropic compression power.

The isentropic power $\dot{W}_{isen}^{HP}$ is obtained by modeling the vapor compression refrigeration cycle. Fig. 4.4 illustrates the single-stage vapor compression refrigeration

cycle in temperature-entropy (T-S) diagram. The points 1, 2, 4 … 8 are the key states of the refrigerant under the operation of heat pump. In counter-clockwise the actual process is represented by 1→2 for the compression in the compressor, 2→4→5→6 for the de-superheating, condensation, and sub-cooling in the condenser, 6→7 for in the expansion valve, 7→8→1 for the vaporization and superheating in the evaporator. The pressures of vaporization and condensation are indicated by P_e and P_c, along with T_e and T_c as of the corresponding temperatures. The process of isentropic compression is represented by the transformation 1→3. The isentropic power is calculated in

$$\dot{W}_{isen}^{Comp} = \dot{m}_r\left(h_{r,3} - h_{r,1}\right), \tag{4.40}$$

where,

$$\dot{m}_r = \frac{\dot{W}^{HP}}{(P_c - P_e)v_{r,1}}, \tag{4.41}$$

$\dot{m}_r$ is the mass flow rate of refrigerant; $h_{r,3}$ is the specific enthalpy of refrigerant at the state 3; $h_{r,1}$ is the specific enthalpy of refrigerant at the state 1; $v_{r,1}$ is the specific volume of refrigerant at the state 1. Eqn. (4.39) to (4.41) are referred to Cengel & Boles (2002).

By consulting the technical information of the case heat pump (GeoSmart 2012), the refrigerant R410A was used in this study, along with the operating parameters presented in Table 4.2. Where the condition, the temperature of water entering the condenser at 21.1 ℃, was determined referring to the leaving temperature of water at the radiant floor (Section 4.6.1).

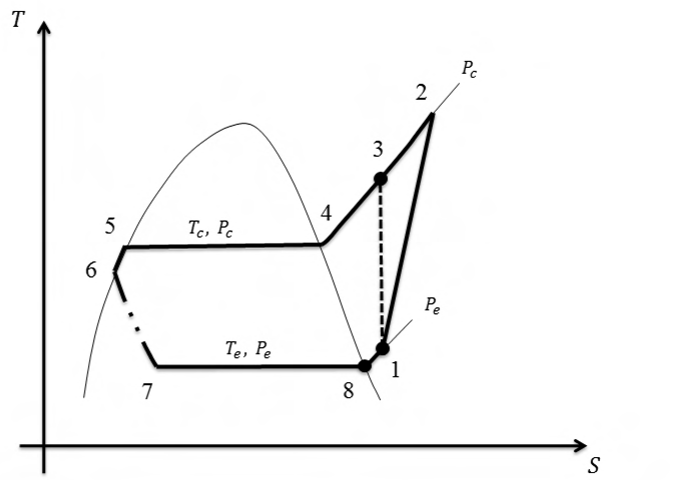

Fig. 4.4 T-S diagram of single-stage vapour compression refrigeration cycle

Table 4.2 Operating parameters of case heat pump (GeoSmart 2012)

Temperature of water entering condenser at 21.1 ℃			
	Temperature of water entering evaporator, ℃		
	t≤ 10	10< t≤ 21.11	t> 21.11
Suction pressure, kPa	468.84	520.55	572.27
Discharge pressure, kPa	1727.14	1825.39	1923.64
Superheat temperature difference, ℃	4.72	5.97	7.22

4.3.6. Heat output

The heat output from the heat pump is transferred to the water storage tank and/or the radiant floor. When only the water storage tank needs heat from the heat pump, the following condition applies:

$$\dot{Q}^{HP4RF} = 0, \tag{4.42}$$

$$\dot{Q}^{HP4WT} = \dot{Q}^{Cond}. \tag{4.43}$$

When both the water storage tank and the radiant floor need heat, the need of the radiant floor is satisfied first while the water storage tank is supplied with the excessive heat. The heat transfer rate from the condenser $\dot{Q}^{Cond}$ is noted as $\dot{Q}^{HP4WT}$ for

the transfer to the water storage tank, and $\dot{Q}^{HP4RF}$ for the transfer to the radiant floor. The heat distribution is computed using the following relations:

$$\begin{cases} \dot{Q}^{HP4RF} = \dot{Q}^{RF}_{demd} \\ \dot{Q}^{HP4WT} = \dot{Q}^{Cond} - \dot{Q}^{RF}_{demd} \end{cases}, \quad if\ \dot{Q}^{RF}_{demd} < \dot{Q}^{Cond}$$
$$\begin{cases} \dot{Q}^{HP4RF} = \dot{Q}^{Cond} \\ \dot{Q}^{HP4WT} = 0 \end{cases}, \quad if\ \dot{Q}^{RF}_{demd} \geq \dot{Q}^{Cond} \tag{4.44}$$

where, $\dot{Q}^{RF}_{demd}$ is the demanded heat transfer rate of the radiant floor.

4.3.7. Exergy analysis of heat pump

This section presents the exergy analysis of the heat pump operation by regarding the heat pump as a thermodynamic open system. The exergy balance equation is established considering the use of electricity, the flows of water, and the exergy destroyed during the operation.

Exergy of water flows through evaporator and condenser

The net exergy transfer rate by water flow through the evaporator, $\dot{X}^{Evap}$, is estimated as

$$\dot{X}^{Evap} = \dot{m}^{Evap}_{w}\psi^{Evap}_{in,w} - \left(\dot{m}^{Evap}_{wf}\psi^{Evap}_{out,wf} + \dot{m}^{Evap}_{wi}\varphi^{Evap}_{out,wi}\right), \tag{4.45}$$

where, $\psi^{Evap}_{in,w}$ is the specific exergy of water entering the evaporator; $\psi^{Evap}_{out,wf}$ is the specific exergy of liquid water leaving the evaporator; $\varphi^{Evap}_{out,wi}$ is the specific exergy of the solid water leaving the evaporator.

The net exergy transfer rate by water flow through the condenser, $\dot{X}^{Cond}$, is estimated as

$$\dot{X}^{Cond} = \dot{m}_w^{Cond}\left(\psi_{out,w}^{Cond} - \psi_{in,w}^{Cond}\right), \tag{4.46}$$

where, $\psi_{out,w}^{Cond}$ is the specific exergy of water leaving the condenser; $\psi_{in,w}^{Cond}$ is the specific exergy of water entering the condenser.

The exergy is transferred through the circulation loop $L3$ from the heat pump condenser to the radiant floor and/or the water storage tank. The exergy transfer rate to the radiant floor is noted as $\dot{X}^{HP4RF}$, and that to the water storage tank as $\dot{X}^{HP4WT}$. Therefore,

$$\dot{X}^{Cond} = \dot{X}^{HP4RF} + \dot{X}^{HP4WT}. \tag{4.47}$$

Exergy destruction and exergetic efficiency

The exergy destruction rate by the heat pump operation, $\dot{X}_{dest}^{HP}$, is obtained from the exergy balance equation:

$$\dot{X}_{dest}^{HP} = \dot{W}^{HP} + \dot{X}^{Evap} - \dot{X}^{Cond}, \tag{4.48}$$

The exergetic efficiency of the heat pump operation, η_{II}^{HP}, is calculated as:

$$\eta_{II}^{HP} = 1 - \frac{\dot{X}_{dest}^{HP}}{\dot{W}^{HP} + \dot{X}^{Evap}}. \tag{4.49}$$

4.4. Mathematical model of ice storage tank

The storage tank (Fig. 4.5) contains water as the storage media, allowing the coexistence of liquid water and solid water. The storage tank is operated between a heat source and a heat sink. The mathematical model simulates the ice storage tank operation to calculate the temperature of water and the mass of ice in the storage tank.

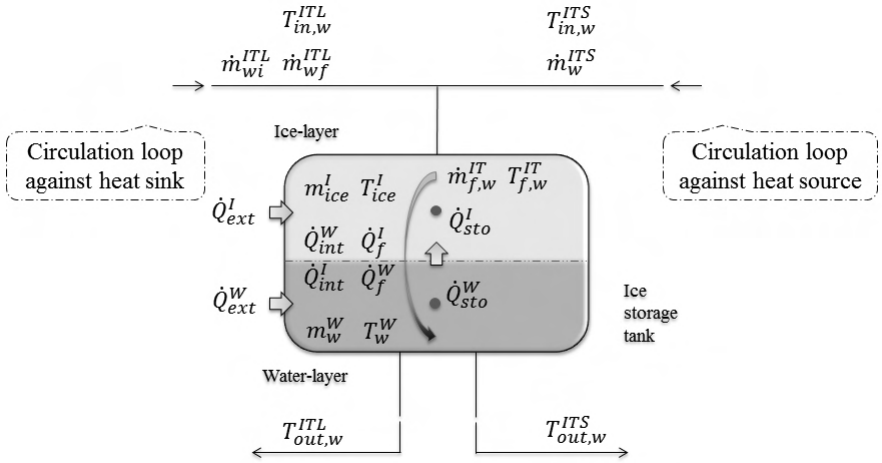

Fig. 4.5 Schematic of ice storage tank model

In the case of only liquid phase, the storage media is one homogeneous water-layer. In the general case of two phases, there is one homogeneous water-layer below one homogeneous ice-layer. When the ice storage tank is under the heat transfer with the heat source and/or the heat sink, there is flow of water through the storage media from top to bottom. In the general case, the water flow contains solid water (ice) and liquid water. The liquid water is called *passing flow* in here, which across the ice-layer flow into the water-layer, while the ice accumulates the ice-layer. The heat transfer of the ice storage tank takes place: (i) across the contact surface between the ice-layer and water-layer; (ii) through the storage tank surface with the surrounding environment; (iii)

by the passing flow with the heat source and heat sink. This section presents the ice storage tank model by Tamasauskas et al. (2012) with modifications.

4.4.1. Energy balance of ice-layer and water-layer

The energy balance equation of the ice-layer is as follows:

$$\dot{Q}^{I}_{sto} = \dot{Q}^{I}_{int} + \dot{Q}^{I}_{ext} + \dot{Q}^{I}_{f} - L_w \dot{m}^{ITL}_{wi}, \tag{4.50}$$

where, $\dot{Q}^{I}_{sto}$ is the energy change rate of the ice-layer; $\dot{Q}^{I}_{int}$ is the heat transfer rate of the ice-layer with the water-layer across the contact surface in between; $\dot{Q}^{I}_{ext}$ is the heat transfer of the ice-layer with the surroundings across the tank surface; $\dot{Q}^{I}_{f}$ is the heat transfer of the ice-layer with the passing flow; L_w is the latent heat of fusion of water; $\dot{m}^{ITL}_{wi}$ is the mass flow rate of solid water (ice) from the heat sink.

Terms in Eqn. (4.50) have following formulations,

$$\dot{Q}^{I}_{sto} = -\frac{dm^{I}_{ice}}{dt} L_w, \tag{4.51}$$

$$\dot{Q}^{I}_{int} = h_{slurry} A^{IT}_{cnt} \left(T^{W}_{w} - T^{I}_{ice}\right), \tag{4.52}$$

$$\dot{Q}^{I}_{ext} = \left(U^{IT}_{vs} A^{I}_{vs} + U^{I}_{hs} A^{IT}_{cnt}\right)\left(T_{ia} - T^{I}_{ice}\right), \tag{4.53}$$

$$\dot{Q}^{I}_{f} = \dot{m}^{ITL}_{wf} {c_p}^{ITL}_{in,wf} T^{ITL}_{in,wf} + \dot{m}^{ITS}_{w} {c_p}^{ITS}_{in,w} T^{ITS}_{in,w} - \left(\dot{m}^{ITL}_{wf} + \dot{m}^{ITS}_{w}\right) {c_p}^{IT}_{f,w} T^{IT}_{f,w}. \tag{4.54}$$

where, t is the time; m^{I}_{ice} is the mass of the ice-layer; $\dot{m}^{ITL}_{wf}$ is the mass flow rate of liquid water from the ice storage tank heat sink; $\dot{m}^{ITS}_{w}$ is the mass flow rate of water from the ice storage tank heat source; T^{I}_{ice} is the temperature of the ice-layer; T^{W}_{w} is the temperature of the water-layer; T_{ia} is the air temperature of the surroundings; $T^{IT}_{f,w}$ is

the temperature of the passing flow; h_{slurry} is the heat transfer coefficient between the slurry ice and liquid water; U_{vs}^{IT} is the thermal transmittance of vertical surface of the ice storage tank; U_{hs}^{I} is the thermal transmittance of the horizontal surface of the ice-layer; A_{cnt}^{IT} is the contact surface area between the ice-layer and the water-layer; A_{vs}^{I} is the vertical surface area of the ice-layer.

The energy balance equation of the water-layer is as follows:

$$\dot{Q}_{sto}^{W} = \dot{Q}_{int}^{W} + \dot{Q}_{ext}^{W} + \dot{Q}_{f}^{W}, \tag{4.55}$$

where, $\dot{Q}_{sto}^{W}$ is the energy change rate of the water-layer; $\dot{Q}_{int}^{W}$ is the heat transfer of the water-layer with ice-layer across the contact surface in between; $\dot{Q}_{ext}^{W}$ is the heat transfer of the water-layer with the surroundings across the tank surface; $\dot{Q}_{f}^{W}$ is the heat transfer of the water-layer with the passing flow.

Terms in Eqn. (4.55) have following formulations,

$$\dot{Q}_{sto}^{W} == \frac{d\left(m_w^W {c_p}_w^W T_w^W\right)}{dt}, \tag{4.56}$$

$$\dot{Q}_{int}^{W} = h_{slurry} A_{cnt}^{IT}\left(T_{ice}^{I} - T_w^W\right), \tag{4.57}$$

$$\dot{Q}_{ext}^{W} = \left(U_{vs}^{IT} A_{vs}^{W} + U_{hs}^{W} A_b^{IT}\right)\left(T_{ia} - T_w^W\right), \tag{4.58}$$

$$\dot{Q}_{f}^{W} = \left(\dot{m}_{wf}^{ITL} + \dot{m}_{w}^{ITS}\right){c_p}_{f,w}^{IT} T_{f,w}^{IT} - (\dot{m}_{w}^{ITL} + \dot{m}_{w}^{ITS}){c_p}_w^W T_w^W. \tag{4.59}$$

where, m_w^W is the mass of the water-layer; U_{hs}^{W} is the thermal transmittance of the horizontal surface of the water-layer; A_{vs}^{W} is the vertical surface area of the water-layer; A_b^{IT} is the base area of the ice storage tank.

4.4.2. Mass content in ice storage tank

The total water mass inside the ice storage tank, m_w^{IT}, consists of the mass of the two layers,

$$m_w^{IT} = m_{ice}^{I} + m_w^{W}. \tag{4.60}$$

The mass fraction of ice in the ice storage tank, γ, is the ratio as of

$$\gamma = \frac{m_{ice}^{I}}{m_w^{IT}}, \tag{4.61}$$

where,

$$m_w^{IT} = \frac{\rho_w^W \rho_{ice}}{\gamma_{max}\rho_w^W + (1-\gamma_{max})\rho_{ice}} V^{IT}, \tag{4.62}$$

and for the rectangular tank,

$$V^{IT} = H^{IT} W^{IT} L^{IT}, \tag{4.63}$$

ρ_w^W is the density of the water-layer, estimated with the maximum temperature of the water-layer, denoted as T_{max}^W; ρ_{ice} is the density of the ice-layer, estimated as 916.2 kg/m^3 for ice at 0 °C; γ_{max} is the maximum mass fraction of ice in the ice storage tank; V^{IT} is the volume of the ice storage tank; H^{IT} is the height of the rectangular tank; W^{IT} is the width of the rectangular tank; L^{IT} is the length of the rectangular tank.

The maximum mass fraction of ice γ_{max}, the maximum temperature of water-layer T_{max}^W, and the three dimensions of tank H^{IT}, W^{IT}, and L^{IT}, are the input parameters. For instance, in the case study, H^{IT} = 2 m, W^{IT} = 2 m, and L^{IT} = 3.5 m. The maximum mass fraction of ice γ_{max} is set for the operational requirement, since certain amount of liquid water should be secured for the circulations with the heat source and

heat sink. Referring to Sunwell (2012), γ_{max}= 0.7. The maximum temperature T_{max}^{W} is set from the economic considerations. High water temperature damages the possibilities of water undergoing phase change, which decreases the thermal storage capacity. Besides, the heat pump acts as the heat sink of the ice storage tank. Heat pumps usually get an operation range, in terms of the entering temperature at the evaporator. Based on the heat pump performance data from GeoSmart (2012), T_{max}^{W}= 37.7 °C.

4.4.3. Heat transfer between layers

The heat transfer between the ice-layer and the water-layer is treated as natural convection of warm water underneath a cold plate (Kreith & Bohn 2001), due to the small magnitude of the passing flow. The intensity of heat transfer between ice and water varies (Maciejewski 1996). The heat transfer coefficient between ice and water is calculated as (Kreith & Bohn 2001),

$$h_{slurry} = \frac{\overline{Nu}_{slurry} k_w^W}{L^I}, \tag{4.64}$$

where, Nu_{slurry} is the Nusselt number of ice slurry; k_w^W is the conductivity of the water-layer; L^I is the characteristic length, taken as the wet perimeter of the ice-layer,

$$L^I = \frac{W^{IT} L^{IT}}{2(W^{IT} + L^{IT})}. \tag{4.65}$$

The Nusselt number piecewise depends on the Rayleigh number (Kreith & Bohn 2001),

$$Nu_{slurry} = \begin{cases} 0, & Ra_{slurry} \leq 10^5 \\ 0.54 Ra_{slurry}^{1/4}, & 10^5 < Ra_{slurry} \leq 10^7, \\ 0.15 Ra_{slurry}^{1/3}, & Ra_{slurry} > 10^7 \end{cases} \quad (4.66)$$

where, Ra_{slurry} is the Rayleigh number for ice slurry,

$$Ra_{slurry} = Gr^I Pr_w^W, \quad (4.67)$$

and

$$Gr^I = \frac{g\beta_w^W \rho_w^W \left(T_w^W - T_{ice}^I\right) {L^I}^3}{{\mu_w^W}^2}. \quad (4.68)$$

Gr^I is the Grashof number of the ice-layer; Pr_w^W is the Prandtl number of the water-layer; g is the gravity acceleration; ρ_w is the density of the water-layer; T_w^W is the temperature of the water-layer; μ_w^W is the viscosity of the water-layer.

The area of contact surface between the ice-layer and the water-layer is calculated as:

$$A_{cnt}^{IT} = \begin{cases} 0, & if\ \gamma < 0 \\ A_b^{IT}, & if\ \gamma > 0 \end{cases}, \quad (4.69)$$

where,

$$A_b^{IT} = W^{IT} L^{IT}, \quad (4.70)$$

for a rectangular storage tank.

4.4.4. Heat transfer with surroundings

The heat transfer between the ice storage tank and its surrounding environment takes place around the storage tank surface. Neglecting the thermal transmittance of

the tank shell, the thermal transmittance of vertical surface of the ice storage tank is calculated with:

$$U_{vs}^{IT} = \frac{1}{\frac{1}{U_{insu}^{IT}} + R_{vs}^{Air}}, \tag{4.71}$$

where, U_{insu}^{IT} is the thermal transmittance of insulation attached to the ice storage tank; R_{vs}^{Air} is the surface film resistance of still air under horizontal heat flow, 0.12 $m^2 \cdot ℃/W$ (ASHRAE 2009c).

The thermal transmittance of the horizontal surface of ice-layer is a piecewise function as follows:

$$U_{hs}^{I} = \begin{cases} U_{hs,down}^{IT}, & T_{ice}^{I} < T_{ia} \\ 0, & T_{ice}^{I} = T_{ia} \\ U_{hs,up}^{IT}, & T_{ice}^{I} > T_{ia} \end{cases}, \tag{4.72}$$

where,

$$U_{hs,down}^{IT} = \frac{1}{\frac{1}{U_{insu}^{IT}} + R_{hs,down}^{Air}}, \tag{4.73}$$

$$U_{hs,up}^{IT} = \frac{1}{\frac{1}{U_{insu}^{IT}} + R_{hs,up}^{Air}}, \tag{4.74}$$

$U_{hs,down}^{IT}$ is the thermal transmittance of ice storage tank horizontal surface under heat flow downward; $U_{hs,up}^{IT}$ is the thermal transmittance of ice storage tank horizontal surface under heat flow upward; $R_{hs,down}^{Air}$ is the film resistance of still air under horizontal surface under heat flow downward, 0.16 $m^2 \cdot ℃/W$ (ASHRAE 2009c); $R_{hs,up}^{Air}$ is

the film resistance of still air under horizontal surface under heat flow upward, 0.11 $m^2 \cdot ^oC/W$ (ASHRAE 2009c).

Respecting the relation between the water-layer temperature and the indoor air temperature, the piecewise function of the thermal transmittance of horizontal surface of the water-layer is as

$$U_{hs}^{W} = \begin{cases} U_{hs,up}^{IT} + U_{hs,down}^{IT}(1 - sgn(\gamma)), & T_w^W < T_{ia} \\ 0, & T_w^W = T_{ia}, \\ U_{hs,down}^{IT} + U_{hs,up}^{IT}(1 - sgn(\gamma)), & T_w^W > T_{ia} \end{cases} \quad (4.75)$$

where, the sign function $sgn(\gamma)$ returns 1 for γ> 0, returns 0 for γ= 0.

The vertical surface area of the ice-layer is estimated as

$$A_{vs}^{I} = \gamma \mathrm{A}_{vs}^{IT}, \quad (4.76)$$

and the vertical surface area of the water-layer

$$A_{vs}^{W} = (1 - \gamma) A_{vs}^{IT}, \quad (4.77)$$

where, the vertical surface area of the ice-storage tank walls is

$$A_{vs}^{IT} = 2(W^{IT} + L^{IT}) H^{IT}. \quad (4.78)$$

The thermal transmittance U_{insu}^{IT} and the temperature T_{ia} are the input parameters. The case study used U_{insu}^{IT}= 0.253 $W/(m^2 \cdot ^oC)$ for the ice storage tank thermal transmittance; the residential environment temperature of 18 ℃ (Leckner & Zmeureanu 2011) as the indoor air temperature.

4.4.5. Passing flow

The passing flow temperature is lower than the entering liquid water temperature, because the ice-layer cools the passing flow. The temperature of the passing flow is calculated as Behschnitt (1996):

$$T_{f,w}^{IT} = \frac{\dot{m}_{wf}^{ITL} T_{in,wf}^{ITL} + \dot{m}_{w}^{ITS} T_{in,w}^{ITS} - \varepsilon\left[\dot{m}_{wf}^{ITL}\left(T_{in,wf}^{ITL} - T_{ice}^{I}\right) + \dot{m}_{w}^{ITS}\left(T_{in,w}^{ITS} - T_{ice}^{I}\right)\right]}{\dot{m}_{w}^{ITS} + \dot{m}_{wf}^{ITL}}, \tag{4.79}$$

where, ε is the cooling effectiveness of the ice-layer, calculated as Tamasauskas et al. (2012):

$$\varepsilon = \begin{cases} 42.35\gamma, & 0 \le \gamma < 0.02 \\ 121.5\gamma^5 - 165.9\gamma^4 + 88.77\gamma^3 + 23.31\gamma^2 + 3.12\gamma + 0.7928, & 0.02 \le \gamma \le 0.44. \\ 1, & 0.44 < \gamma \le 1 \end{cases} \tag{4.80}$$

4.4.6. Temperatures in ice storage tank

The temperature of the ice-layer is estimated at constant temperature of 0 ℃ (Tamasauskas et al. 2012). The water-layer temperature is calculated by solving the energy balance Eqns (4.50) and (4.55). By employing backward Euler method to discretize the ordinary differential equations, we obtain:

$$\dot{Q}_{sto}^{I} = -\frac{m_{ice\,t_j}^{I} - m_{ice\,t_{j-1}}^{I}}{\Delta t} L_w, \tag{4.81}$$

$$\dot{Q}_{sto}^{W} = \frac{\left(m_w^W c_{p_w}^{\ W}\right)_{t_{j-1}} \left(T_w^W{}_{t_j} - T_w^W{}_{t_{j-1}}\right)}{\Delta t}, \tag{4.82}$$

where,

$$\Delta t = t_j - t_{j-1}. \tag{4.83}$$

Δt is the time step; t_j is the current time; t_{j-1} is the previous time. Rearranging Eqns. (4.81) and (4.82) we have:

$$m^I_{ice_{t_j}} = m^I_{ice_{t_{j-1}}} - \frac{\dot{Q}^I_{sto}\Delta t}{L_w}, \tag{4.84}$$

$$T^W_{w\ t_j} = T^W_{w\ t_{j-1}} + \frac{\dot{Q}^W_{sto}\Delta t}{\left(m^W_w c_{p_w}{}^W\right)_{t_{j-1}}}. \tag{4.85}$$

The temperature of the water-layer is calculated by simultaneously solving above two equations with $m^W_w = m^{IT} - m^I_{ice}$ substituted.

The time step Δt is the input parameter, the case study used Δt= 900 s.

4.4.7. Interchange of energy in solid-liquid equilibrium

Interchange of energy for solid-liquid equilibrium is a procedure to amend the discretized solutions for the occasions involving the phase changing. Phase change occurs during the heat charging and discharging of the ice storage tank. In the numerical solution of the discretized energy balance equations of the ice storage tank, the final moments of phase change may take place during one of the calculation time period. In the final moments the ice could completely disappeared, or the water eventually reached the solidification temperature of 0 ℃. The calculation time period refers to the time step used to discretize the ordinary differential equations of the energy balances. The discretized solution cannot tell the final moments, but only given for the fixed time step, e.g. t_j and t_{j-1}. If the moments take place between t_j and t_{j-1}, the calculations

should able to handle, or the numerical solutions as $m^I_{ice_{t_j}} < 0$ or $T^W_{w\ t_j} < 0$ are possible to present. Smaller time steps mitigate but do not eliminate the potential problem.

With the procedure employed in this thesis, the limit states of heat charging and discharging are counted. Reaching the limit states, the amount of heat that is unable to be charged onto the ice-layer is charged onto the water-layer instead; and the amount of heat that is unable to be discharged from the water-layer is discharged from the ice-layer. Two new variables are introduced for counting the dispatch: (i) The heat transfer rate, denoted by $\dot{Q}^{I2W}$, is the interchange of energy from the ice-layer to the water-layer; (ii) The heat transfer rate, denoted by $\dot{Q}^{W2I}$, is the interchange of energy from the water-layer to the ice-layer.

I. The ice-layer

The procedure starts with the pre-estimation of the energy change rate of the ice-layer, $\dot{Q}^I_{sto_{pre}}$, with:

$$\dot{Q}^I_{sto_{pre}} = \dot{Q}^I_{\text{int}} + \dot{Q}^I_{ext} + \dot{Q}^I_f - L_w \dot{m}^{ITL}_{wi}. \tag{4.86}$$

Because of not knowing if exists enough ice to fulfill the heat charging, the calculation by Eqn. (4.50) is distinguished by the pre-estimated quantity.

The pre-estimation of the mass of the ice-layer, $m^I_{ice_{pre}}$, at time t_j is calculated with:

$$m^I_{ice_{pre_{t_j}}} = m^I_{ice_{t_{j-1}}} - \frac{\dot{Q}^I_{sto_{pre}} \Delta t}{L_w}. \tag{4.87}$$

If the pre-estimated mass $m^I_{ice_{pre}} \geq 0$, then at the time t_j, $m^I_{ice_{t_i}} = m^I_{ice_{pre}{}_{t_j}}$; if $m^I_{ice_{pre}} < 0$, $m^I_{ice_{t_j}}$ is set equal to zero.

The heat storage capacity of the ice-layer is calculated with Eqn. (4.81). The heat transfer rate $\dot{Q}^{I2W}$ is calculated as the difference between the pre-estimated demand for heat storage and the capacity of the ice-layer as:

$$\dot{Q}^{I2W} = \dot{Q}^I_{sto_{pre}} - \dot{Q}^I_{sto}. \tag{4.88}$$

II. The water-layer

The heat transfer rate $\dot{Q}^{I2W}$ is added to Eqn. (4.55):

$$\dot{Q}^W_{sto_{pre}} = \left(\dot{Q}^W_{int} + \dot{Q}^W_{ext} + \dot{Q}^W_f\right) + \dot{Q}^{I2W}. \tag{4.89}$$

The pre-calculation of the temperature of the water-layer at time t_j, $T^W_{w\ pre}$, is pre-calculated as:

$$T^W_{w\ pre_{t_j}} = T^W_{w\ t_{j-1}} + \frac{\dot{Q}^W_{sto_{pre}} \Delta t}{\left(m^W_w c_{p_w}\right)_{t_{j-1}}}. \tag{4.90}$$

If $T^W_{w\ pre_{t_j}} \geq 0$, congelation does not commence, and hence $T^W_{w\ t_j} = T^W_{w\ pre_{t_j}}$; if $T^W_{w\ pre} < 0$, $T^W_{w\ t_j}$ is set equal to zero. With the temperature $T^W_{w\ t_j}$, the heat storage capacity of the water-layer is calculated with Eqn. (4.82). The heat transfer rate $\dot{Q}^{W2I}$ is calculated as:

$$\dot{Q}^{W2I} = \dot{Q}^W_{sto_{pre}} - \dot{Q}^W_{sto}, \tag{4.91}$$

which corresponds to the amount of ice frozen from water in extra. The mass of ice-layer, therefore, should be:

$$m^I_{ice_{t_j}} = m^I_{ice_{pre}} + m^I_{ice_{extra}}, \tag{4.92}$$

where, $m^I_{ice_{extra}}$ is the extra mass of ice,

$$m^I_{ice_{extra}} = \frac{\dot{Q}^{W2I}\Delta t}{L_w}. \tag{4.93}$$

4.4.8. Entering conditions of heat transfer fluid

The entering conditions of heat transfer fluid are determined by the operation of other devices connected to the ice storage tank. The entering conditions are the ice storage tank model inputs, related to the storage tank heat source and heat sink.

The solar thermal collector is the heat source of ice storage tank in the solar combisystem. The leaving conditions of the heat transfer water from the solar thermal collector are the entering conditions to the ice storage tank:

$$\dot{m}^{ITS}_w = \dot{m}^{Coll}_w, \tag{4.94}$$

$$T^{ITS}_{in,w} = T^{Coll}_{out,w}, \tag{4.95}$$

$$c_{p}{}^{ITS}_{in,w} = c_{p}{}^{Coll}_{out,w}. \tag{4.96}$$

The heat pump is the heat sink of ice storage tank in the solar combisystem. The leaving conditions of the heat transfer water from the heat pump evaporator are the entering conditions to the ice storage tank:

$$\dot{m}_{wi}^{ITL} = \dot{m}_{wi}^{Evap}, \quad (4.97)$$

$$\dot{m}_{wf}^{ITL} = \dot{m}_{wf}^{Evap}, \quad (4.98)$$

$$T_{in,wf}^{ITL} = T_{out,wf}^{Evap}, \quad (4.99)$$

$$c_{p_{in,wf}}^{ITL} = c_{p_{out,wf}}^{Evap}. \quad (4.100)$$

4.4.9. Exergy analysis of ice storage tank

This section presents the exergy analysis of the ice storage tank operation by regarding the ice storage tank as a thermodynamic open system. The exergy balance equation is established considering the flow of water, the heat transfer between the storage tank and surroundings, the inter-layer heat transfer between the two control volumes, and the exergy destroyed during the operation.

Exergy transfer with heat source and heat sink

When the solar thermal collector is operated against the ice storage tank, the net exergy transfer rate from the heat source, $\dot{X}^{ITS}$, is:

$$\dot{X}^{ITS} = \dot{X}^{Coll4IT}. \quad (4.101)$$

When the heat pump is turned on, the net exergy transfer rate to the heat sink, $\dot{X}^{ITL}$, is:

$$\dot{X}^{ITL} = \dot{X}^{Evap}. \quad (4.102)$$

Exergy transfer with surroundings

The exergy transfer between the ice storage tank and the surroundings, $\dot{X}_{ext}^{IT}$, is calculated with:

$$\dot{X}_{ext}^{IT} = \dot{X}_{ext}^{I} + \dot{X}_{ext}^{W}, \tag{4.103}$$

where,

$$\dot{X}_{ext}^{I} = \dot{Q}_{ext}^{I}|\tau_{ia}|, \tag{4.104}$$

$$\dot{X}_{ext}^{W} = \dot{Q}_{ext}^{W}|\tau_{ia}|, \tag{4.105}$$

$\dot{X}_{ext}^{I}$ is the exergy transfer rate of the ice-layer with the indoor surroundings; $\dot{X}_{ext}^{W}$ is the exergy transfer rate of the water-layer with the indoor surroundings; τ_{ia} is the quality factor of conduction-convection with respect to the indoor air temperature TK_{ia},

$$\tau_{ia} = 1 - \frac{TK_0}{TK_{ia}}. \tag{4.106}$$

For the quality factor of conduction-convection, generally expressed as τ= 1- $\frac{TK_0}{TK}$, when TK> TK_0, the quality factor is positive, indicating the conduction-convection embodies warm exergy with respect to the reference state. When TK< TK_0, the quality factor is negative, indicating cold exergy embodied. When TK= TK_0, the quality factor is zero, indicating no exergy is transferred due to the conduction-convection. By taking the quality factor in absolute value, the sign convention of the quality factor is withdrawn, so that no confliction would be caused against the sign convention of energy transfer process.

Exergy destroyed by inter-layer heat transfer

The heat transfer between the ice-layer and water-layer due to the temperature difference degrades the quality of the heat. The inter-layer exergy destruction rate, $\dot{X}_{int,dest}^{IT}$, is calculated as:

$$\dot{X}_{int,dest}^{IT} = \dot{X}_{int}^{I} - \dot{X}_{int}^{W}, \tag{4.107}$$

where, $\dot{X}_{int}^{I}$ is the exergy transfer rate of the ice-layer with the water-layer; $\dot{X}_{int}^{W}$ is the exergy transfer rate of the water-layer with the ice-layer. Further transforming,

$$\dot{X}_{int,dest}^{IT} = \dot{Q}_{int}^{I}\left(\left|\tau^{W}\right| - \left|\tau^{I}\ \right|\right), \tag{4.108}$$

where, τ^{W} is the quality factor of the transferred heat with respect to the water-layer temperature, TK_{w}^{W}, as:

$$\tau^{W} = 1 - \frac{TK_0}{TK_{w}^{W}}; \tag{4.109}$$

τ^{I} is the quality factor of the transferred heat with respect to the ice-layer temperature, TK_{ice}^{I}, as:

$$\tau^{I}\ = 1 - \frac{TK_0}{TK_{ice}^{I}}. \tag{4.110}$$

Change of exergy during heat storage process in ice storage tank

The exergy variation rate within the ice storage tank, $\Delta\dot{X}^{IT}$, is calculated as the sum of that of the two layers,

$$\Delta\dot{X}^{IT} = \Delta\dot{X}^{I} + \Delta\dot{X}^{W}, \tag{4.111}$$

where, $\Delta\dot{X}^{I}$ is the exergy variation rate of the ice-layer,

$$\Delta\dot{X}^{I} = \frac{\left(m_{ice_{t_j}}^{I} - m_{ice_{t_{j-1}}}^{I}\right)\varphi_{ice}^{I}}{\Delta t}; \tag{4.112}$$

$\Delta\dot{X}^{W}$ is the exergy variation rate of the water-layer,

$$\Delta\dot{X}^{W} = \frac{m^{W}_{w\,t_j}\psi^{W}_{w\,t_j} - m^{W}_{w\,t_{j-1}}\psi^{W}_{w\,t_{j-1}}}{\Delta t}; \tag{4.113}$$

φ^{I}_{ice} is the specific exergy of ice in the ice-layer; ψ^{W}_{w} is the specific exergy of water in the water-layer.

Exergy destruction and exergetic efficiency

The exergy destruction rate by the ice storage tank operation, $\dot{X}^{IT}_{dest}$, is obtained from the established exergy balance:

$$\dot{X}^{IT}_{dest} = \dot{X}^{ITS} - \dot{X}^{ITL} + \dot{X}^{IT}_{ext} + \dot{X}^{IT}_{int,dest} - \Delta\dot{X}^{IT}. \tag{4.114}$$

The exergetic efficiency of the ice storage tank operation, η^{IT}_{II}, is calculated as:

$$\eta^{IT}_{II} = 1 - \frac{\sum_0^{t_j} X^{IT}_{dest}}{\sum_0^{t_j} X^{ITS}}. \tag{4.115}$$

$\sum_0^{t_j} X^{IT}_{dest}$ is the sum of exergy destruction of the ice storage tank since the start time of operation, where,

$$X^{IT}_{dest} = \dot{X}^{IT}_{dest}\Delta t, \tag{4.116}$$

$\sum_0^{t_j} X^{ITS}$ is the sum of exergy transfer from the heat source of ice storage tank since the start time of operation, where,

$$X^{ITS} = \dot{X}^{ITS}\Delta t. \tag{4.117}$$

4.5. Mathematical model of water storage tank

The water storage tank (Fig. 4.6) contains water as the thermal storage media. Two immersion heat exchangers are mounted inside the storage tank, as part of two

circulation loops connecting the storage tank to the heat sources and heat sinks. Inside the circulation loops, water is the heat transfer fluid. Heat transfers between the heat transfer fluid and the storage media by the immersion heat exchangers. Cold water from the city main flows into the storage tank to compensate the hot water drawn off. Whenever the draw-off temperature below the set temperature, an inline heater on the draw-off pipeline starts up to reheat the hot water using electricity. The mathematical model simulates the water storage tank operation to calculate the temperature of water in the storage tank and the electric power input to the inline heater.

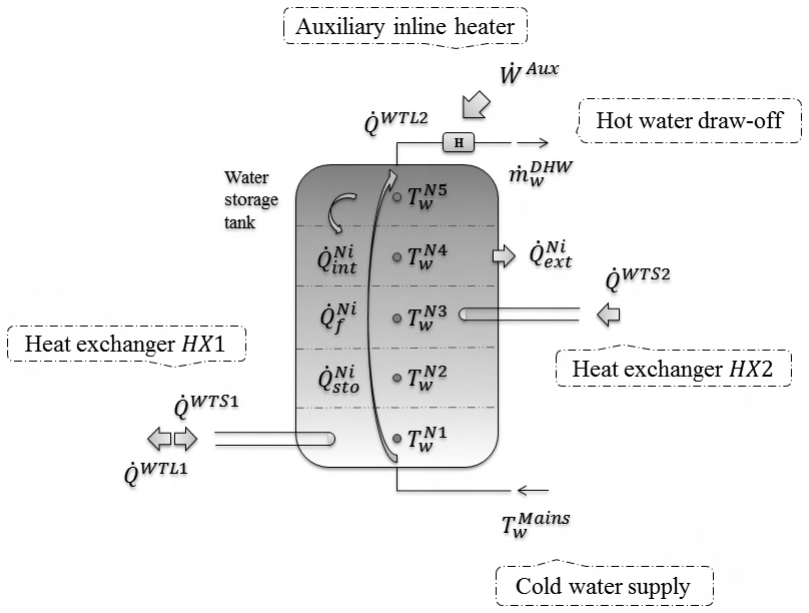

Fig. 4.6 Schematic of water storage tank model

The modeling of water storage tank is based on Duffie & Beckman (2006) and Cruickshank & Harrison (2010). The storage media is regarded as five distinct homogeneous layers in equal mass. Each layer is identified as one water-node, denoted as Ni, i = 1, 2… 5 in sequence from the bottom to top. One immersion heat exchanger

$HX1$ locates at the water-node $N1$, the other immersion heat exchanger $HX2$ locates at the water-node $N3$. The heat transfer of water-nodes takes place across the contact surface between adjacent water-nodes, tank surface, and immersion heat exchanger surfaces. The cold water port locates at the water-node $N1$, the hot water port locates at the water-node $N5$. The water flow created by the leaving hot water and entering cold water is called *jet flow* in here, which is involved with the transfer of heat with the water-nodes as well. The modeling assumes that the jet flow takes place as water moving from the lower node to the right above higher node, which is a pattern of relay in the bottom-up direction. A premise implied is that the amount of jet flow at one time step does not exceed the mass of the one water-node.

4.5.1. The energy balance of water-nodes

Energy balance is established for the water-node Ni as:

$$\dot{Q}_{sto}^{Ni} = \dot{Q}_{HX}^{Ni} + \dot{Q}_{int}^{Ni} + \dot{Q}_{ext}^{Ni} + \dot{Q}_{f}^{Ni} \tag{4.118}$$

where, $\dot{Q}_{sto}^{Ni}$ is the energy change rate of the water-node Ni; $\dot{Q}_{HX}^{Ni}$ is the heat transfer rate of the immersion heat exchanger; $\dot{Q}_{int}^{Ni}$ is the heat transfer rate of the water-node Ni with the adjacent nodes across the contact surface in between; $\dot{Q}_{ext}^{Ni}$ is the heat transfer rate of the water-node Ni with the surroundings across the tank surface; $\dot{Q}_{f}^{Ni}$ is the heat transfer rate of the water-node Ni with the jet flow.

Terms in Eqn. (4.118) have following formulations,

$$\dot{Q}_{sto}^{Ni} = \frac{d\left(m_w^N c_{p_w}^{Ni} T_w^{Ni}\right)}{dt}, \tag{4.119}$$

$$\dot{Q}_{HX}^{Ni} = \dot{Q}_{WTS1}^{Ni} + \dot{Q}_{WTS2}^{Ni} + \dot{Q}_{WTL1}^{Ni}, \tag{4.120}$$

$$\dot{Q}_{int}^{Ni} = \begin{cases} \frac{k^{WTi+1}}{L^{WTi+1}}\left(A_b^{WT} + A_{cs,shell}^{WT}\right)\left(T_w^{Ni+1} - T_w^{Ni}\right), & i = 1 \\ \frac{k^{WTi}}{L^{WTi}}\left(A_b^{WT} + A_{cs,shell}^{WT}\right)\left(T_w^{Ni-1} - T_w^{Ni}\right) + & \\ \quad \frac{k^{WTi+1}}{L^{WTi+1}}\left(A_b^{WT} + A_{cs,shell}^{WT}\right)\left(T_w^{Ni+1} - T_w^{Ni}\right), & i = 2,3,4 \\ \quad \frac{k^{WTi}}{L^{WTi}}\left(A_b^{WT} + A_{cs,shell}^{WT}\right)\left(T_w^{Ni-1} - T_w^{Ni}\right), & i = 5 \end{cases}, \tag{4.121}$$

$$\dot{Q}_{ext}^{Ni} = \begin{cases} \left(U_{vs}^{WT} A_{vs}^{Ni} + U_{hs}^{WT} A_b^{WT}\right)\left(T_{ia} - T_w^{Ni}\right), & i = 1,5 \\ U_{vs}^{WT} A_{vs}^{Ni}\left(T_{ia} - T_w^{Ni}\right), & i = 2,3,4 \end{cases}, \tag{4.122}$$

$$\dot{Q}_f^{Ni} = \begin{cases} \dot{m}_w^{DHW}\left(c_{p_w}^{Mains} T_w^{Main} - c_{p_w}^{Ni} T_w^{Ni}\right), & i = 1 \\ \dot{m}_w^{DHW}\left(c_{p_w}^{Ni-1} T_w^{Ni-1} - c_{p_w}^{Ni} T_w^{Ni}\right), & i = 2,3,4,5 \end{cases}. \tag{4.123}$$

where, $\dot{Q}_{WTS1}^{Ni}$ is the heat transfer rate from the heat source through the heat exchanger $HX1$ to the water-node Ni; $\dot{Q}_{WTS2}^{Ni}$ is the heat transfer rate from the heat source through the heat exchanger $HX2$ to the water-node Ni; $\dot{Q}_{WTL1}^{Ni}$ is the heat transfer rate from the water-node Ni to the heat sink through the heat exchanger $HX1$; m_w^N is the mass of the water-node; $\dot{m}_w^{DHW}$ is the mass flow rate of domestic hot water drawn; T_w^{Ni} is the temperature of the water-node Ni; T_w^{Ni+1} is the temperature of the of the water-node Ni+1; T_w^{Ni-1} is the temperature of the of the water-node Ni-1; T_w^{Main} is the temperature of water from the city main; k^{WTi} is the thermal conductivity of water given by Eqn. (4.140) (similar to k^{WTi+1}); U_{vs}^{WT} is the thermal transmittance of vertical surface of the water storage tank; U_{hs}^{WT} is the thermal transmittance of the horizontal surface of the water storage tank; L^{WTi} is the length given by Eqn. (4.144) (similar to

L^{WTi+1}); A_b^{WT} is the base area of the water storage tank; $A_{cs,shell}^{WT}$ is the cross-sectional area of the water storage tank shell; A_{vs}^{Ni} is the vertical surface area of the water-node Ni.

4.5.2. Heat transfer of immersion heat exchangers

The heat transfer by conduction takes place in the water storage tank between the adjacent nodes, in functional of the temperature gradient and thermal conductivity. The dependent quantities generally are available for the modeling. In contrast, the heat transfer by convection is more complex, and the modeling does not have an approach widely being accepted for all situations. However, the convection cannot be abandon. Without employing certain computational approach, large temperature difference present among the *exchanger node* (the node with the heat exchanger) and *non-exchanger node* (the node without the heat exchanger).

Because the convection caused by the fluid mechanism of buoyancy effect is unknown, a new concept of so-called ***continuous node*** is conceived for modeling stratified thermal storage tank. The concept is presented in this section, with a series of definition including ***node exchange heat***, ***node exchange contribution***, and ***node exchange mass*** for explicate the continuous node components. The application approach is given by case of this study.

The heat transfer of immersion heat exchanger HX with the node Ni is defined as ***node exchange heat***. Denoting the node exchange heat rate by $\dot{Q}_{HX}^{Ni}$, the overall heat transfer rate of immersion heat exchanger HX by $\dot{Q}^{HX}$, here has

$$\sum_{i=1}^{n} \dot{Q}_{HX}^{Ni} = \dot{Q}^{HX}, \quad (i = 1 \dots n), \tag{4.124}$$

where, n is the number of nodes in the stratified thermal storage tank. The ratio of the node exchange heat rate to the overall heat transfer rate of immersion heat exchanger HX is defined as ***node exchange contribution***, denoting by α^{Ni},

$$\alpha^{Ni} = \frac{\dot{Q}_{HX}^{Ni}}{\dot{Q}^{HX}}. \quad (i = 1 \dots n) \tag{4.125}$$

For a single heat exchanger HX, the summation of all node exchange contributions equals to 1,

$$\sum_{i=1}^{n} \alpha^{Ni} = 1 \quad \left(0 \le \alpha^{Ni} \le 1\right), \tag{4.126}$$

where, α^{Ni}= 0 indicates that the node Ni is not influenced by the heat transfer of immersion heat exchanger HX; α^{Ni}> 0 indicates that the node Ni is influenced by the heat transfer of immersion heat exchanger HX; if α^{Ni}= 1, the node Ni is the only one node that undergoes the heat transfer with the immersion heat exchanger HX.

The ***continuous node*** is a lumped node aggregated with the nodes that undergoing the transfer of heat with the immersion heat exchanger. By assigning the indices $p \dots q$ to the component nodes, the continuous node is composed of the node Ni (i= $p \dots q$), and the component node exchanger contribution is subject to:

$$\alpha^{Ni} > 0. \quad (i = p \dots q) \tag{4.127}$$

Because the component nodes aggregate into one continuous body, each has an *equal node exchange contribution*. The magnitude of the node exchange contribution is, therefore, the reciprocal of the component number,

$$\alpha^{Ni} = \frac{1}{q - p + 1}. \quad (i = p \dots q) \tag{4.128}$$

The continuous node includes the exchanger node, and, maybe, non-exchanger node. Being with the immersion heat exchanger, an exchanger node is always under the influence of the heat transfer and, therefore, Eqn. (4.127) is applied and an exchanger node is always the continuous node component. As for the non-exchanger node, it could be or not be involved in the heat transfer of immersion heat exchanger. The situation for a non-exchanger node involved the transfer of heat and becomes the continuous node component is: (i) its adjacent higher temperature node in positive α^{Ni} under a heat charging process, or (ii) its adjacent lower temperature node in positive α^{Ni} under a heat discharging process.

During a heat charging process, the node exchange heat rate is calculated as:

$$\dot{Q}_{HX}^{Ni} = \alpha^{Ni}\dot{Q}^{HX}. \quad (i = 1 \dots n) \tag{4.129}$$

Both of the quantities at the right side are known. During a heat discharging process, the ***node exchange mass*** is defined as the partial mass of node Ni that is upon the discharge, denoted by m_{HX}^{Ni}. The magnitude of the node exchange mass is between 0 and the mass of the node, inclusive. The node that does not belong to the continuous

node has the node exchange mass of zero. The component nodes of continuous node have *equal node exchange mass* for each, denoted by m_{HX}^{N},

$$m_{HX}^{N} = \frac{\dot{Q}^{HX}\Delta t}{\sum_{i=1}^{n}\left[sgn\left(\alpha^{Ni}\right)\left(C_p{}^{Ni}T^{Ni} - C_{p_{in}}{}^{HX}T_{in}^{HX}\right)\right]}, \quad (i = 1 \dots n) \tag{4.130}$$

where T^{Ni} is the temperature of the node Ni; T_{in}^{HX} is the temperature of the heat transfer fluid entering the immersion heat exchanger HX. And the discharging temperature of the immersion heat exchanger operation is the arithmetic mean temperature of the component nodes, calculated as:

$$T_{out}^{HX} = \frac{\sum_{i=p}^{q} sgn\left(\alpha^{Ni}\right)T^{Ni}}{q - p + 1}. \quad (i = p \dots q) \tag{4.131}$$

The node exchange mass features the heat discharging process, used to calculate the node exchange mass of node Ni,

$$m_{HX}^{Ni} = sgn\left(\alpha^{Ni}\right)m_{HX}^{N}. \quad (i = 1 \dots n) \tag{4.132}$$

Whereupon, the node exchange heat is calculated as:

$$\dot{Q}_{HX}^{Ni} = \frac{m_{HX}^{Ni}\left(C_p{}^{Ni}T^{Ni} - C_{p_{in}}{}^{HX}T_{in}^{HX}\right)}{\Delta t}. \quad (i = 1 \dots n) \tag{4.133}$$

A brief summary is given for the above concept development: The simplest situation for a continuous node being formed is with one exchanger node; the utmost is with all nodes in a storage tank. Within a continuous node, the temperature of an exchanger node is the highest during the heat charging, the lowest during the heat discharging. If a non-exchanger node joins a continuous node depends on: (i) the

temperature difference with the adjacent nodes; and (ii) the operation status of an immersion heat exchanger, in heat charging or heat discharging. Each node in a storage tank is appointed a node exchange contribution. The heat charging/discharging impacts made by an immersion heat exchanger on each of the nodes are calculated.

The following subsections are presented how the concept is applied. The water storage tank has two immersion heat exchangers, $HX1$ and $HX2$, operated in three ways: the immersion heat exchanger $HX1$ in heat charging mode; the immersion heat exchanger $HX2$ in heat charging mode; the immersion heat exchanger $HX1$ in heat discharging mode.

I. The immersion heat exchanger $HX1$ in the heat charging mode

The heat transfer rate $\dot{Q}_{WTS1}^{Ni}$ is calculated as:

$$\dot{Q}_{WTS1}^{Ni} = \alpha_{WTS1}^{Ni}\dot{Q}^{WTS1}, \tag{4.134}$$

where, $\dot{Q}^{WTS1}$ is the heat charging rate of the immersion heat exchanger $HX1$; α_{WTS1}^{Ni} is the node Ni exchange contribution with respect to the heat transfer rate $\dot{Q}^{WTS1}$.

The node exchange contribution α_{WTS1}^{Ni} is determined with the water-node temperatures in the heat charging mode, shown in Table 4.3.

Table 4.3 Node exchange contributions of immersion heat exchanger HX1 in heat charging mode

Conditions	Decisions
$T_w^{N1} < T_w^{N2}$	α_{WTS1}^{N1}= 1 and α_{WTS1}^{Ni}= 0 (i= 2, 3… 5)
$T_w^{N1} \geq T_w^{N2} < T_w^{N3}$	α_{WTS1}^{Ni}= 1/2 (i= 1, 2) and α_{WTS1}^{Ni}= 0 (i= 3, 4, 5)
$T_w^{N1} \geq T_w^{N2} \geq T_w^{N3} < T_w^{N4}$	α_{WTS1}^{Ni}= 1/3 (i= 1, 2, 3) and α_{WTS1}^{Ni}= 0 (i= 4, 5)
$T_w^{N1} \geq T_w^{N2} \geq T_w^{N3} \geq T_w^{N4} < T_w^{N5}$	α_{WTS1}^{Ni}= 1/4 (i= 1, 2… 4) and α_{WTS1}^{N5}= 0
$T_w^{N1} \geq T_w^{N2} \geq T_w^{N3} \geq T_w^{N4} \geq T_w^{N5}$	α_{WTS1}^{Ni}= 1/5 (i= 1, 2… 5)

II. The immersion heat exchanger $HX2$ in the heat charging mode

The heat transfer rate $\dot{Q}_{WTS2}^{Ni}$ is calculated as:

$$\dot{Q}_{WTS2}^{Ni} = \alpha_{WTS2}^{Ni}\dot{Q}^{WTS2}, \tag{4.135}$$

where, $\dot{Q}^{WTS2}$ is the heat charging rate of the immersion heat exchanger $HX2$; α_{WTS2}^{Ni} is the node Ni exchange contribution with respect to the heat charging rate $\dot{Q}^{WTS2}$.

The node exchange contribution α_{WTS2}^{Ni} is determined with the water-node temperatures in the heat charging mode, shown in Table 4.4.

Table 4.4 Node exchange contributions of immersion heat exchanger HX2 in heat charging mode

Conditions	Decisions
$T_w^{N2} > T_w^{N3} < T_w^{N4}$	α_{WTS2}^{N3}= 1 and α_{WTS2}^{Ni}= 0 (i= 1, 2, 4, 5)
$T_w^{N1} > T_w^{N2} \leq T_w^{N3} < T_w^{N4}$	α_{WTS2}^{Ni}= 1/2 (i= 2, 3) and α_{WTS2}^{Ni}= 0 (i= 1, 4, 5)
$T_w^{N1} \leq T_w^{N2} \leq T_w^{N3} < T_w^{N4}$	α_{WTS2}^{Ni}= 1/3 (i= 1, 2, 3) and α_{WTS2}^{Ni}= 0 (i= 4, 5)
$T_w^{N2} > T_w^{N3} \geq T_w^{N4} < T_w^{N5}$	α_{WTS2}^{N3}= 1/2 (i= 3, 4) and α_{WTS2}^{Ni}= 0 (i= 1, 2, 5)
$T_w^{N1} > T_w^{N2} \leq T_w^{N3} \geq T_w^{N4} \geq T_w^{N5}$	α_{WTS2}^{Ni}= 1/3 (i= 3, 4, 5) and α_{WTS2}^{Ni}= 0 (i= 1, 2)
$T_w^{N1} \leq T_w^{N2} \leq T_w^{N3} \geq T_w^{N4} \geq T_w^{N5}$	α_{WTS2}^{Ni}= 1/4 (i= 1, 2… 4) and α_{WTS2}^{N5}= 0
$T_w^{N2} > T_w^{N3} \geq T_w^{N4} \geq T_w^{N5}$	α_{WTS2}^{Ni}= 1/3 (i= 3, 4, 5) and α_{WTS2}^{Ni}= 0 (i= 1, 2)
$T_w^{N1} > T_w^{N2} \leq T_w^{N3} \geq T_w^{N4} \geq T_w^{N5}$	α_{WTS2}^{Ni}= 1/4 (i= 2, 3… 5) and α_{WTS2}^{N1}= 0
$T_w^{N1} \leq T_w^{N2} \leq T_w^{N3} \geq T_w^{N4} \geq T_w^{N5}$	α_{WTS2}^{Ni}= 1/5 (i= 1, 2… 5)

III. The immersion heat exchanger $HX1$ in the heat discharging mode

The heat transfer rate $\dot{Q}^{WTL1}$ is calculated as:

$$\dot{Q}_{WTL1_{t_j}}^{Ni} = \frac{m_{WTL1_{t_j}}^{Ni}\left(C_{p_{w\ t_{j-1}}}^{Ni}\ T_{w\ t_{j-1}}^{Ni} - C_{p_{in,w}\ t_j}^{WTL1}\ T_{in,w\ t_j}^{WTL1}\right)}{\Delta t}, \tag{4.136}$$

where,

$$m_{WTL1_{t_j}}^{Ni} = sgn\left(\alpha_{WTL1_{t_j}}^{Ni}\right) m_{WTL1_{t_j}}^{N}, \tag{4.137}$$

and

$$m_{WTL1_{t_j}}^{N} = \frac{\dot{Q}^{WTL1}{}_{t_j} \Delta t}{\sum\left[sgn\left(\alpha_{WTL1_{t_j}}^{Ni}\right)\left(C_{p_w}{}^{Ni}{}_{t_{j-1}} T_w^{Ni}{}_{t_{j-1}} - C_{p_{in,w}}{}^{WTL1}{}_{t_j} T_{in,w}^{WTL1}{}_{t_j}\right)\right]}, \tag{4.138}$$

$\dot{Q}^{WTL1}$ is the heat discharging rate of the immersion heat exchanger $HX1$; $T_{in,w}^{WTL1}$ is the temperature of water entering the immersion heat exchanger $HX1$; m_{WTL1}^{Ni} is the node Ni exchange mass with respect to the heat discharging rate $\dot{Q}^{WTL1}$; α_{WTL1}^{Ni} is the node Ni exchange contribution respecting the heat discharging rate $\dot{Q}^{WTL1}$; m_{WTL1}^{N} is the node exchange mass respecting the heat discharging rate $\dot{Q}^{WTL1}$.

The node exchange contribution α_{WTL1}^{Ni} was determined with the water-node temperatures for the heat discharging mode, shown in Table 4.5.

Table 4.5 Node exchanger contributions of immersion heat exchanger HX1 in heat discharging mode

Conditions	Decisions
$T_w^{N1} > T_w^{N2}$	α_{WTL1}^{N1}= 1 and α_{WTL1}^{Ni}= 0 (i= 2, 3…5)
$T_w^{N1} \leq T_w^{N2} > T_w^{N3}$	α_{WTL1}^{Ni}= 1/2 (i= 1, 2) and α_{WTL1}^{Ni}= 0 (i= 3, 4, 5)
$T_w^{N1} \leq T_w^{N2} \leq T_w^{N3} > T_w^{N4}$	α_{WTL1}^{Ni}= 1/3 (i= 1, 2, 3) and α_{WTL1}^{Ni}= 0 (i= 4, 5)
$T_w^{N1} \leq T_w^{N2} \leq T_w^{N3} \leq T_w^{N4} > T_w^{N5}$	α_{WTL1}^{Ni}= 1/4 (i= 1, 2…4) and α_{WTL1}^{N5}= 0
$T_w^{N1} \leq T_w^{N2} \leq T_w^{N3} \leq T_w^{N4} \leq T_w^{N5}$	α_{WTL1}^{Ni}= 1/5 (i= 1, 2…5)

As for the discharging temperature of the immersion heat exchanger $HX1$, the calculation is as:

$$T_{out,w}^{WTL1}{}_{t_j} = \frac{\sum_{i=p}^{q} sgn\left(\alpha_{WTL1_{t_j}}^{Ni}\right) T_w^{Ni}{}_{t_{j-1}}}{q-p+1}, \tag{4.139}$$

where, $T_{out,w}^{WTL1}$ is the temperature of water leaving the immersion heat exchanger $HX1$.

Substituting Eqns. (4.134), (4.135), and (4.136) to Eqn. (4.120), the determined node exchange contributions α_{WTS1}^{Ni}, α_{WTS2}^{Ni}, and α_{WTL1}^{Ni}, based on the node temperatures of previous time ${T_w^{Ni}}_{t_{j-1}}$, will be used to calculate $\dot{Q}_{HX}^{Ni}$, the heat transfer rate of the immersion heat exchanger of node Ni. The node temperatures at the current time, ${T_w^{Ni}}_{t_j}$, is calculated by solving the energy balance equations of the five nodes of the water storage tank.

The approach presented above was used to estimate the immersion heat exchanger operation onto the stratified nodes. The concept of continuous node was developed by acknowledging that the fluid motion of convection takes place in the presence of temperature difference. The existence of flow motion can be recognized by the temperature differences among the nodes: From the point of view of fluid mechanics, the temperature difference indicates the diffusion and collisions in the fluid, especially when large temperature difference in place, the buoyancy is bustling about to homogenize the density of fluid (Turner 1973). With the concept of continuous node, to model the flow motion is avoided. Instead, by designating thermodynamic system in a flexible way, the approach replaces the need for modeling the convection. From the thermodynamic point of view, how the continuous node concept works can be explicated this way: The establishment of energy balance equation (4.118) upon controlled mass implies that, one node is one thermodynamic system, and the storage tank operation is represented by several thermodynamic systems. When the continuous node has more than one component nodes, the multiple thermodynamic systems of the

component nodes (each in one-node-magnitude) are regarded as one thermodynamics system (in multiple-nodes-magnitude) undergoing the heat charging or discharging process. In this perspective, the node exchange contribution is assigned. Afterwards, the multiple thermodynamic systems are resumed, the energy balance equation (4.118) is valid and the unknown temperature of each node can be solved.

4.5.3. Heat transfer between nodes

The inter-nodal heat transfer takes place under the temperature difference between adjacent water-nodes in the vertical direction by conduction. In addition, the heat conduction through the tank shell is calculated. It was assumed that the inner vertical surface of tank shell has the temperature equal to the temperature of the water-node at the same height.

The thermal conductivity k^{WTi} is an area-weighted property as

$$k^{WTi} = \frac{k_{shell}^{WT} A_{cs,shell}^{WT} + k_{avg,w}^{WTi} A_{\mathrm{b}}^{WT}}{A_{cs,shell}^{WT} + A_{b}^{WT}}, \qquad i = 2, 3 \dots 5, \tag{4.140}$$

where, k_{shell}^{WT} is the thermal conductivity of the water storage tank shell; $k_{avg,w}^{WTi}$ is the thermal conductivity of water with respect to the temperature,

$$T_{avg,w}^{WTi} = \begin{cases} \dfrac{T_w^{Mains} + T_w^{Ni}}{2}, & i = 1 \\ \dfrac{T_w^{Ni-1} + T_w^{Ni}}{2}, & i = 2, 3 \dots 5 \end{cases}. \tag{4.141}$$

For a vertical cylinder tank, the areas $A_{cs,shell}^{WT}, A_{b}^{WT}$ are calculated as:

$$A_{cs,shell}^{WT} = \pi D^{WT} \delta_{shell}^{WT}, \tag{4.142}$$

$$A_b^{WT} = \frac{\pi}{4} D^{WT\,2}, \tag{4.143}$$

where, D^{WT} is the diameter of the cylinder water storage tank; δ_{shell}^{WT} is the thickness of the water storage tank shell.

The distance that corresponds to the inter-nodal heat conduction is calculated in

$$L^{WTi} = \frac{L_{Ni-1}^{WT} + L_{Ni}^{WT}}{2}, \qquad i = 2, 3 \dots 5, \tag{4.144}$$

where,

$$L_{Ni}^{WT} = \frac{m_w^N}{\rho_w^{Ni} A_b^{WT}}, \tag{4.145}$$

L_{Ni}^{WT} is the thickness of the water-node Ni. For a five-nodes water storage tank model,

$$m_w^N = \frac{1}{5}\left(\rho_w^{WT} A_b^{WT} H^{WT}\right), \tag{4.146}$$

where, ρ_w^{WT} is the density of water in the water storage tank, estimated at 99 °C; H^{WT} is the height of the water storage tank.

The thermal conductivity k_{shell}^{WT} and tank dimensions $\delta_{shell}^{WT}, D^{WT}, H^{WT}$ are the input parameters. For instance, in the case study: k_{shell}^{WT}= 13.64 W/(m·°C) for stainless steel at 40 °C, and δ_{shell}^{WT}= 0.002 m, D^{WT}= 1.3 m, H^{WT}= 1.657 m (Consolar 2012).

4.5.4. Heat transfer with surroundings

The heat transfer between the water storage tank and the surrounding environment takes place through the storage tank walls. The thermal transmittance is

calculated with the thermal transmittance of the storage tank insulation and the surface film resistance of still air.

The thermal transmittance of water storage tank horizontal surface under heat flow upward is denoted by $U_{hs,up}^{WT}$; the thermal transmittance of water storage tank horizontal surface under heat flow downward is denoted by $U_{hs,down}^{WT}$. The calculations for $U_{hs,up}^{WT}$ and $U_{hs,down}^{WT}$, and U_{vs}^{WT} as well, are similar to Eqns. (4.71), (4.74), and (4.73), respectively (Section 4.4.4), except using U_{insu}^{WT} (the thermal transmittance of insulation attached to the water storage tank) instead of using U_{insu}^{IT}. The thermal transmittance of horizontal surface of the water storage tank is calculated in a piecewise function with respect to the relation between the bottom and top nodes temperatures and the indoor air temperature as:

$$U_{hs}^{WT} = \begin{cases} U_{hs,up}^{WT}, & T_w^{N1} < T_{ia} \ or \ T_w^{N5} > T_{ia} \\ 0, & T_w^{N1} = T_{ia} \ or \ T_w^{N5} = T_{ia} \\ U_{hs,down}^{WT}, & T_w^{N1} > T_{ia} \ or \ T_w^{N5} < T_{ia} \end{cases}. \quad (4.147)$$

For a cylinder storage tank, the vertical surface area of the water-node Ni is calculated as:

$$A_{vs}^{Ni} = \pi D^{\mathrm{WT}} L_{Ni}^{WT}. \quad (4.148)$$

The thermal transmittance U_{insu}^{WT} is the input parameter. In the case study, U_{insu}^{WT}= 0.286 W/(m^2·°C).

4.5.5. Domestic hot water makeup

Due to the discharge of hot water, heat output rate from the water storage tank is calculated as:

$$\dot{Q}^{WTL2} = \dot{m}_w^{DHW}\left(c_{p_w}^{N5} T_w^{N5} - c_{p_w}^{Mains} T_w^{Mains}\right), \tag{4.149}$$

where,

$$\dot{m}_w^{DHW} = \rho_w^{Main} \dot{V}_w^{DHW}. \tag{4.150}$$

$\dot{Q}^{WTL2}$ is the heat output rate of the water storage tank onto heating water for the domestic draw-off; $\dot{V}_w^{DHW}$ is the volume flow rate of the domestic hot water draw-off.

The temperature T_w^{Main} is the input variable. For instance, the case study used the correlated data by Hugo (2008) based on the measured temperature of the city main of Montreal by Dumas & Marcoux (2004),

$$\begin{aligned} T_w^{Main} = e + f_1\cos(\omega N) + g_1\sin(\omega N) + f_2\cos(2\omega N) + g_2\sin(2\omega N) + \cdots \\ + f_{17}\cos(17\omega N) + g_{17}\sin(17\omega N), \end{aligned} \tag{4.151}$$

where, ω, e, f_i, g_i (i= 1, 2 … 7) are the coefficients cited in Table 4.6.

The flow rate $\dot{V}_w^{DHW}$ is the input variable. The case study used data by Ulrike Jordan & Vajen (2001) with average daily domestic hot water consumption of 266 L (Aguilar et al. 2005); The published consumption rate in one-minute time scale was transformed to 15 min time scale.

Eqn. (4.123) calculates the heat transfer rate due to the hot water draw-off. The formulation implies a premise that the mass of the jet flow is not greater than the mass of the water-node. The studied case satisfied the premise, that is,

$$\dot{m}_w^{DHW}\Delta t \leq m_w^N, \tag{4.152}$$

where, Δt is the time step, Δt= 900 s.

Table 4.6 Coefficients of city main temperature of case study

		Units			Units
ω	0.0086904	dimensionless	e	11.490452	℃
f_1	0.1839946	℃	g_1	0.0905672	℃
f_2	-6.7763674	℃	g_2	-7.3992997	℃
f_3	-0.0965715	℃	g_3	-0.2033946	℃
f_4	0.0843686	℃	g_4	0.8829336	℃
f_5	-0.0031887	℃	g_5	-0.0370572	℃
f_6	-0.0969744	℃	g_6	0.1161188	℃
f_7	0.0140706	℃	g_7	-0.0229117	℃
f_8	-0.3362503	℃	g_8	-0.0142773	℃
f_9	-0.0277629	℃	g_9	-0.0179754	℃
f_{10}	-0.0362475	℃	g_{10}	-0.1390454	℃
f_{11}	-0.0136723	℃	g_{11}	-0.0541225	℃
f_{12}	-0.0187207	℃	g_{12}	0.1353561	℃
f_{13}	-0.0066015	℃	g_{13}	-0.0206411	℃
f_{14}	-0.0893228	℃	g_{14}	0.0843321	℃
f_{15}	-0.0449833	℃	g_{15}	-0.0122686	℃
f_{16}	0.1727085	℃	g_{16}	0.0686489	℃
f_{17}	0.0242816	℃	g_{17}	0.0008067	℃

4.5.6. Temperatures in water storage tank

The water-node temperature is calculated by solving the energy balance formulated for the water storage tank. Employing backward Euler method to discretize the Eqn. (4.119), we obtain:

$$\dot{Q}_{sto}^{Ni} = \frac{\left(m_w^N c_{p_w}^{Ni}\right)_{t_{j-1}} \left(T_w^{Ni}{}_{t_j} - T_w^{Ni}{}_{t_{j-1}}\right)}{\Delta t}. \quad (4.153)$$

By rearranging we have:

$$T_w^N{}_{t_j} = T_w^N{}_{t_{j-1}} + \frac{\dot{Q}_{sto}^{Ni} \Delta t}{\left(m_w^N c_{p_w}^{Ni}\right)_{t_{j-1}}}. \quad (4.154)$$

4.5.7. Electric power of heater

The electric power of the heater is calculated as:

$$\dot{W}^{Aux} = \dot{m}_w^{DHW} \left(C_{p_{w,set}}^{Aux} T_{w,set}^{Aux} - C_{p_w}^{N5} T_w^{N5}\right), \quad (4.155)$$

where, $\dot{W}^{Aux}$ is the electric power of the auxiliary heater; $T_{w,set}^{Aux}$ is the set point temperature of domestic hot water.

The set temperature T_{set}^{Aux} is the input parameter. For instance, the studied case set T_{set}^{Aux}= 40.5 ℃ (California Energy Commission 2005).

4.5.8. Heat transfer with heat source and heat sink

The heat transfer rates of the water storage tank with the heat sources and heat sink are the input of the water storage tank model. Determined by the operating conditions of the devices connected to the immersion heat exchangers, the heat transfer rates are as below.

For the immersion heat exchanger $HX1$, the heat transfer rate in the heat charging mode is corresponded to the heat transfer from the heat pump as:

$$\dot{Q}^{WTS1} = \dot{Q}^{HP4WT}. \tag{4.156}$$

In the heat discharging mode, the entering condition of the heat transfer water is taken as the leaving condition from the radiant floor,

$$T_{in,w}^{WTL1} = T_{out,w}^{RF}, \tag{4.157}$$

where, $T_{out,w}^{RF}$ is the temperature of water leaving the radiant floor. The heat discharging rate is corresponded to the heat transfer to the radiant floor as:

$$\dot{Q}^{WTL1} = \dot{Q}^{WT4RF}, \tag{4.158}$$

where,

$$\dot{Q}^{WT4RF} = \dot{Q}_{demd}^{RF}. \tag{4.159}$$

$\dot{Q}^{WT4RF}$ is the heat transfer rate from the water storage tank to the radiant floor; $\dot{Q}_{demd}^{RF}$ is the heat transfer rate demanded by the indoor space onto the radiant floor.

For the immersion heat exchanger $HX2$, the heat charging rate is corresponded to the heat transfer from the solar thermal collector as:

$$\dot{Q}^{WTS2} = \dot{Q}^{Coll4WT}. \tag{4.160}$$

4.5.9. Heating load of water storage tank

The heating load of water storage tank has two components: the heat discharging of heat exchanger $HX1$ and the domestic hot water makeup. Therefore, the heat output rate of water storage tank, $\dot{Q}^{WTL}$, is calculated as:

$$\dot{Q}^{WTL} = \dot{Q}^{WTL1} + \dot{Q}^{WTL2}. \tag{4.161}$$

4.5.10. Exergy analysis of water storage tank

This section presents the exergy analysis of the water storage tank operation by regarding the water storage tank as a thermodynamic open system. The exergy balance equation is established considering the flow of water, the heat transfer between the storage tank and surroundings, the inter-nodal heat transfer between adjacent water-nodes, and the exergy destroyed during the operation.

Exergy transfer with heat source and heat sink

The net exergy transfer rate from the water storage tank heat sources, $\dot{X}^{WTS}$, is calculated as:

$$\dot{X}^{WTS} = \dot{X}^{WTS1} + \dot{X}^{WTS2} \tag{4.162}$$

where, $\dot{X}^{WTS1}$ is the net exergy transfer rate of the immersion heat exchanger $HX1$; $\dot{X}^{WTS2}$ is the net exergy input rate of the immersion heat exchanger $HX2$; both are the input of the water storage tank model. When the water storage tank receives exergy from the heat pump,

$$\dot{X}^{WTS1} = \dot{X}^{HP4WT}; \tag{4.163}$$

When water storage tank receives exergy from the solar thermal collector,

$$\dot{X}^{WTS2} = \dot{X}^{Coll4WT}. \tag{4.164}$$

The exergy transfer rate $\dot{X}^{HP4WT}$ is calculated with:

$$\dot{X}^{HP4WT} = \dot{X}^{Cond} - \dot{X}^{HP4RF}. \tag{4.165}$$

The net exergy transfer rate to the water storage tank heat sink, $\dot{X}^{WTL1}$, is the input of the water storage tank model. When the water storage tank output exergy to the radiant floor,

$$\dot{X}^{WTL1} = \dot{X}^{WT4RF}. \tag{4.166}$$

where, $\dot{X}^{WT4RF}$ is the exergy transfer rate from the water storage tank to the radiant floor.

Exergy transfer with surroundings

The exergy transfer between the water storage tank and the surroundings, $\dot{X}_{ext}^{WT}$, is calculated as:

$$\dot{X}_{ext}^{WT} = \sum_{i=1}^{5} \dot{X}_{ext}^{Ni}, \tag{4.167}$$

where,

$$\dot{X}_{ext}^{Ni} = \dot{Q}_{ext}^{Ni} |\tau_{ia}|, \tag{4.168}$$

$\dot{X}_{ext}^{Ni}$ is the exergy transfer rate of the water-node Ni with the indoor surroundings.

Exergy destroyed by inter-nodal heat transfer

Due to the temperature difference among the adjacent nodes, the inter-nodal exergy destruction rate of the water storage tank, $\dot{X}_{int,dest}^{WT}$, is calculated as:

$$\dot{X}_{int,dest}^{WT} = \sum_{i=1}^{4} \left| \dot{Q}_{int,Ni+1}^{Ni} \left(|\tau^{Ni}| - |\tau^{Ni+1}| \right) \right| \tag{4.169}$$

where,

$$\dot{Q}_{int,Ni+1}^{Ni} = \frac{k^{WTi+1}}{L^{WTi+1}}\left(A_b^{WT} + A_{cs,shell}^{WT}\right)\left(T_w^{Ni+1} - T_w^{Ni}\right), \tag{4.170}$$

$$\tau^{Ni} = 1 - \frac{TK_0}{TK_w^{Ni}}, \tag{4.171}$$

$$\tau^{Ni+1} = 1 - \frac{TK_0}{TK_w^{Ni+1}}, \tag{4.172}$$

$\dot{Q}_{int,Ni+1}^{Ni}$ is the heat transfer rate of the water-node Ni with the node Ni+1, τ^{Ni} is the quality factor of conduction-convection with respect to the water-node Ni absolute temperature TK_w^{Ni}.

Change of exergy during heat storage process in water storage tank

The exergy variation rate within the ice storage tank, $\Delta\dot{X}^{WT}$, is calculated as the sum of that of the water-nodes,

$$\Delta\dot{X}^{WT} = \sum_{i=1}^{5} \frac{m_w^N\left(\psi_{w\ t_j}^{Ni} - \psi_{w\ t_{j-1}}^{Ni}\right)}{\Delta t}, \tag{4.173}$$

where, $\psi_{w\ t_j}^{Ni}$ is the specific exergy of water in the water-node Ni.

Exergy destruction and exergetic efficiency

The exergy destruction rate by the water storage tank operation, $\dot{X}_{dest}^{WT}$, is obtained from the established exergy balance:

$$\dot{X}_{dest}^{WT} = \dot{X}^{WTS} - \dot{X}^{WTL} + \dot{X}_{ext}^{WT} + \dot{X}_{int,dest}^{WT} - \Delta\dot{X}^{WT}. \tag{4.174}$$

The exergetic efficiency of the ice storage tank operation, η_{II}^{WT}, is calculated as:

$$\eta_{II}^{WT} = 1 - \frac{\sum_0^{t_j} X_{dest}^{WT}}{\sum_0^{t_j} X^{WTS}}, \tag{4.175}$$

The calculations for $\sum_0^{t_j} X_{dest}^{WT}$, and $\sum_0^{t_j} X^{WTS}$ are similar to the Eqns. (4.116) and (4.117), respectively.

Exergy output for heating

The exergy output rate of the water storage tank onto heating, $\dot{X}^{WTL}$, is calculated as:

$$\dot{X}^{WTL} = \dot{X}^{WTL1} + \dot{X}^{WTL2}, \tag{4.176}$$

where,

$$\dot{X}^{WTL2} = \dot{m}_w^{DHW}\left(\psi_w^{DHW} - \psi_w^{Mains}\right), \tag{4.177}$$

$\dot{X}^{WTL1}$ is the exergy output rate of the immersion heat exchanger $HX1$; $\dot{X}^{WTL2}$ is the exergy output rate for domestic hot water makeup; ψ_w^{DHW} is the specific exergy of water with respect to the temperature of the domestic hot water drawn-off; ψ_w^{Mains} is the specific exergy of water with respect to the temperature of the city main.

4.6. Mathematical model of radiant floor

The radiant floor (Fig. 4.7) takes heat from the heat source to emit to the residential space, which is the heat sink of the radiant floor. The mathematical model simulates the radiant floor operation to calculate the radiant floor heat supply to the residential space.

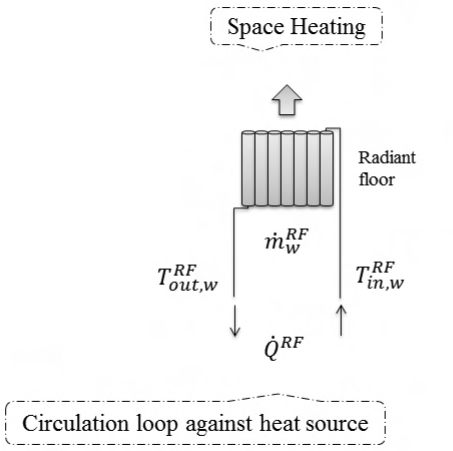

Fig. 4.7 Schematic of radiant floor model

4.6.1. Heat transfer flow

The mass flow rate of water through the radiant floor, $\dot{m}_w^{RF}$, is calculated as:

$$\dot{m}_w^{RF} = \frac{\dot{Q}^{RF}}{C_{p_{in,w}}^{RF} T_{in,w}^{RF} - C_{p_{out,w}}^{RF} T_{out,w}^{RF}}, \tag{4.178}$$

where, $\dot{Q}^{RF}$ is the heat input rate to the radiant floor; $T_{in,w}^{RF}$ is the temperature of water entering the radiant floor; $T_{out,w}^{RF}$ is the temperature of water leaving the radiant floor.

According to ASHRAE (2004), the minimum floor surface temperature is 19 ℃. The temperature of water leaving the radiant floor is set at 20 ℃.

4.6.2. Supply conditions

The supply conditions are the inputs of the radiant floor model, determined by the leaving conditions of the devices connected. The heat transfer rate from the radiant floor heat source is as:

$$\dot{Q}^{RF} = \begin{cases} \dot{Q}^{WT4RF}, & when\ water\ storage\ tank\ supplies \\ \dot{Q}^{HP4RF}, & when\ \ heat\ pump\ supplies \end{cases}. \quad (4.179)$$

The temperature of water entering the radiant floor is as:

$$T_{in,w}^{RF} = \begin{cases} T_{out,w}^{WTL1}, & when\ water\ storage\ tank\ supplies \\ T_{out,w}^{Cond}, & when\ \ heat\ pump\ supplies \end{cases}. \quad (4.180)$$

4.6.3. Exergy analysis of radiant floor

This section presents the exergy analysis of the radiant floor operation by regarding the radiant floor as a thermodynamic open system. The exergy balance equation is established considering the flow of water, the heat transfer between the radiant floor and indoor space, and the exergy destroyed during the operation.

Exergy of water flow through radiant floor

The exergy transfer rate by water flow through the radiant floor, $\dot{X}^{RFS}$, is calculated as:

$$\dot{X}^{RFS} = \dot{m}_w^{RF}\left(\psi_{in,w}^{RF} - \psi_{out,w}^{RF}\right), \quad (4.181)$$

where, $\psi_{in,w}^{RF}$ is the specific exergy of water entering the radiant floor; $\psi_{out,w}^{RF}$ is the specific exergy of water leaving the radiant floor.

The exergy transfer rate $\dot{X}^{RFS}$ is noted as $\dot{X}^{HP4RF}$ for the heat pump as the heat source, and $\dot{X}^{WT4RF}$ for the water storage tank supplying the radiant floor.

Exergy flow into indoor space

The exergy output rate of the radiant floor, $\dot{X}^{RFL}$, is calculated as:

$$\dot{X}^{RFL} = \dot{Q}^{RF}\left|\tau_{ia}\right|. \tag{4.182}$$

Destroyed exergy and exergetic efficiency

The exergy destruction rate by the radiant floor operation, $\dot{X}_{dest}^{RF}$, is obtained from the exergy balance equation:

$$\dot{X}_{dest}^{RF} = \dot{X}^{RFS} - \dot{X}^{RFL}, \tag{4.183}$$

The exergetic efficiency of the radiant floor operation, η_{II}^{RF}, is calculated as:

$$\eta_{II}^{RF} = 1 - \frac{\dot{X}_{dest}^{RF}}{\dot{X}^{RFS}}. \tag{4.184}$$

4.7. Mathematical model of circulating pump

The circulating pump (Fig. 4.8) drives water flow along the circulation loop. The mathematical model simulates the circulating pump operation to calculate the electric power input.

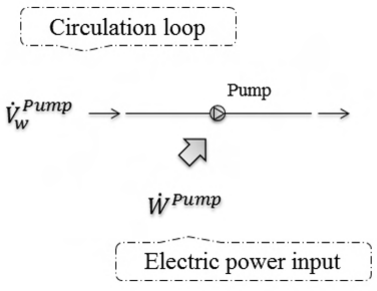

Fig. 4.8 Schematic of circulating pump model

4.7.1. Electric power

The pump performance is calculated using polynomial model (ASHRAE 2009a). Electric power input is calculated using a regression model with the following formulation:

$$\dot{W}^{Pump} = \Big(c_0 + c_1\dot{V}_w^{Pump} + c_2\dot{V}_w^{Pump^2} + c_3\dot{V}_w^{Pump^3} + c_4\dot{V}_w^{Pump^4} + c_5\dot{V}_w^{Pump^5} + c_6\dot{V}_w^{Pump^6} + c_7\dot{V}_w^{Pump^7} + c_8\dot{V}_w^{Pump^8}\Big) F^{Pump}, \quad (4.185)$$

where, $\dot{W}^{Pump}$ is the electric power input to the circulating pump; c_0 … c_8 are the coefficients; $\dot{V}_w^{Pump}$ is the volume flow rate of water through the circulating pump; F^{Pump} is the flow fraction,

$$F^{Pump} = \frac{\dot{V}_w^{Pump}}{\dot{V}_{max}^{Pump}}, \quad (4.186)$$

and $\dot{V}_{max}^{Pump}$ is the maximum volume flow rate of water through the circulating pump.

The coefficients c_0 … c_8 and the quantity $\dot{V}_{max}^{Pump}$ are given for a specific pump by the user extracted from the manufacture catalogue. Fig. 4.9 shows the coefficients and the performance curve of the pump, Wilo-Star 16F (Wilo 2012), used in the case study. Eqn. (4.187) is the specific formulation prepared to model the case pump, used onto all pumps of the solar combisystem. Regarding the flow fraction, a minimum is required for the sake of avoiding low flow damage, such as, temperature rise, radial bearing loads, axial thrust, etc. Recommended minimum flow rate ranges from 10% to 80% of the flow at best efficiency point; however, the same type of pump may have the

recommendation in a range for a given application (Volk 2005). The case study set the minimum as F_{min}^{Pump}= 0.1.

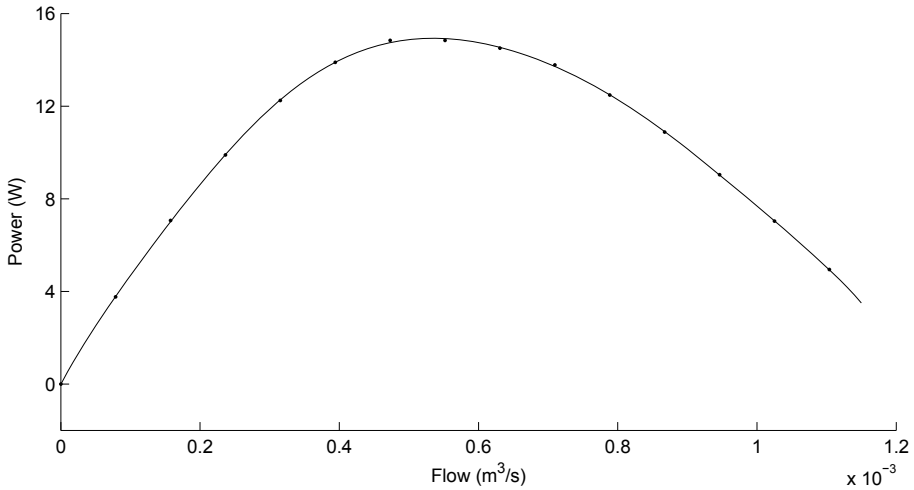

c_0, W	c_1, W·s/m^3	c_2, W·s^2/m^6	c_3, W·s^3/m^9	c_4, W·s^4/m^{12}	c_5, W·s^5/m^{15}	c_6, W·s^6/m^{18}	c_7, W·s^7/m^{21}	c_8, W·s^8/m^{24}
14.918	-0.55325	-5.423	1.9018	-0.76084	-0.76548	0.74376	0.1408	-0.15351

Fig. 4.9 Performance curve of case pump

$$\dot{W}^{Pump} = \Big(14.918 - 0.55325\,\dot{V}_w^{Pump} - 5.423\,\dot{V}_w^{Pump^2} + 1.9018\,\dot{V}_w^{Pump^3} - 0.76084\,\dot{V}_w^{Pump^4} - 0.76548\,\dot{V}_w^{Pump^5} + 0.74376\,\dot{V}_w^{Pump^6} + 0.1408\,\dot{V}_w^{Pump^7} + 0.15351\,\dot{V}_w^{Pump^8}\Big)\frac{\dot{V}_w^{Pump}}{0.001041}. \quad (4.187)$$

The flow rate $\dot{V}_w^{Pump}$ is noted by $\dot{V}_w^{Pump1}$, $\dot{V}_w^{Pump2}$ and $\dot{V}_w^{Pump3}$ for the pump $P1$, $P2$, and $P3$ connected to the circulation loop $L1$, $L2$, and $L3$, respectively. Also, the power input $\dot{W}^{Pump}$ is noted by $\dot{W}_w^{Pump1}$, $\dot{W}_w^{Pump2}$ and $\dot{W}_w^{Pump3}$. For the solar combisystem, the overall electric power input of the circulating pumps is calculated as:

$$\dot{W}_{supp}^{Pump} = \dot{W}^{Pump1} + \dot{W}^{Pump2} + \dot{W}^{Pump3}. \quad (4.188)$$

4.7.2. Flow rates

The volume flow rate is the input of the circulating pump model, determined by the operation of the circulation loop connected. On the circulation loop $L1$, the flow rate is that through the solar thermal collector,

$$\dot{V}_w^{Pump1} = \dot{V}_w^{Coll}. \tag{4.189}$$

On the circulation loop $L2$, the flow rate is that through the heat pump evaporator,

$$\dot{V}_w^{Pump2} = \dot{V}_w^{Evap}. \tag{4.190}$$

On the circulation loop $L2$, the flow rate is that through the heat pump condenser,

$$\dot{V}_w^{Pump3} = \dot{V}_w^{Cond}. \tag{4.191}$$

4.7.3. Exergy analysis of circulating pump

For the operation of circulating pump $P1$, $P2$, and $P3$, the exergy destruction rate, denoted by $\dot{X}_{dest}^{Pump1}$, $\dot{X}_{dest}^{Pump2}$, and $\dot{X}_{dest}^{Pump3}$, are calculated as the following:

$$\dot{X}_{dest}^{Pump1} = \dot{W}^{Pump1}. \tag{4.192}$$

$$\dot{X}_{dest}^{Pump2} = \dot{W}^{Pump2}. \tag{4.193}$$

$$\dot{X}_{dest}^{Pump3} = \dot{W}^{Pump}. \tag{4.194}$$

For the solar combisystem, the overall exergy destruction of circulating pump operations, $\dot{W}_{dest}^{Pump}$, is calculated as:

$$\dot{W}_{dest}^{Pump} = \dot{W}_{supp}^{Pump}. \tag{4.195}$$

4.8. Mathematical model of system

The mathematical model of system is developed by coupling all the mathematical models of the component devices. For the whole combisystem, the thermodynamic system boundary was drawn around the combisystem physical parts (II in Fig. 4.10) to isolate the combisystem from the outer and indoor environment, which are the thermodynamic system surroundings.

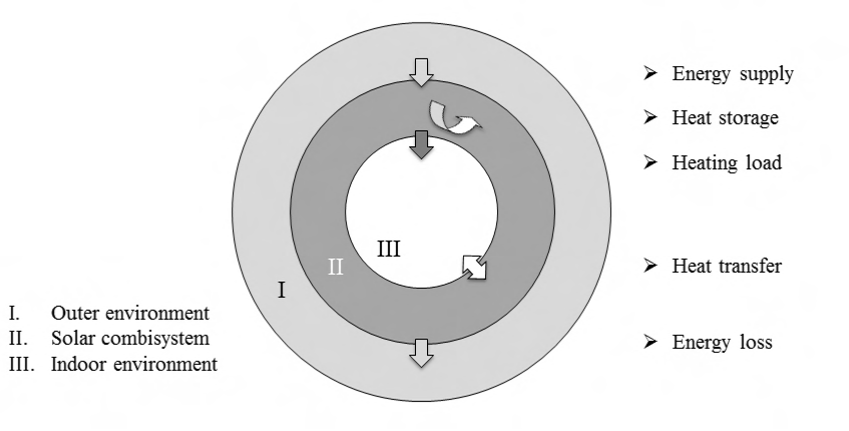

Fig. 4.10 Thermodynamic system boundary of solar combisystem

4.8.1. Heating load

The combisystem heat output rate for heating, $\dot{Q}_{load}^{Sys}$, includes that for the preparation of domestic hot water and that for space heating,

$$\dot{Q}_{load}^{Sys} = \dot{Q}^{WTL2} + \dot{Q}^{RF}. \tag{4.196}$$

4.8.2. Energy supply and loss

The energy supply rate of the combisystem, $\dot{E}_{supp}^{Sys}$, is calculated as:

$$\dot{E}_{supp}^{Sys} = \dot{E}_{sol}^{Sys} + \dot{W}_{ele}^{Sys}, \tag{4.197}$$

where, $\dot{E}_{sol}^{Sys}$ is the solar energy supply rate to the combisystem,

$$\dot{E}_{sol}^{Sys} = \dot{Q}_{sol}^{Coll}; \tag{4.198}$$

$\dot{W}_{ele}^{Sys}$is the electric power input rate to the combisystem,

$$\dot{W}_{ele}^{Sys} = \dot{W}^{Aux} + \dot{W}^{HP} + \dot{W}_{supp}^{Pump}. \tag{4.199}$$

The energy loss rate of the combisystem, $\dot{E}_{loss}^{Sys}$, is the energy loss rate at the solar thermal collector,

$$\dot{E}_{loss}^{Sys} = \dot{E}_{loss}^{Coll}. \tag{4.200}$$

4.8.3. Heat transfer with environment

The heat transfer rate of the combisystem with the environment, $\dot{Q}_{ext}^{Sys}$, includes that of the ice storage tank and that of the water storage tank,

$$\dot{Q}_{ext}^{Sys} = \dot{Q}_{ext}^{IT} + \dot{Q}_{ext}^{WT}. \tag{4.201}$$

4.8.4. Heat storage

The energy change rate of the combisystem, $\dot{Q}_{sto}^{Sys}$, includes that in the ice storage tank and that in the water storage tank,

$$\dot{Q}_{sto}^{Sys} = \dot{Q}_{sto}^{IT} + \dot{Q}_{sto}^{WT}. \tag{4.202}$$

4.8.5. System performance

The performance of the solar combisystem is examined over the whole simulation period using indicators: (i) the Coefficient of Performance, (ii) the solar energy contribution, and (iii) the solar energy fraction.

System COP

The combisystem COP is calculated as the overall combisystem heating load, $\sum_{t=0}^{t} Q_{load}^{Sys}$, divided by the overall combisystem electricity consumption, $\sum_{t=0}^{t} W_{ele}^{Sys}$, as:

$$COP = \frac{\sum_{t=0}^{t} Q_{load}^{Sys}}{\sum_{t=0}^{t} W_{ele}^{Sys}}. \quad (4.203)$$

where,

$$Q_{load}^{Sys} = \dot{Q}_{load}^{Sys} \Delta t, \quad (4.204)$$

$$W_{ele}^{Sys} = \dot{W}_{ele}^{Sys} \Delta t. \quad (4.205)$$

Solar energy contribution

The solar energy contribution of the combisystem, SC_E , is calculated as the overall solar energy supplied to the combisystem, $\sum_{t=0}^{t} E_{sol}^{Sys}$, divided by the overall energy supplied to the combisystem, $\sum_{t=0}^{t} E_{supp}^{Sys}$, as:

$$SC_E = \frac{\sum_{t=0}^{t} E_{sol}^{Sys}}{\sum_{t=0}^{t} E_{supp}^{Sys}}, \quad (4.206)$$

where,

$$E_{sol}^{Sys} = \dot{E}_{sol}^{Sys} \Delta t, \quad (4.207)$$

$$E_{supp}^{Sys} = \dot{E}_{supp}^{Sys} \Delta t. \quad (4.208)$$

Solar energy fraction

Solar energy fraction evaluates the contribution of solar devices of a solar system. The evaluation of the solar energy fraction requires the comparison with a reference system that does not include any solar device but meets the same heating needs as the solar system does. In this study, an all electrical heating system is used as the reference system.

The solar energy fraction of the combisystem, SF_E, is calculated as the overall solar energy supplied by the solar thermal collector, $\sum_{t=0}^{t} Q^{Coll}$, to the energy used by the reference system, $\sum_{t=0}^{t} E_{supp}^{refSys}$, as:

$$SF_E = \frac{\sum_{t=0}^{t} Q^{Coll}}{\sum_{t=0}^{t} E_{supp}^{refSys}}, \quad (4.209)$$

where,

$$Q^{Coll} = \dot{Q}^{Coll} \Delta t, \quad (4.210)$$

$$E_{supp}^{refSys} = \dot{E}_{supp}^{refSys} \Delta t. \quad (4.211)$$

4.9. Mathematical model of control system

The mathematical model simulates the operation controls of the valves, circulating pumps, and auxiliary heater. The control system simulation is accomplished by customizing the controlled variables, set points, and organizing the control logic.

4.9.1. Controlled variables

The control system sends out operation instructions by control signals. In the control system modeling, the control signals are simulated using controlled variables. Controlled variables are customized for the combisystem to control the flows of heat transfer fluids, to operate the auxiliary heater. The developed mathematical models of combisystem devices are integrated with the controlled variables, particularly into those model sections that are related to the heat transfer fluid flows and the electric power of the auxiliary heater. Table 4.7 shows the controlled variables with respect to the devices being controlled (see Fig. 4.1).

Table 4.7 Controlled variables of devices

Devices	Controlled variables
Circulating pump $P1$	θ^{Coll}
Circulating pump $P2$	θ^{HP}
Circulating pump $P3$	$\theta^{HP}, \theta^{WT4RF}$
Three-way valve $V1$, L-type	$\theta^{Coll4WT}, \theta^{Coll4IT}$
Three-way valve $V2$, T-type	$\theta^{HP4WT}, \theta^{HP4RF}, \theta^{WT4RF}$
Bypass valve $V3$	$\theta^{HP}, \theta^{WT4RF}$
Auxiliary heater	θ^{Aux}

I. The circulation loop $L1$

The solar thermal collector and the two storage tanks are linked by the circulation loop $L1$, which has the circulating pump $P1$ and the valve $V1$. When the circulation loop is on operation, heat is transferred from the solar thermal collector to the storage tanks. The valve $V1$ is simulated as a three-way valve of L-type, so that one

of the storage tanks, either the water storage tank or the ice storage tank, can receive the heat transferred.

The controlled variable $\boldsymbol{\theta^{Coll}}$ is defined for the control of circulating pump $P1$: θ^{Coll}= 1 for turning on the pump, θ^{Coll}= 0 for turning off. The controlled variable $\boldsymbol{\theta^{Coll4WT}}$ is defined for the control of valve $V1$ to connect the solar thermal collector with the water storage tank, $\theta^{Coll4WT}$= 1 for opened connection, $\theta^{Coll4WT}$= 0 for closed. The controlled variable $\boldsymbol{\theta^{Coll4IT}}$ is defined for the control of valve $V1$ to connect the solar thermal collector with the ice storage tank: $\theta^{Coll4IT}$= 1 for opened connection, $\theta^{Coll4IT}$= 0 for closed.

With the controlled variables defined, Eqn. (4.5) is modified as:

$$T_{in,w}^{Coll}{}_{t} = \begin{cases} T_{w}^{N1}{}_{t-\Delta t'} & \theta^{Coll4WT} = 1 \\ T_{w}^{W}{}_{t-\Delta t'} & \theta^{Coll4IT} = 1 \end{cases}. \tag{4.212}$$

II. The circulation loops $L2$ and $L3$

The operation of the circulation loop $L2$ is related to the operation of the circulation loop $L3$, due to both are connected to the heat pump. The controlled variable $\boldsymbol{\theta^{HP}}$ is defined for the control of heat pump: θ^{HP}= 1 for turning up, θ^{HP}= 0 for shutting down. The circulating pumps $P2$ and $P3$ are operated together with the heat pump, and therefore both are controlled by the controlled variable θ^{HP}.

The heat pump, the water storage tank, and the radiant floor are linked up by the circulation loop $L3$, which has the circulating pump $P3$, and the valve $V2$. The valve

$V2$ is simulated as a three-way valve of T-type. The circulation loop $L3$ has one bypass for the switch of heat sources. By controlling the bypass valve $V3$, either the heat pump or the water storage tank is switched to be the heat source of the circulation loop $L3$. The operation is a sole source situation: When the circulation loop $L3$ is on operation with the heat pump as the heat source, heat is transferred from the heat pump to either the water storage tank, or the radiant floor, or both. When the circulation loop is on operation with the water storage tank as the heat source, heat is transferred from the water storage tank to the radiant floor. The operation of circulation loop $L3$ synchronized the operation of the circulating pump $P3$.

The controlled variables $\boldsymbol{\theta^{HP4WT}}$, $\boldsymbol{\theta^{HP4RF}}$, and $\boldsymbol{\theta^{WT4RF}}$ are defined for the specified device connections along the circulation loop $L3$, either one of controlled variables influences the operations of valve $V2$ and valve $V3$ at the same time. The controlled variable $\boldsymbol{\theta^{HP4WT}}$ is defined for the connection between the heat pump and the water storage tank: θ^{HP4WT}= 1 for opened connection, θ^{HP4WT}= 0 for closed. The controlled variable $\boldsymbol{\theta^{HP4RF}}$ is defined for the connection between the heat pump and radiant floor: θ^{HP4RF}= 1 for opened connection, θ^{HP4RF}= 0 for closed. The controlled variable $\boldsymbol{\theta^{WT4RF}}$ is defined for the connection between the water storage tank and radiant floor, θ^{WT4RF}= 1 for opened connection, θ^{WT4RF}= 0 for closed.

The controlled variables θ^{HP} and θ^{WT4RF} never both equal to 1 at the same time, because the heat pump does not work simultaneously with the hot water storage tank

to heat the radiant floor. For the controlled variables θ^{HP4RF} and θ^{HP4WT}, if one or both equal to 1, then θ^{HP}= 1.

With the controlled variables defined, Eqns. (4.23) and (4.24) is modified as:

$$TK_{in,w}^{Evap}{}_{t} = 273.15 + T_{w}^{W}{}_{t-\Delta t}, \tag{4.213}$$

and

$$TK_{in,w}^{Cond}{}_{t} = \begin{cases} 273.15 + T_{out,w}^{RF}, & \theta^{HP4WT} = 0 \; and \; \theta^{HP4RF} = 1 \\ 273.15 + T_{w}^{N1}{}_{t-\Delta t}, & \theta^{HP4WT} = 1 \; and \; \theta^{HP4RF} = 0 \\ 273.15 + \dfrac{\dot{m}_{w}^{RF} T_{out,w}^{RF} + \left(\dot{m}_{w}^{Cond} - \dot{m}_{w}^{RF}\right) T_{w}^{N1}{}_{t-\Delta t}}{\dot{m}_{w}^{Cond}}, & \theta^{HP4WT} = 1 \; and \; \theta^{HP4RF} = 1 \end{cases}. \tag{4.214}$$

III. The heater

The controlled variable $\boldsymbol{\theta^{Aux}}$ is defined for the control of the auxiliary heater: θ^{Aux}= 1 for turning on, θ^{Aux}= 0 for turning off.

4.9.2. Set points

The set point is the constant assigned to a setting variable for specifing the designed/expected operation state represented by the variable. Any departure of the current operation state from the expected state would make the control system to send new control instruction for adjustment. The control settings are presented in Table 4.8, where, the set points are given by quantities so for the user to assign values.

Table 4.8 Settings of solar combisystem component models

Devices	Setting variables	Set points
Radiant floor	$T_{in,w}^{RF}$	T_{com}^{RF}
Ice storage tank	γ, T_w^W	γ_{max}, T_{max}^W
Water storage tank	$T_w^{N1}, T_w^{N3}, T_w^{N5}$	$T_{set}^{WT}, T_{var}^{WT}, T_{max}^{WT}$

I. The radiant floor

The supply temperature to the radiant floor is limited to a lower bound. The setting is

$$T_{in,w}^{RF} \geq T_{com}^{RF}, \tag{4.215}$$

where, T_{com}^{RF} is the comfort temperature of radiant floor. In the study, the value was T_{com}^{RF}= 25 ℃. The setting was referred to the optimal temperature for sedentary in terms of thermal comfort by Olesen (1977).

II. The ice storage tank

The mass fraction of ice in the ice storage tank is limited to an upper limit. The setting is

$$\gamma \leq \gamma_{max}, \tag{4.216}$$

where, γ_{max} is the maximum mass fraction of ice in the ice storage tank. In the case study, γ_{max}= 0.7±0.01, as the maximum value of 0.7, allowing the variation of 0.01 in the simulation.

The temperature of liquid water in the ice storage tank is limited to an upper limit. The setting is

$$T_w^W \leq T_{max}^W, \tag{4.217}$$

where, T_{max}^W is the maximum temperature of the water-layer in the ice storage tank. In the case study, T_{max}^W= 37.8±1 ℃, as the maximum temperature of 37.8 ℃, allowing the variation of 1 ℃ in the simulation. The setting complied with the heat pump catalogue in terms of the operation temperatures of the heat source (GeoSmart 2012). To limit with a maximum was also regarded in favor of making use of thermal capacity of water under phase changing, since the storage tank is operated as a cold energy store.

III. The water storage tank

Temperatures in the water storage tank are subject to a maximum, denoted by T_{max}^{WT}. The basic settings are the water temperature of three nodes in the water storage tank as follows.

$$T_w^{N1} \geq T_{set}^{WT} - T_{var}^{WT}, \tag{4.218}$$

$$T_w^{N3} \geq T_{set}^{WT}, \tag{4.219}$$

$$T_{set}^{WT} \leq T_w^{N5} \leq T_{set}^{WT} + T_{var}^{WT}, \tag{4.220}$$

where, T_{set}^{WT} is the temperature set for the water storage tank; T_{var}^{WT} is the variation allowed with respect to the water storage tank setting temperature.

In the case study, T_{max}^{WT}= 60 ℃, T_{set}^{WT}= 40 ℃, and T_{var}^{WT}= 5 ℃. With the maximum limit, the operation range for the bottom, middle, and top section temperatures are 35 ℃ ≤ T_w^{N1}≤ 60 ℃, 40 ℃ ≤ T_w^{N3}≤ 60 ℃, and 40 ℃ ≤ T_w^{N5}≤ 45 ℃, respectively. For the top water-node $N5$, the upper bound is to meet the temperature requirement of domestic hot water use, the safety requirement of not exceed 50 ℃ from scald, as well as

avoiding the Legionella pneumophila to be "in the 60 ℃ range" (ASHRAE 2007). For the bottom water-node $N1$, the setting was referred to the supply temperature requirement of the radiant floor. The impact made by the low temperature of the heat source of heat pump was also taken into account. For the middle water-node $N3$, the setting was in between of the top and the bottom, the lower bound was set the same as of the top node.

4.9.3. Control logic

The control logic is modeling the decision making at the control hub of mechanical system based on setting values and the deviations of corresponding measures taken by sensors, before control actuators setting out control directives to regulate the behavior of system devices (ASHRAE 2011). Table 4.9 sorted the controlled variables for the combisystem component devices. Each of the devices is under the operation control directives delivered by the listed controlled variables.

Table 4.9 Controlled variables of solar combisystem component

Devices	Controlled variables
Solar thermal collector	θ^{Coll} ($\theta^{Coll4WT}$, $\theta^{Coll4IT}$)
Heat pump	θ^{HP} (θ^{HP4WT}, θ^{HP4RF})
Ice storage tank	$\theta^{Coll4IT}$, θ^{HP}
Water storage tank	$\theta^{Coll4WT}$, θ^{HP4WT}, θ^{WT4RF}
Radiant floor	θ^{HP4RF}, θ^{WT4RF}

Fig. 4.11 illustrates the control logic of the non-heating season operation of the combisystem. Fig. 4.12 illustrates the control logic of the heating season operation of the combisystem. The control logic direct the integral response of the solar

combisystem operation based on the conditions of: (i) the relations of the current values of setting variables and the set points, (ii) the availability of insolation, and (iii) the residential heating demands. The conditions are represented by diamond conditional boxes on the figures. To have the graphic presentations in concise, a couple of premises are not detailed: (i) $\dot{G} > 0$ for θ^{Coll}= 1, also $\theta^{Coll4WT}$= 1 or $\theta^{Coll4IT}$= 1, that is, only when insolation is available, the solar thermal collector might start on to collect solar heat. (ii) $T_w^W < T_{max}^W$ for $\theta^{Coll4IT}$= 1, that is, only when the ice storage tank water-layer temperature below its set point, the heat is possibly allowed to transfer from the solar thermal collector to the ice storage tank.

Control directives are firmed by assigning values to the controlled variables, which are enclosed in the rectangular boxes and trapezoidal boxes on the figures. The control directives are decisions made for the conditions based on *True* or *False*, denoted by *T* and *F* on the figures. These control directives would control the auxiliary heater (circled by the line in oval on the figures), manipulate the operations of circulation loop $L1$, $L2$, and $L3$ by control the operations of circulating pumps and valves. Control directives enclosed in the trapezoidal boxes are flexible situations with one decision in higher priority over the other. Flexibility is granted regarding the heat transfer from the solar thermal collector to one of the two storage tanks, when neither of the storage tanks in urge of heat charging.

The control logic is not exclusive to obtain the same series control directives. However, any change is believed very likely to yield different results. The presented control logic is used in this study.

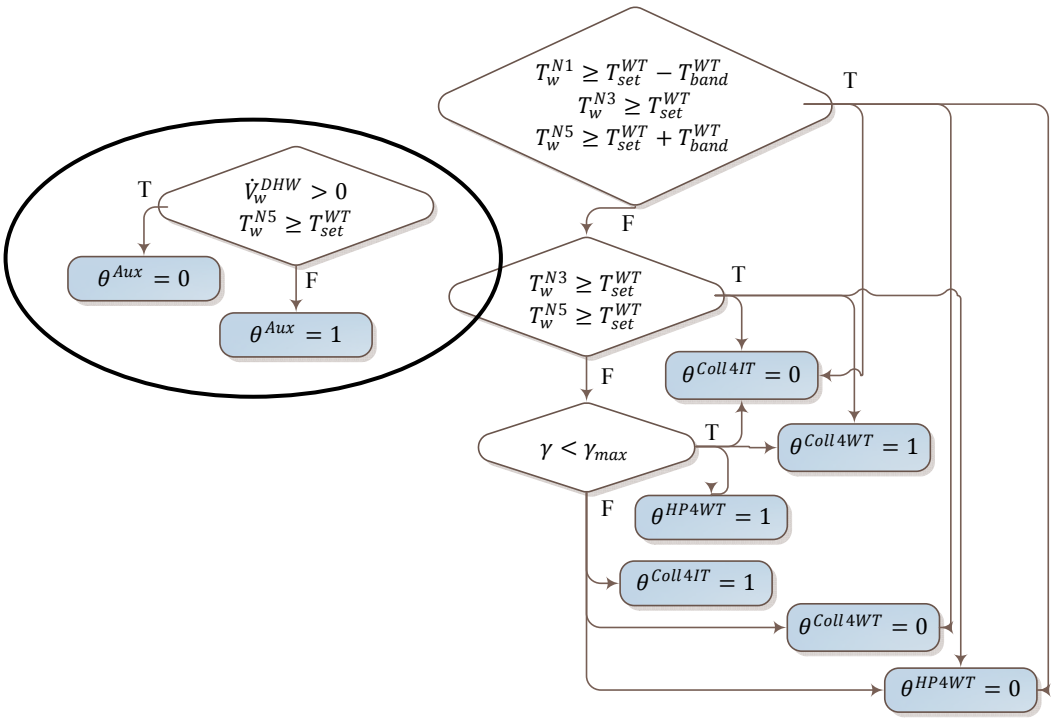

Fig. 4.11 Flowchart of operation control algorithm for non-heating season

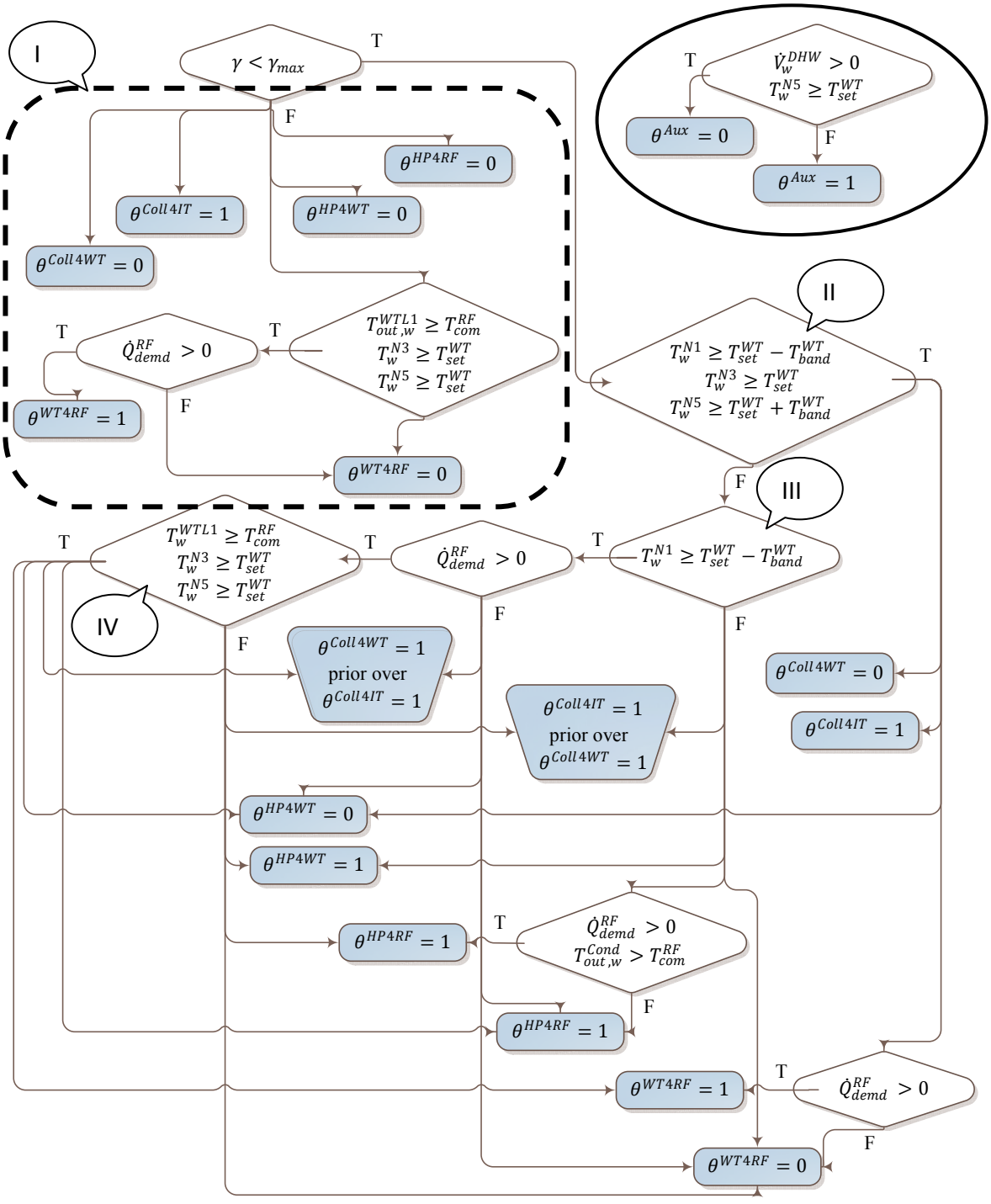

Fig. 4.12 Flowchart of operation control algorithm for heating season

The control for the non-heating season operation (Fig. 4.11) is relative simple. During then, the water storage tank takes on the heat distribution center of the combisystem. In contrast, the control for the heating season operation (Fig. 4.12) is relative complex. To ensure the residential heating demands being met, the thermal storage capacity of the ice storage tank is crucial. On Fig. 4.12, the top left part is circled by dashed outline noted with the callout I, which corresponds the situation of ice storage tank lacked of heat storage capacity, featured by $\gamma \geq \gamma_{max}$. This part of control flows indicate: If the ice storage tank is crippled, so is the heat pump, and the water storage tank becomes the sole device that can respond to the heating demands. In such situation, the combisystem is completely climate-dependent. With only water storage tank and solar thermal collector be functional, the combisystem supplies heat far from enough as being demanded.

If the ice storage tank has the capacity to store heat, the control logic would flow to the situation that has the water storage tank status being focused, noted by the callout II, III, and IV on Fig. 4.12. For the condition in callout II, the water storage tank is sufficient with heat in storage, and would supply heat if needed but not take in any. The condition in callout III represents the bottom line of water storage tank in heat reservation, for space heating. Reaching this bottom line, the heat pump is to be employed for heat input to the water storage tank. The condition in callout IV represents that the water storage tank can be used to heat the radiant floor. And at this situation, the solar thermal collector is employed as the heat source of water storage tank. The control strategy suggested in here is that, using the water storage tank to

respond the heating demands of radiant floor at the higher priority than using the heat pump. The reason is that unlike the water storage tank, the heat pump output is lack of flexibility.

On Fig. 4.12, the condition regarding heat supply to the radiant floor, as formulated by Eqn. (4.215), is distinguished into conditions of two forms:

$$T_{out,w}^{WTL1} \geq T_{com}^{RF}, \tag{4.221}$$

for the water storage tank on the supply, and

$$T_{out,w}^{Cond} \geq T_{com}^{RF}, \tag{4.222}$$

for the heat pump condenser on the supply.

4.10. Integration of mathematical models in complete computer model

The solar combisystem mathematical model is built from integrated component models, including the control system model, the system model, and the component equipment models. The component equipment models, including the solar thermal collector model, heat pump model, ice storage tank model, water storage tank model, radiant floor model, and circulating pump model, are coupling one with the other through the relations that represent the heat transfer water behaviors within the circulation loops. The integration of control system model with the coupled component equipment models is practiced by not only including the control algorithm, but also by

modifying those relations regarding circulation loops with appropriate controlled variables to represent the *controlled* heat transfer through the circulation loops.

The solar combisystem computer model is achieved by implementing the solar combisystem mathematical model onto a computer program. Where, interface was created for inputs. The solar combisystem operation can be modeled by running computer simulation with the computer model. This research used the EES program (Klein 2012) for the implementation. EES is a general purpose equation-solving program handling coupled non-linear algebraic and differential equations. The program has built-in functions calculating the thermodynamic and transport properties of substances. Such features make the program suitable for this study to use.

Reading previous values in quasi-static approach

The combisystem thermodynamic model is developed in quasi-static approach. This implies the thermodynamic process of the combisystem is regarded as steady state over each of the time interval Δt. Because of thermal storage process involved, as given by Eqns. (4.87), (4.90), and (4.154), the state of one time interval is related to the state of the previous time interval. This requires the computer model should be able to carry the previous state over to the current time for the thermal storage process to be computed.

Two variables are introduced for the purpose of continuous computation: Run as the sequencing number of simulation runs, which starts from 1 at the initiation; $Time$

for the combisystem operation time simulated, which is the input starting from 0 s at the initiation. The following relation is subjected:

$$Run = \frac{Time}{\Delta t} + 1. \tag{4.223}$$

For example, the case study has Δt= 900 s, with $Time$= 0, 900, 1800 … input, Run= 1, 2, 3 … are obtained.

Certain types of variables

A few variables are functional for the computer model to compute, presented in Table 4.10. These variables are grouped into three types by their functions. The time variables are the input variables of the combisystem model, varying at each time step. The differential variables are the variables from the differential equations of storage tank models. This type of variables needs the initial value input, the case study used: m_{ice}^{I}= 0, T_w^W= 18 ℃, and T_w^{Ni}= 18 ℃. The tracing variables are the variables being traced for the previous values. Those differential variables are belonging to this type too.

Multiple so-called Parametric Tables are created for these variables. The number of parametric tables depends on the number of simulation runs. Because each table, named, can hold a limited number of rows, one row corresponding to one simulation run. The parametric tables are jointly used with the build-in TableValue FUNCTION,

$$variable = \text{TableValue FUNCTION}(table, row, variable), \tag{4.224}$$

where, $table$ denotes the name of the parametric table; row denotes the number of the row in the parametric table; $variable$ is the name of the variable included in the parametric table. By assigning the argument row as,

$$row = Run - 1, \tag{4.225}$$

the function reads and assigns the previous value of the given variable from the specified parametric table.

Table 4.10 Variables in parametric tables of EES-based solar combisystem model

Symbols	Descriptions	Type
$\dot{G}$	Insolation on tilted panel	Time variable
T_{oa}	Outdoor air temperature	
T_w^{Main}	City main water temperature	
$\dot{V}_w^{DHW}$	Domestic hot water volume flow rate	
$\dot{Q}_{demd}^{RF}$	Space heating demand	
$Time$	Simulation time	
m_{ice}^{I}	Ice-layer mass	Differential variable
T_w^W	Water-layer temperature	Tracing variable
T_w^{Ni}	Water-node temperature	
γ	Ice mass fraction	Tracing variable
m_w^W	Water-layer mass	
$\dot{m}_w^{RF}$	Water mass flow rate of radiant floor	
θ^{HP4WT}	Controlled variable of heat pump charging water storage tank	
θ^{HP4RF}	Controlled variable of heat pump charging radiant floor	

Model parameters

The so-called Lookup Tables are created to store the model parameters input by the user. One table is used for one component equipment, plus a common one for the simulation operation (including parameters such as the time step Δt). The built-in Lookup FUNCTION is used for the program to read and assign the parameter values,

$$parameter = \text{Lookup FUNCTION}(table, row, parameter), \tag{4.226}$$

where, $table$ denotes the name of the lookup table; row denotes the number of the table row; $parameter$ is the parameter to be looked up for values.

Programming

At this stage, each of the component models needs to be broken down to parts for each part to be written as a procedure. The procedures, along with some user-written functions, become the subroutines of the combisystem computer model. The subroutines, either saved as stand-alone EES library files under particular directory or arranged within a so-called Equation Window, are to be used by the main routine of the combisystem computer model. The main routine is written in the equation window, with functions and directives compiled in sequence. Arranging the sequence is necessary for solving the unknown with the known in ready (appeared earlier). The programmed model can pre-calculate, such as the imminent capacities of component equipment. This was used by the control algorithm for adjusting the device operation. Values were read from the lookup tables and parametric tables using the specific functions, the directives call procedures and export results.

Solving

Running simulation is executed upon the parametric tables using the so-called Solve Table COMMAND. While the solving is processed row by row on the parametric tables, the combisystem operation is simulated from one time step to the next. During each run of simulation, the variables in the parametric tables (except the input time variables) are written with results that are just solved by going through the main routine to compute for all the unknowns. The solving operation employs iterative computation technique, starting from a guess value for an unknown, and terminating till the stop criteria being reached. The case study applied the default setting of criteria tolerances

of EES: number of iterations > 100, relative residuals < 10^{-6}, change in variables < 10^{-9}, elapsed time > 3600 s.

4.11. Model validation and verification

After completing the model implementation, model validation and verification were conducted following two of the four processes presented by Sargent (2011) (Fig. 4.13): the conceptual model validation and the computerized model verification. The former verifies the solar combisystem mathematical model's representation is for the intended purpose of the modeling of the system operation. The latter verifies the programming and implementation in the EES program was correct.

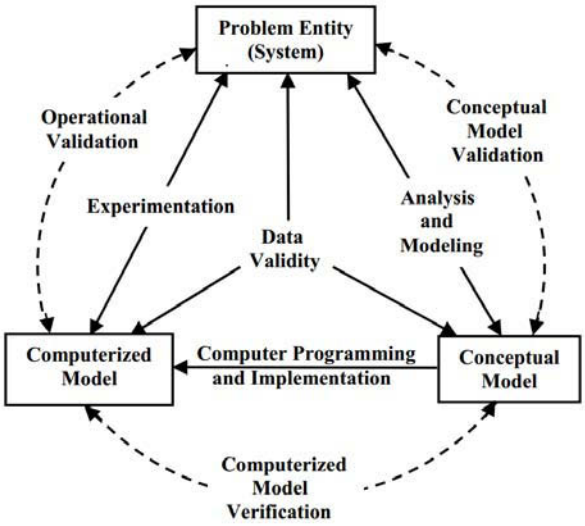

Fig. 4.13 Simplified version of the modeling process (Sargent 2011)

The mathematical and logical relationships of the combisystem component models and the overall combisystem model were examined for validation. The

component energy models, either from previous studies, current industry practice or new developments underwent the *checkup* of the Second Law of thermodynamics. Whenever the models failed to comply with both the First Law of thermodynamic and the Second Law of thermodynamic, the models were modified.

For computer model verification, structured walkthroughs and correctness proofs were performed, as of the static testing approach. Dynamic testing was executed under simulation tests with various simulation time spans, for day, for season (i.e., heating season and non-heating season), and for a complete simulation year. Detailed output from the test simulations were traced for investigating the input-output relations, the model internal consistency, etc. Energy balance was checked for each component equipment models, as well as for the complete combisystem model. Efforts were made to look for the hidden errors, for instance checking dimensionless numbers, such as thermal efficiency, which bears values in a range between 0 and 1. The feature of checking unit consistency in the EES program was used to reduce errors for this complex combisystem model.

5. Results and discussions

The case study house is in Montreal, Canada. The heating season is from October 17 to April 30, followed by the non-heating season from May 1 to October 16. The design indoor temperature of the house is 18 ℃. The building geometry and physical characteristics can be found in Leckner & Zmeureanu (2011). The solar combisystem computer model was simulated to meet the case house residential heating requirements during a year. The input space heating demand was from the study by Leckner & Zmeureanu (2011) with a seasonal overall of 8,323 kWh and a peak of 12.992 kW in January. The input domestic hot water consumption was from the study by Ulrike Jordan & Vajen (2001) with a daily average of 266 L (Aguilar et al. 2005). The input cold water temperature was from the study by Hugo (2008), who correlated the temperature of the city main of Montreal measured by Dumas & Marcoux (2004).

Table 5.1 presents the capacity and control settings of the solar combisystem equipment in the simulated case. The water storage tank (Consolar 2012), heat pump (GeoSmart 2012), and solar thermal collector (SunEarth 2012) are products available for purchase; the size of ice storage tank was studied as customized. Their capacities and the node setting temperatures were finalized after analyses performed using the developed computer model. The decision was made based on: to meet the case heating requirements using equipment in the lowest capacities.

Table 5.1 Capacities and control settings of solar combisystem simulated case

Component equipment	Capacity	Settings
Radiant floor loop	-	Minimum supply temperature 25 ℃ (Olesen 1977) Return temperature 20 ℃ (ASHRAE (2004) Nodes setting temperature 40±5 ℃
Water storage tank	2.2 m^3	Maximum allowable temperature 60 ℃ (ASHRAE 2007) Auxiliary heater start-up temperature 40.5 ℃ (California Energy Commission 2005)
Ice storage tank	14 m^3	Maximum ice fraction 70% (Sunwell 2012) Maximum water temperature 37.8 ℃ (GeoSmart 2012)
Heat pump	12.95 kW COP 3.1	-
Solar thermal collectors	27.58 m^2	Tilt angle 60° (Hugo 2008) Orientation due South

The initial conditions of the simulation were the temperatures in the storage tanks, which were taken as the indoor air temperature 18 ℃. The impact of the initial values was eliminated by simulating the combisystem operation for a simulation time of three continuous years. Results of the third year were used for the analysis.

5.1. Energy performance of solar combisystem

5.1.1. Overview of annual energy flow

The solar combisystem used solar heat and electricity to meet the residential heating needs. The annual energy flows among the system components are plotted in Fig. 5.1. The rectangular boxes by continuous line represent the system components. The rectangular boxes by dotted line represent the supply of energy (at the top) and the heating loads (at the bottom). The boxes in irregular shape represent the outdoor environment and the indoor surroundings. The arrows connecting the boxes show the direction of the flow paths.

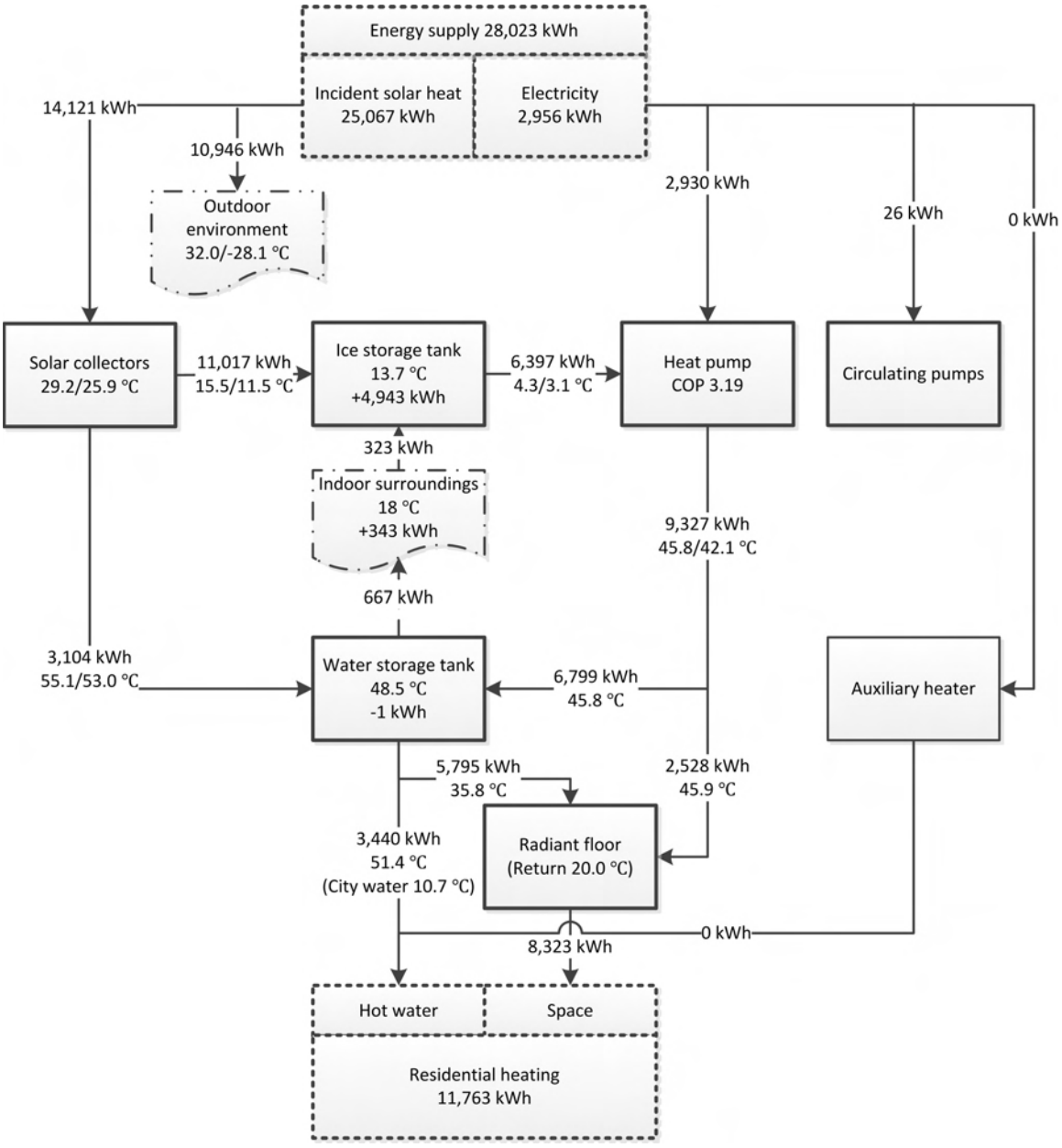

Fig. 5.1 Flowchart of energy flows of solar combisystem annual operation

System COP: 3.98. Solar energy contribution: 89.5%. Solar energy fraction (reference): 1.3.

The annual energy use was quantified in kWh. The amount of change of energy was indicated for the storage tanks, positive for energy stored and negative for energy extracted. Similar convention was used for the indoor surroundings. The operation temperatures were labeled. For instance, in the case of solar collectors, $\overline{T}_{out}/\overline{T}_{in}$ is the

mean outlet temperature followed by the mean inlet temperature. In the case of outdoor environment, T_{max}/T_{min} is the upper limit and the lower limit of outdoor temperature. Some cases were labelled with one temperature: mean temperature of the ice storage tank water-layer, mean temperature of the water storage tank nodes, or supply temperature along the flow path.

5.1.2. Combisystem energy performance

Combisystem COP

The system COP was calculated as the ratio of the system heating load to the system electricity consumption. Annual operation of the combisystem used 2,956 kWh of electricity meeting the heating needs of 11,763 kWh. The combisystem had an annual system COP of 3.98.

$$System\ COP = \frac{system\ heating\ load}{system\ electricity\ consumption} = \frac{11{,}763}{2{,}956} = 3.98 \quad (5.1)$$

Solar energy fraction compared to reference system

A compared non-solar system is supposed to satisfy the same heating needs as of a solar system (Hastings & Wall 2007). The reference system compared was consisted of electric water heater and electric baseboard heater (Table 5.2).

By comparing the two systems, the solar energy fraction of a solar system is calculated as a ratio of the solar energy collection of a solar system to the energy used by the reference system,

$$Solar\ energy\ fraction\ (SF_E) = \frac{solar\ energy\ collection\ of\ solar\ system}{energy\ used\ by\ reference\ system} = \frac{14{,}121}{10{,}850} = 1.3 \quad (5.2)$$

The solar combisystem had an annual solar energy fraction of 1.3. April had the solar energy fraction peak of 5.39, and the minimum appeared in December as of 0.52.

Table 5.2 Reference system energy use vs. solar energy collection of solar combisystem

	Reference system			Solar combisystem	
	Electricity consumption of baseboard heater, kWh	Electricity consumption of water heater, kWh	Total energy use, kWh	Collected solar radiation, kWh	Solar energy fraction, dimensionless
January	2,331.04	277.51	2,608.55	1,707.84	0.65
February	1,721.11	262.53	1,983.64	2,222.92	1.12
March	949.38	306.54	1,255.92	2,807.75	2.24
April	182.27	283.44	465.72	2,511.75	5.39
May	0.00	213.88	213.88	433.03	2.02
June	0.00	156.79	156.79	342.73	2.19
July	0.00	117.67	117.67	298.52	2.54
August	0.00	100.80	100.80	274.45	2.72
September	0.00	145.52	145.52	350.41	2.41
October	171.68	171.73	343.41	1,018.88	2.97
November	976.15	218.15	1,194.30	974.43	0.82
December	1,991.79	271.83	2,263.62	1,178.00	0.52
Year	8,323	2,526	10,850	14,121	1.30

Solar energy contribution

Among 28,023 kWh of energy, a sum of the annual incident solar energy (25,067 kWh) and the annual electricity consumption, the annual incident solar energy contribution was 89.5%.

$$Incident\ solar\ energy\ contribution\ (SC_E) = \frac{incident\ solar\ energy}{system\ energy\ input} \times 100$$
$$= \frac{25{,}067}{28{,}023} \times 100\% = 89.5\% \quad (5.3)$$

Among 17,077 kWh of energy, a sum of the annual solar energy collection (14,121 kWh) and the annual electricity consumption, the annual collected solar energy contribution was 82.7%.

$$Collected\ solar\ energy\ contribution\ (SC_E) = \frac{solar\ energy\ collection}{system\ energy\ input} \times 100$$
$$= \frac{14{,}121}{17{,}077} \times 100\% = 82.7\% \quad (5.4)$$

Energy efficiency

The system operation used 28,023 kWh of energy to meet the heating needs of 11,763 kWh over one year. The annual system energy efficiency of 42.0% was calculated as the ratio of the annual heating load to the annual energy input:

$$System\ energy\ efficiency = \frac{system\ heating\ load}{system\ energy\ input} \times 100$$
$$= \frac{11{,}763}{28{,}023} \times 100\% = 42.0\% \quad (5.5)$$

If counting the energy use since the heat input by the solar thermal collector, to supply the heating load led the energy efficiency of 68.9% (among 17,077 kWh).

5.1.3. Electricity consumption and combisystem COP

Table 5.3 presents the electricity consumption of heat pump and circulating pumps, along with the system COP calculated as the average of the system COPs over the corresponding time period.

Table 5.3 Results of electricity consumption and system COP of solar combisystem annual operation

	Heat pump, kWh	Circulating pumps, kWh				System COP, dimensionless
		P1	P2	P3	Overall	
January	854.89	1.58	1.54	1.73	4.85	3.07
February	564.02	1.84	1.03	1.18	4.04	3.55
March	264.50	2.21	0.48	0.59	3.29	4.84
April	99.43	2.36	0.19	0.23	2.78	4.94
May	-	0.78	-	-	0.78	449.77
June	-	0.67	-	-	0.67	420.69
July	-	0.47	-	-	0.47	491.50
August	-	0.55	-	-	0.55	380.45
September	-	0.51	-	-	0.51	553.23
October	64.64	1.16	0.12	0.17	1.44	6.54
November	367.64	1.27	0.65	0.83	2.75	3.31
December	714.98	1.30	1.29	1.49	4.08	3.19
Year	2,930	15	5	6	26	3.98

The heat pump used 2930 kWh of electricity in the year, with the highest consumption in January followed by December. The circulation pumps $P2$ & $P3$ were operated during January to April and October to December in the heating season. The circulation pump $P1$ has been operated throughout the year. The auxiliary heater, not shown, was never used without any consumption. In the heating season, the monthly averaged system COP was over 3 from January to April and from October to December. From May to December monthly averaged system COP represented large values, due to small amount of electricity was consumed on operating the circulating pump $P1$. The monthly averaged system COP in October was larger than in the rest heating season months, because half of the month was in non-heating season.

5.1.4. Major flows of energy

The energy flows of solar combisystem annual operation shown in Fig. 5.1 are detailed by month in the followed Table 5.4.

Table 5.4 Results of energy flows of solar combisystem annual operation

	Energy input, kWh			Heating load, kWh	Heat transferred with indoor surroundings, kWh	Heat lost to outdoor environment, kWh	Heat storage, kWh
	Incident solar heat	Electricity	Overall				
January	2,823.18	859.75	3,682.93	2,640.14	66.91	1,115.34	-10.49
February	3,680.97	568.06	4,249.02	2,014.13	25.57	1,458.05	798.38
March	4,714.15	267.79	4,981.94	1,295.93	-51.51	1,906.41	1,724.80
April	4,015.50	102.22	4,117.72	504.91	-59.81	1,503.75	2,046.47
May	1,200.62	0.78	1,201.40	351.81	-65.85	767.59	15.36
June	948.72	0.67	949.39	279.79	-64.76	605.99	-1.82
July	725.36	0.47	725.83	233.21	-68.20	426.83	-2.88
August	758.99	0.55	759.53	208.46	-68.79	484.53	-2.80
September	875.64	0.51	876.16	284.46	-62.49	525.23	3.46
October	1,783.80	66.08	1,849.88	431.87	-53.31	764.91	598.34
November	1,530.94	370.39	1,901.33	1,224.29	17.47	556.51	135.25
December	2,008.93	719.06	2,728.00	2,294.88	41.29	830.94	-360.62
Year	25,067	2,956	28,023	11,764	-343	10,946	4,943

Heating load and energy use

The combisystem supplied 11,764 kWh of heating load for the space heating (8,323 kWh) and the preparation of domestic hot water (3,440 kWh) during an annual operation. Fig. 5.2 presents the monthly profile of space heating load and water heating load. The simulated space heating load matched the input heating demand appeared from October to April, corresponding the heating season started from October 17 to April 30. The water heating load continued throughout the 12 months.

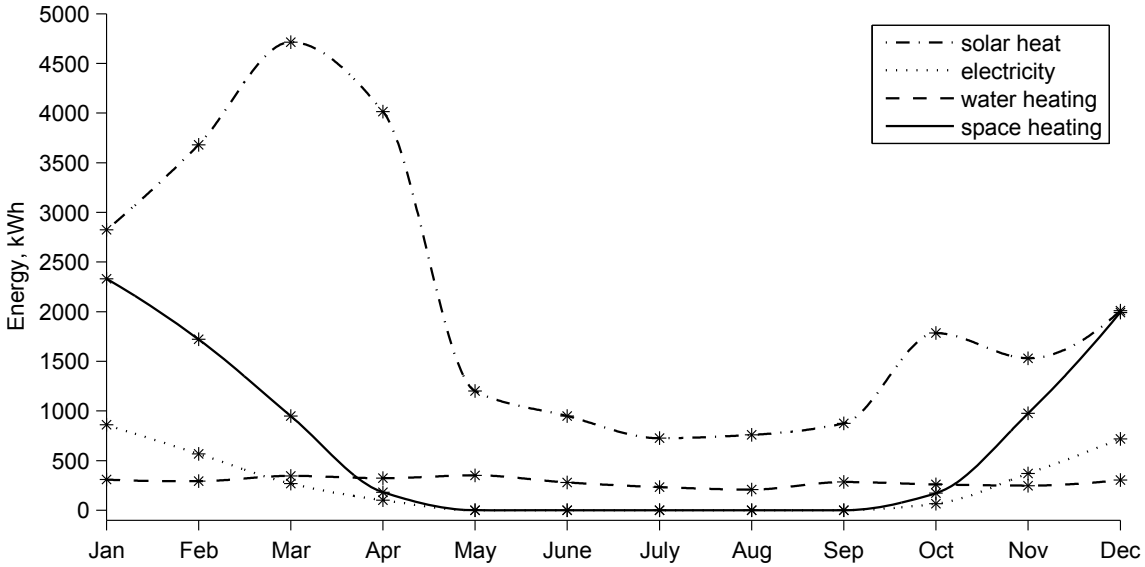

Fig. 5.2 Energy supply and heating load of solar combisystem

The total 28,023 kWh of energy input to the system included 2,956 kWh of electricity and 25,067 kWh of incident solar heat during the operation periods. The profile of monthly energy use from the two sources is also presented in Fig. 5.2.

Heat transfer between combisystem and indoor environment

The combisystem lost 343 kWh of heat to the indoor environment throughout an entire year. The loss was the results of transfer of heat between the water storage tank and the surroundings, and between the ice storage tank and the surroundings. Fig. 5.3 shows the monthly profile of the heat transfer, where the positives represent the heat transferred from the indoor environment to the storage tanks, the negatives represent the heat transferred from the storage tanks to the indoor environment.

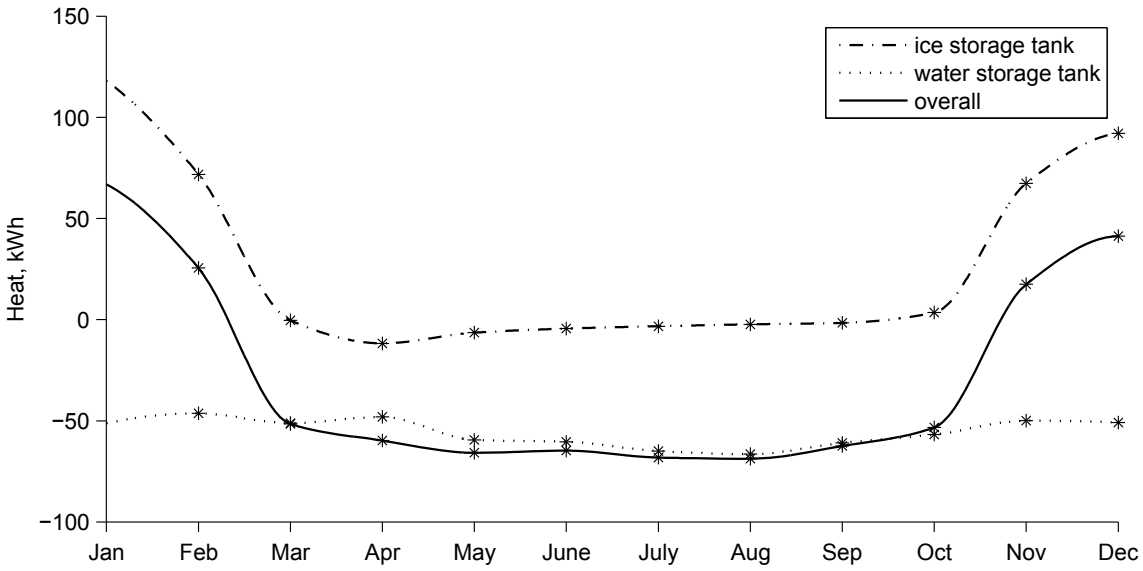

Fig. 5.3 Heat transfer between storage tanks and indoor surroundings

(positive values represent tanks in heat gain; negative values represent tanks in heat loss)

Heat loss to outdoor environment

The combisystem lost 10,946 kWh of heat to the outdoor environment during the annual operation. The loss was accounted for the amount of solar heat failed to be absorbed by the solar thermal collectors.

Heat storage

The combisystem using the water storage tank and the ice storage tank stored 4,943 kWh of heat throughout an entire year. Fig. 5.4 presents the storage of heat by month, where the positives represent the heat stored in the storage tanks, the negatives represent the heat released from the storage tanks. The monthly profile shows the ice storage tank in active of storing and releasing heat from January to May and from September till December during the heating season. The most amount of heat stored appears at the ice storage tank in April, the most amount of heat released at the

ice storage tank in December. The results showed smaller magnitude of storage of heat took place in the water storage tank, in contrast to the ice storage tank.

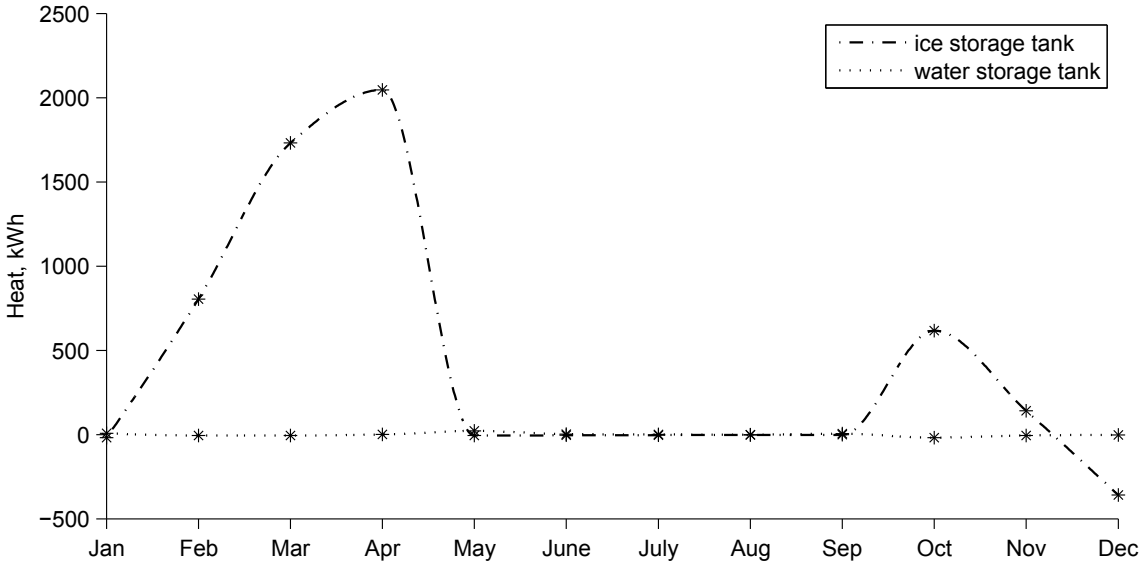

Fig. 5.4 Heat storage of solar combisystem

(positive values represent heat stored; negative values represent heat released)

5.2. Combisystem operation in non-heating season

The combisystem had non-heating season operation of 169 days, from May 1 to October 16, producing the domestic hot water. The non-heating season operation is discussed with the hourly results of three continuous calendar days from July 20 to July 22.

Heating load and use of heat

Fig. 5.5 presents the heating load of the solar combisystem for domestic hot water production. The water storage tank, where to prepare the domestic hot water,

had two heat sources: the heat pump and the solar thermal collectors. But the results showed that the idle status of heat pump during the non-heating season. This indicated the use of solar thermal collectors in non-heating season was sufficient. The heat charge from the solar thermal collectors to the water storage tank is presented in Fig. 5.6.

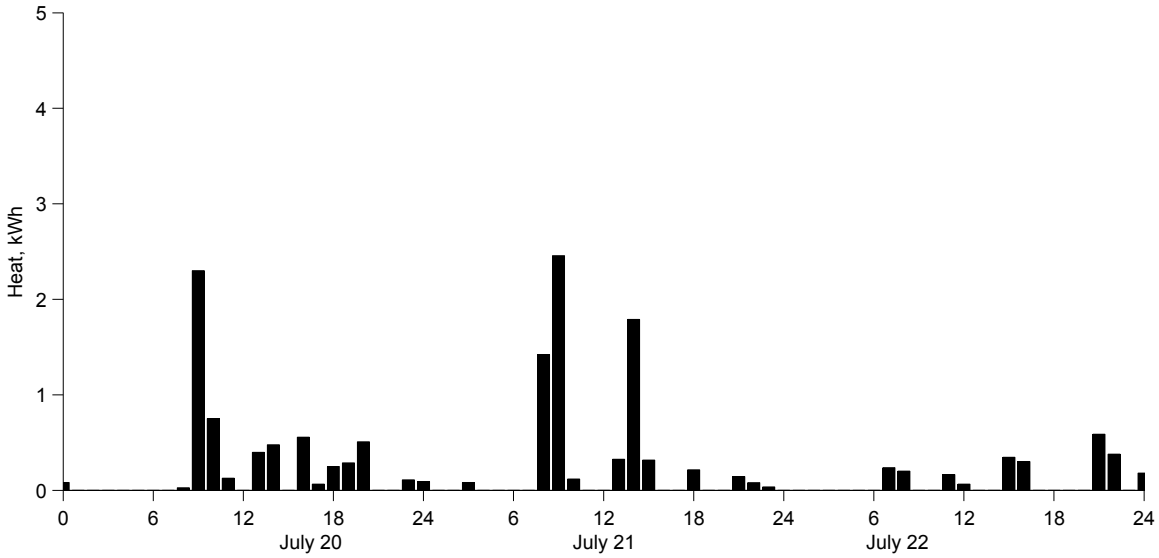

Fig. 5.5 Heating load of solar combisystem from July 20 to July 22

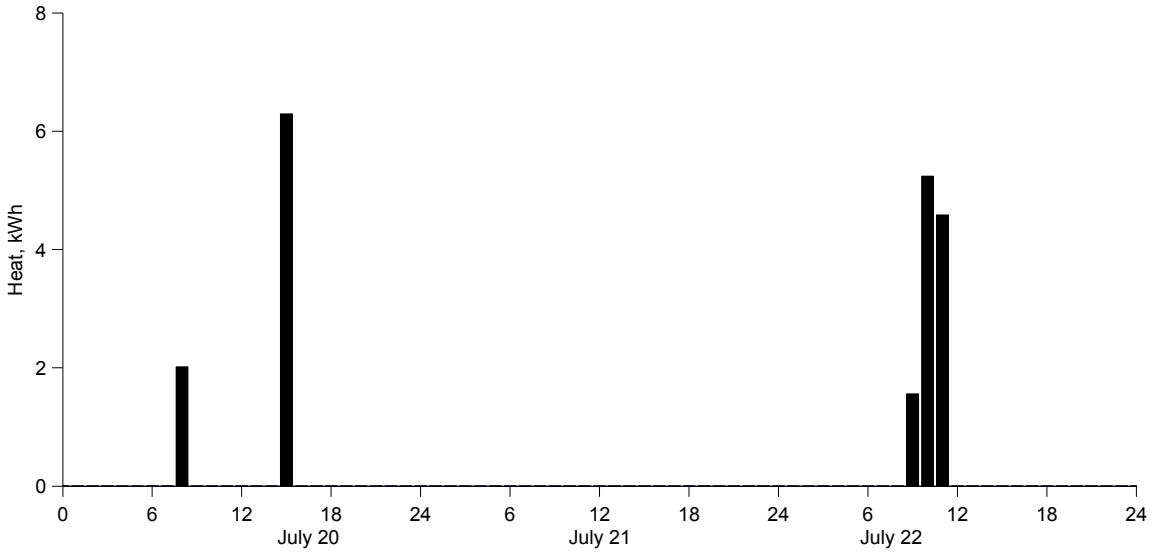

Fig. 5.6 Solar heat collection charging water storage tank from July 20 to July 22

Fig. 5.7 presents the solar radiation and the heat flows at the solar thermal collectors. The available solar incident is referred to the incident solar energy on the surfaces of solar thermal collectors regardless the collector operation. The utilized solar incident is referred to the incident solar energy on the surfaces of solar thermal collectors during the *on* operation of solar thermal collectors. When the solar thermal collectors were *on*, solar heat was collected charging to the storage tanks. The results show the heat charging only took place from the solar thermal collectors to the water storage tank, nothing for the ice storage tank.

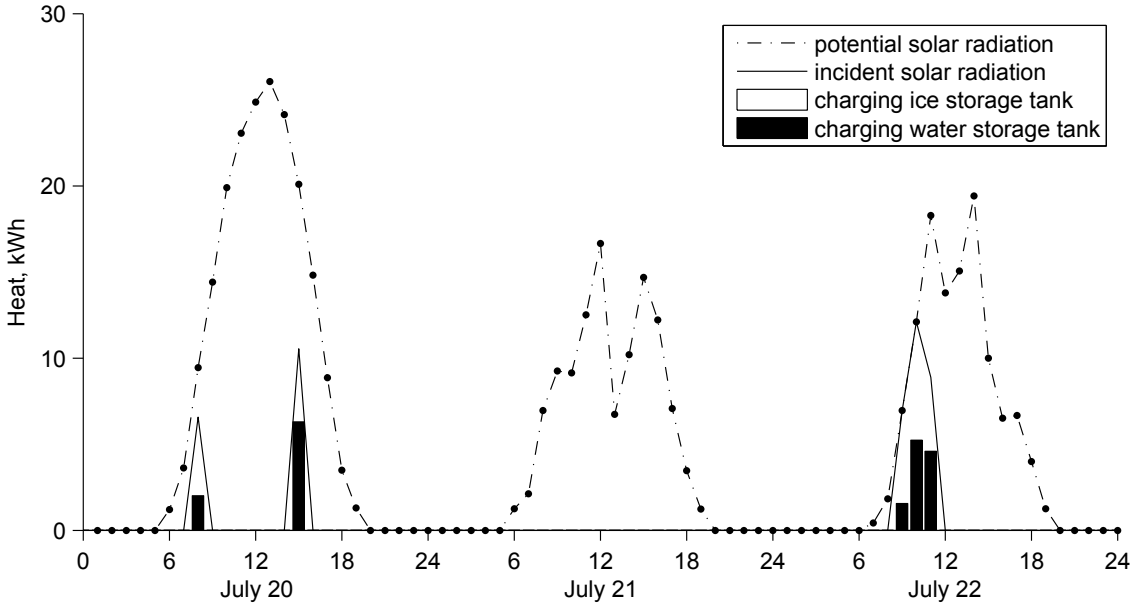

Fig. 5.7 Solar heat collection and storage from July 20 to July 22

The solar thermal collectors have been operated within two hours on July 20 and within 3 hours on July 22, no operation on July 21. This suggested that the domestic hot water production on July 21 used the heat stored in the water storage tank. After the release of heat from storage, the solar thermal collectors collected heat on July 22 for

the water storage tank, more than on July 20. This showed how the solar thermal collector operation serving the short period heat storage operation of water storage tank.

Heat storage

Fig. 5.8 presents the change of heat in the water storage tank. The positive values indicate the water storage tank was under the heat charging, the negative values indicate the water storage tank was under the heat discharging.

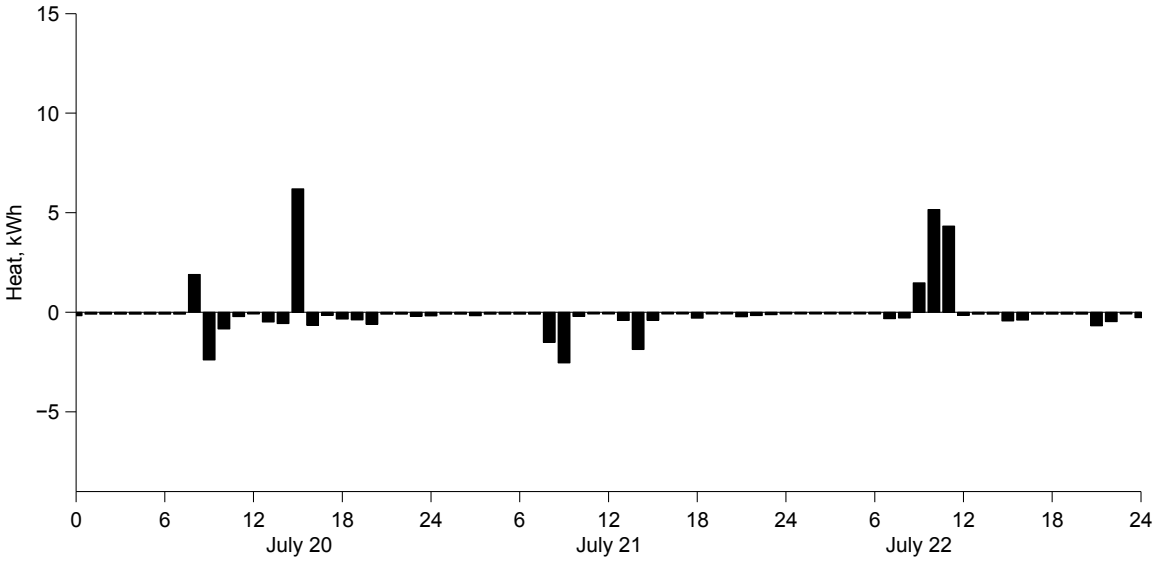

Fig. 5.8 Heat storage of water storage tank from July 20 to July 22

Storage temperature

Fig. 5.9 presents the temperature variation of five water-nodes ($N1$ to $N5$) in the water storage tank. After the domestic hot water production on July 21, the temperature of node $N1$ dropped down to 35.5 ℃, near the set point of 35 ℃. This led the solar thermal collectors to start operation on the next day July 22 as soon as solar heat was available. The combisystem control system allowed the charge of heat to the

water storage tank when the temperature in water storage tank is below 60 ℃. For this reason, as the temperature reached 62 ℃ at the node $N4$ and 61 ℃ at the node $N5$, the solar thermal collectors stopped the *on* operation (Fig. 5.7) though solar heat was still available. The temperature profile indicated thermal stratification in the water storage tank.

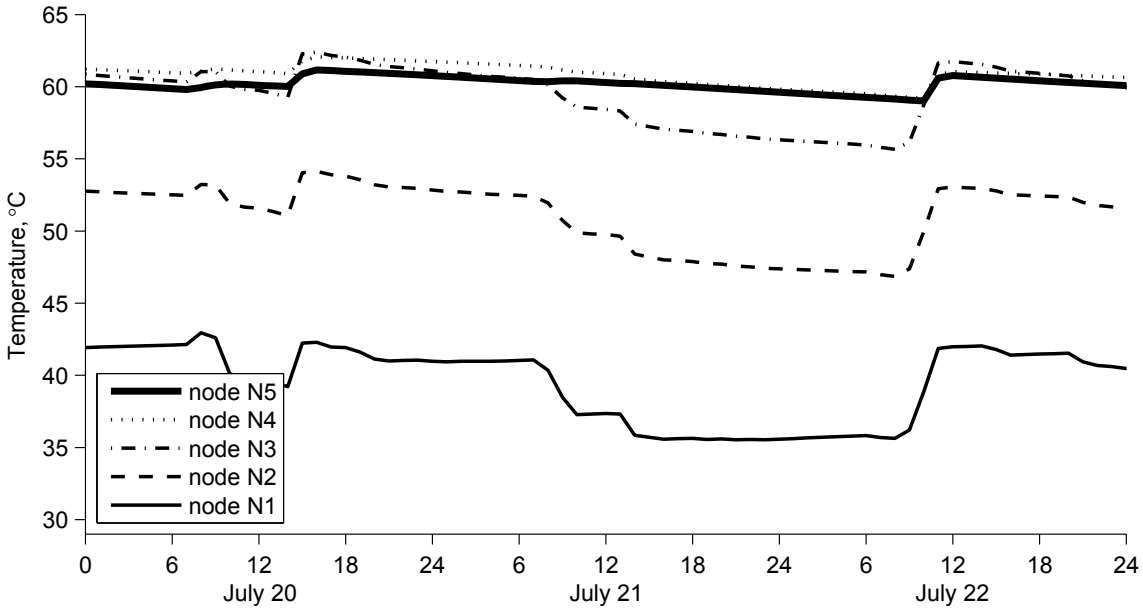

Fig. 5.9 Node temperature of water storage tank from July 20 to July 22

Electricity use

Fig. 5.10 presents the electricity used by the combisystem operation. The electricity consumption was solely due to the operation of pump $P1$ to circulate water along the loop $L1$ for the transfer of heat from the solar thermal collectors to the water storage tank.

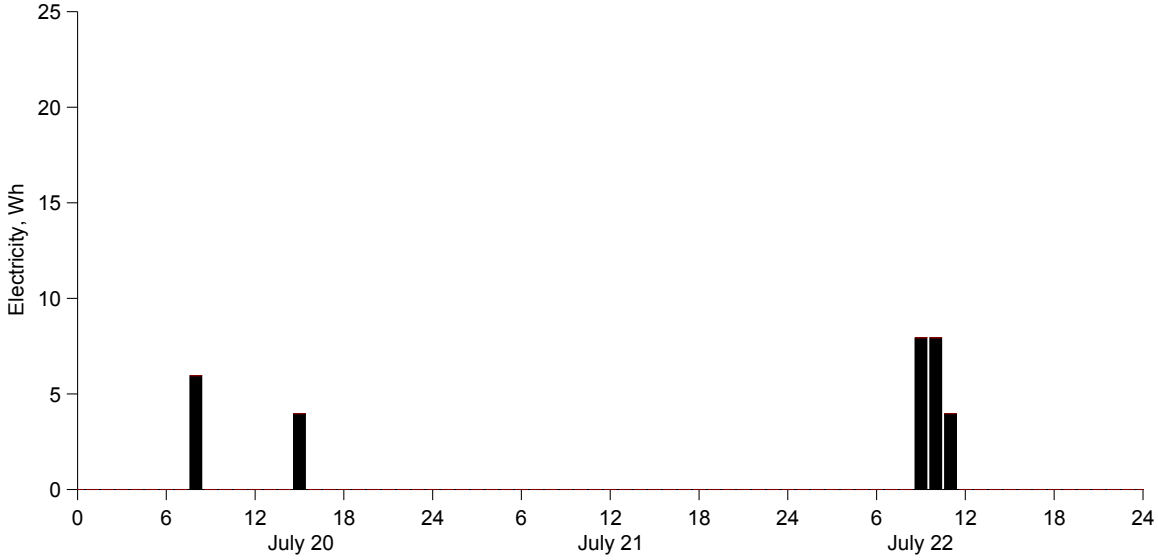

Fig. 5.10 Electricity consumption of solar combisystem from July 20 to July 22

5.3. Combisystem operation in heating season

The combisystem had the heating season operation of 196 days from October 17 to April 30. The combisystem covered the heating needs for the domestic hot water and the space heating. The operation at the peak space heating is to be overviewed in this section, followed by the heating season operating condition discussed with the hourly results of three continuous calendar days from January 11 to January 13.

Peak space heating

The residential space heating demand reached the peak of 12,992 W at 7:15 a.m. on January 12, and there was also domestic hot water use at this moment (Fig. 5.11).

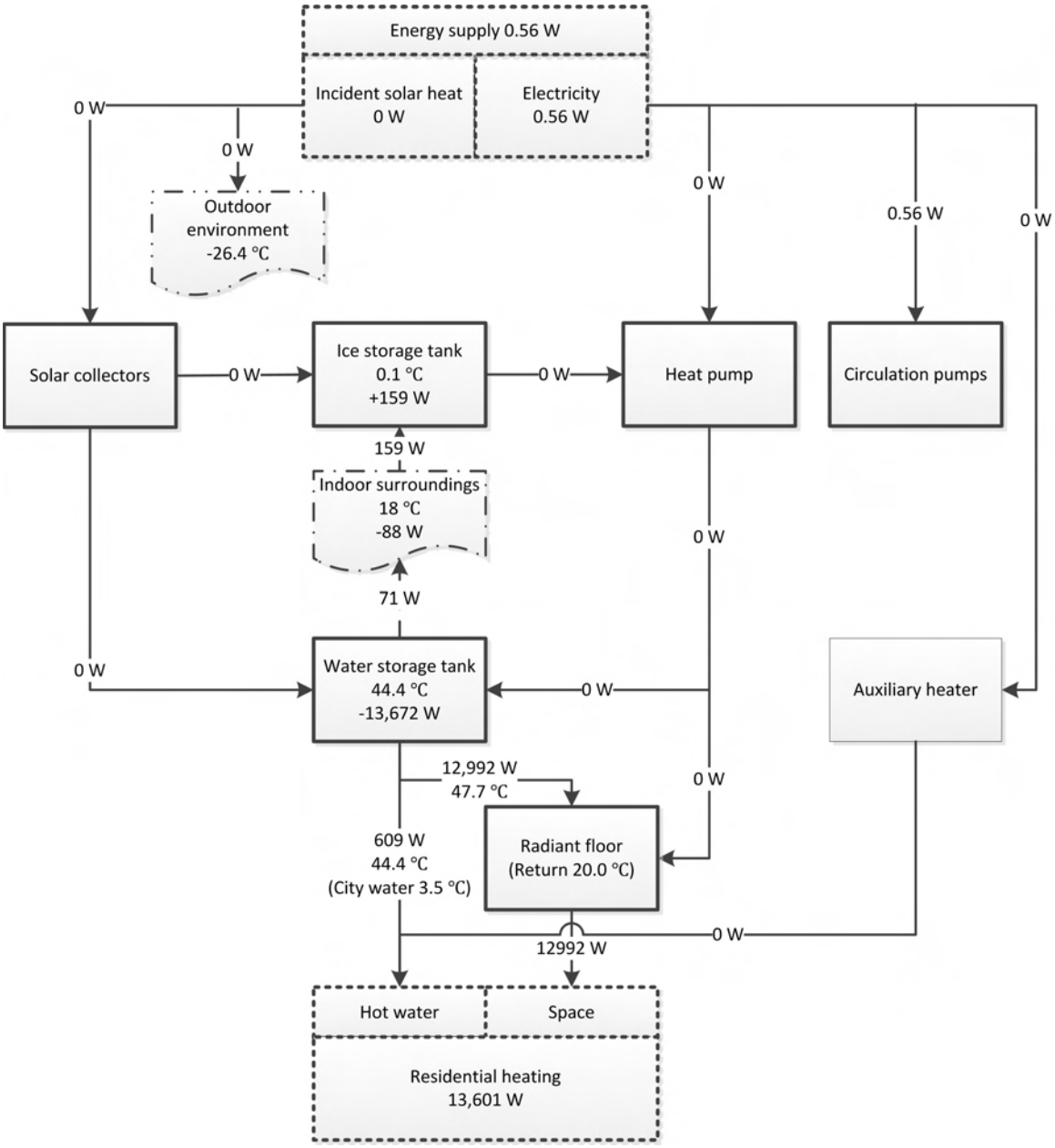

Fig. 5.11 Flowchart of energy flows of solar combisystem at space heating peak

Above flowchart presents the operation temperatures along with the energy flow rates in W. At this peak time, the outdoor temperature was -26.4 ℃, city water temperature was 3.5 ℃, and the indoor temperature was 18 ℃. The combisystem used

electricity (0.56 W) to run a circulation pump for the space heating, which was supplied by the radiant floor using the heat from water storage tank (12,992 W). The water storage tank also covered the heat meeting the domestic hot water needs (609 W). The supply temperature was 47.7 ℃ for the radiant floor and 44.4 ℃ for the domestic hot water. The total heat transfer rate from the water storage tank for the heating was 13,601 W.

Terrell (1979) has reported the possibility of a solar heating system satisfying the heating demand during the coldest months without directly using solar energy. Instead, the solar energy stored from the previous time was released to meet the heating needs, and the store temperature was reduced by such operation. The reported results were confirmed by the results shown in this simulated case: The combisystem satisfied the heating demand at the residential peak space heating time using the heat stored from the previous time.

The surroundings of the combisystem underwent the heat transfer with the storage tanks. The water storage tank lost heat (71 W) to the surroundings, whereas the ice storage tank gained heat (159 W) from the surroundings. The water storage tank operation at this peak decreased the heat stored at the rate of 13,672 W. At this peak, the solar thermal collectors, heat pump, and the auxiliary heater were idle.

Heating load

Fig. 5.12 presents the combisystem heating load for the space heating and the domestic hot water. The space heating was supplied by the radiant floor using the heat

from heat pump and water storage tank. The domestic hot water was prepared in the water storage tank. The space heating load exhibited similar patterns of variation through the hours of each day. The heat provided by water storage tank for the space heating was no less than the heat provided by heat pump, when the space heating load were relative low. When the space heating load was high, the heat pump provided most amount of heat for the space heating. This indicated the operation difference between the heat pump and the water storage tank, in terms of matching the space heating demand respecting its own capability.

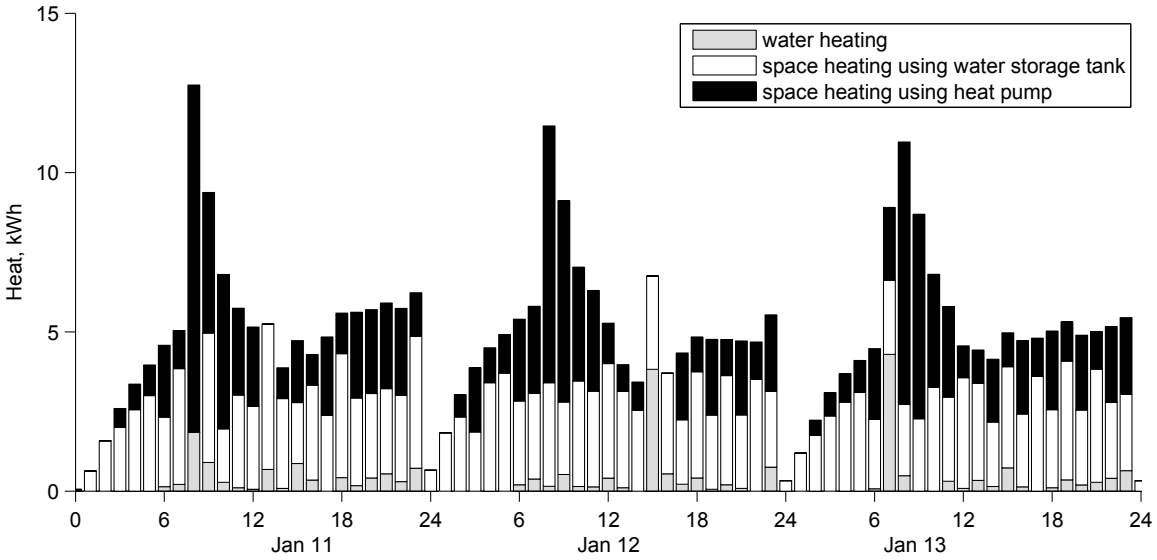

Fig. 5.12 Heating load of solar combisystem from Jan. 11 to Jan. 13

Heat pump output

Fig. 5.13 presents the use of the heat output from heat pump. The heat output was transferred to the water storage tank and the radiant floor. Within the hours with higher output, the heat pump provided the radiant floor more heat than does the water

storage tank. On the contrary, the water storage tank received heat from the heat pump more than the radiant floor did within the hours that the heat pump made outputs.

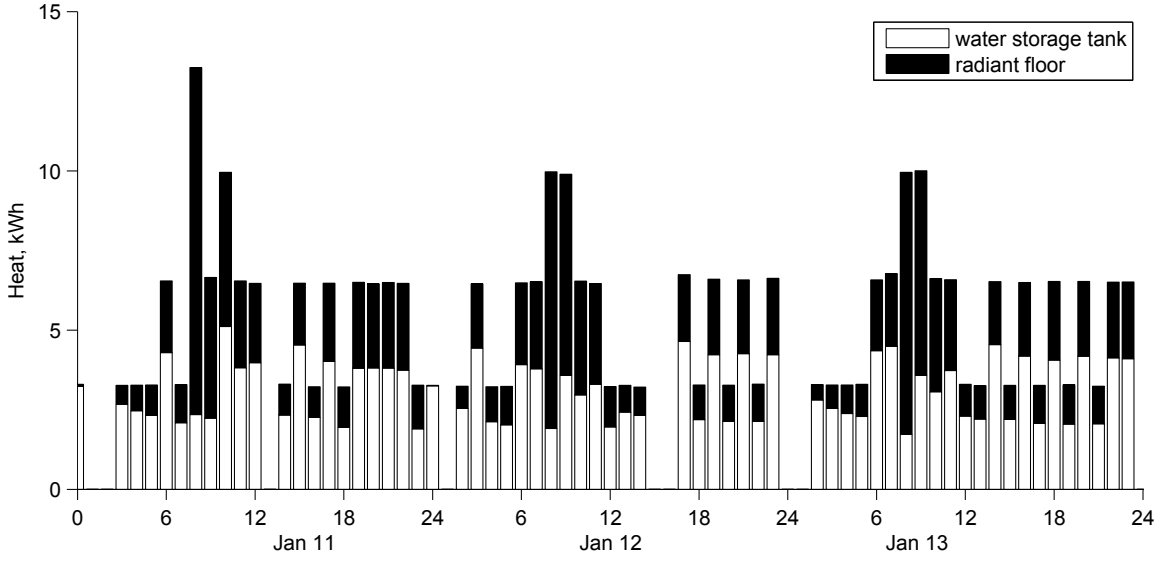

Fig. 5.13 Heat output of heat pump from Jan. 11 to Jan. 13

Solar heat collection

Solar heat was the sole source providing the combisystem with heat. Fig. 5.14 presents the solar radiation and the heat flows at the solar thermal collectors. Solar heat was available around the middle house each day, and the solar thermal collectors were *on* operation during then. The collected heat was input to the ice storage tank and the water storage tank for storage. The results show that the ice storage tank received more heat than the water storage tank during these days. The seasonal peak space heating took place on January 12. The results show that the solar thermal collectors had *on* operation during most of the time when solar heat was available.

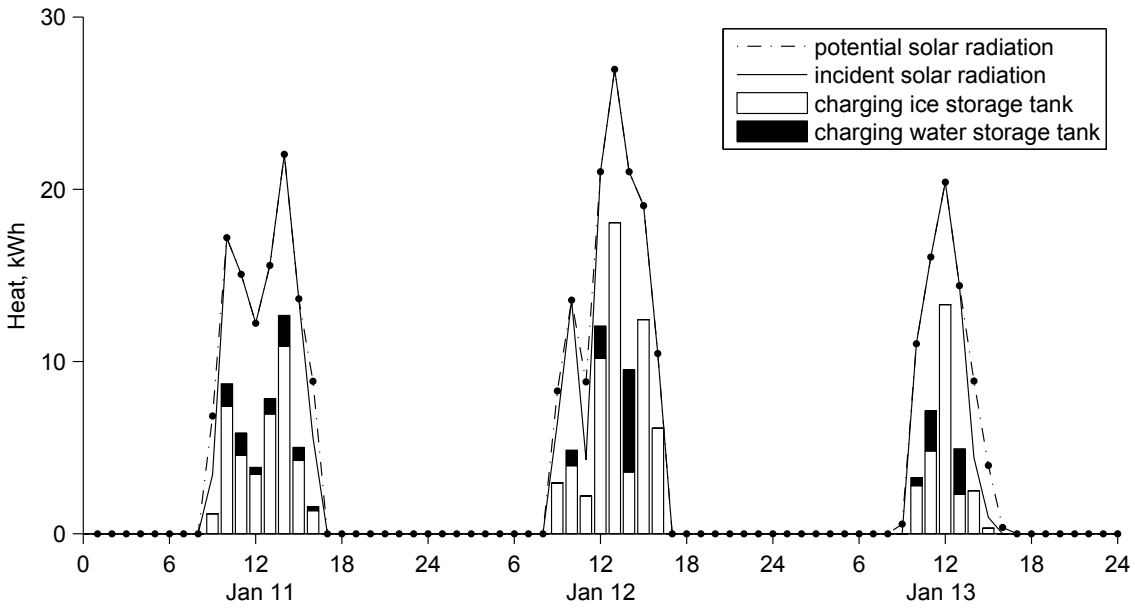

Fig. 5.14 Solar incidence and solar heat collection from Jan. 11 to Jan. 13

Heat storage

I. Water storage tank

Fig. 5.15 presents the heat charging to the water storage tank, by the heat pump and the solar thermal collectors. The water storage tank started to take in heat at every early morning from the heat pump. Around the middle hours of each day, there was heat transferred from the solar thermal collectors.

Fig. 5.16 presents the change of heat in the water storage tank, exhibited the short term heat storage. The positive values were corresponded to the heat gains, the negative values were corresponded to the heat losses. The greatest magnitude of heat gain was on January 12, which occurred hours after the peak space heating load.

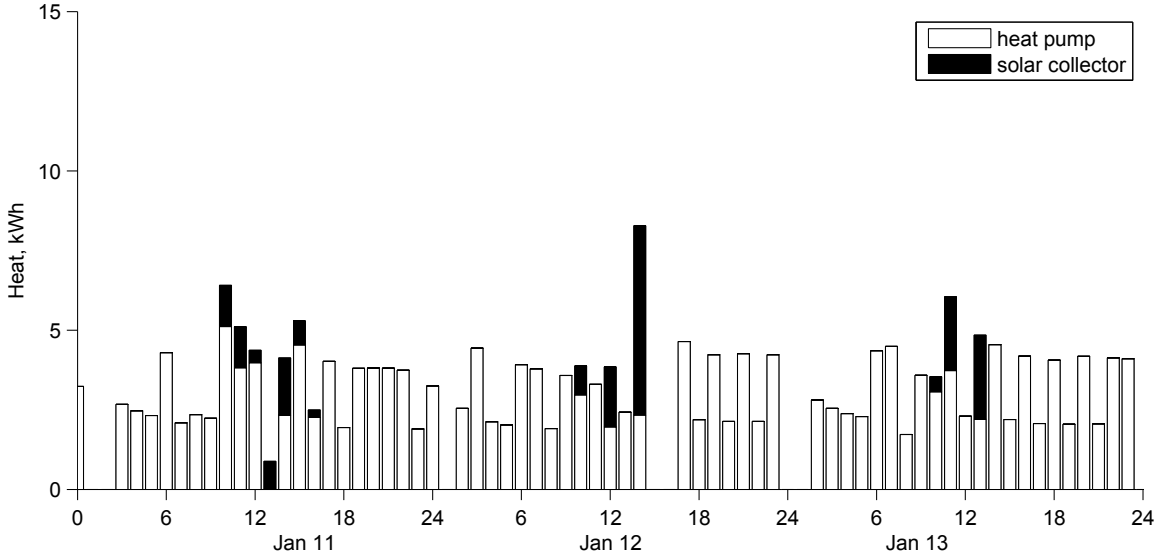

Fig. 5.15 Heat input to water storage tank from Jan. 11 to Jan. 13

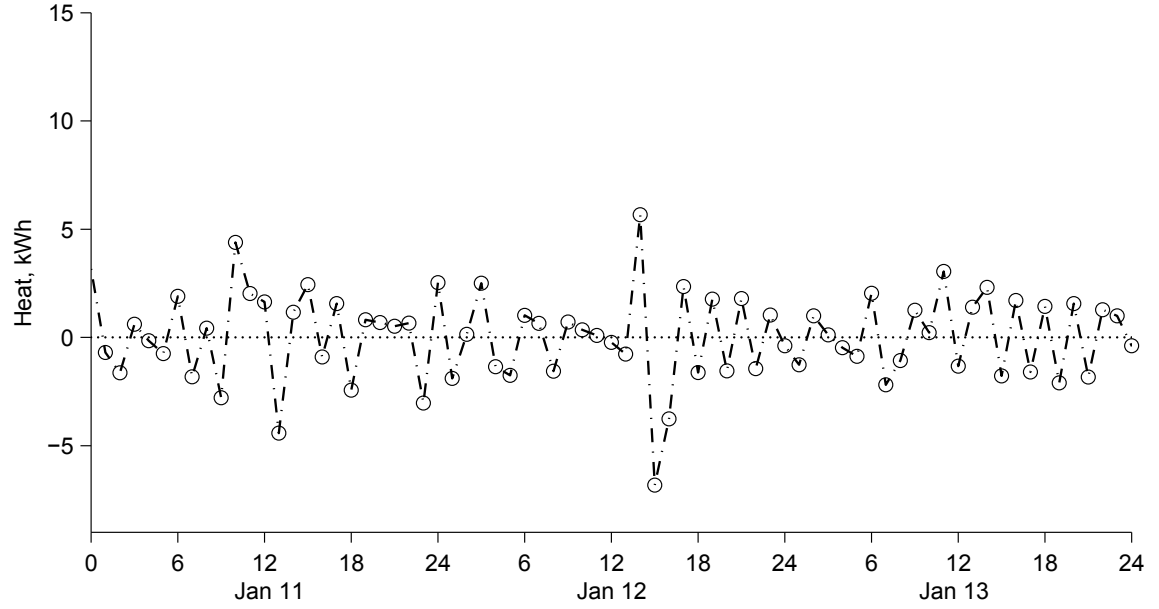

Fig. 5.16 Heat storage of water storage tank from Jan. 11 to Jan. 13

II. Ice storage tank

The ice storage tank is the thermal energy storage operated between the solar thermal collectors and the heat pump. Fig. 5.17 presents the input and output of heat of

ice storage tank. The results showed the ice storage tank output heat more frequently than input.

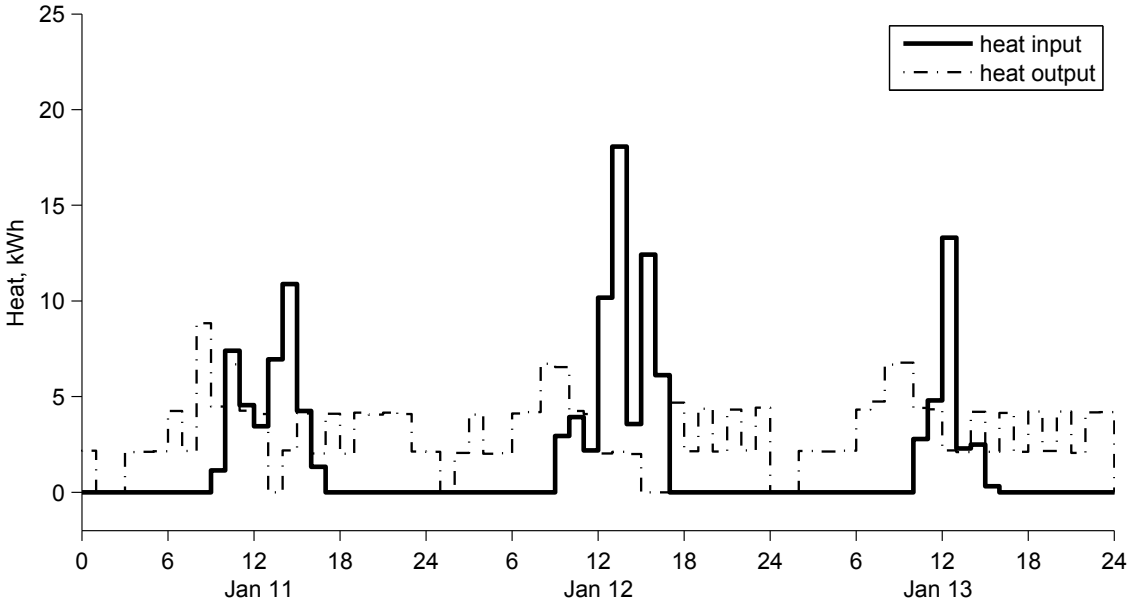

Fig. 5.17 Heat input and heat output of ice storage tank from Jan. 11 to Jan. 13

Fig. 5.18 presents the change of heat in the ice storage tank. Compared to the water storage tank, the ice storage tank had larger magnitude of change of during the day. This suggested the ice storage tank was operated with larger storage capacity than the water storage tank.

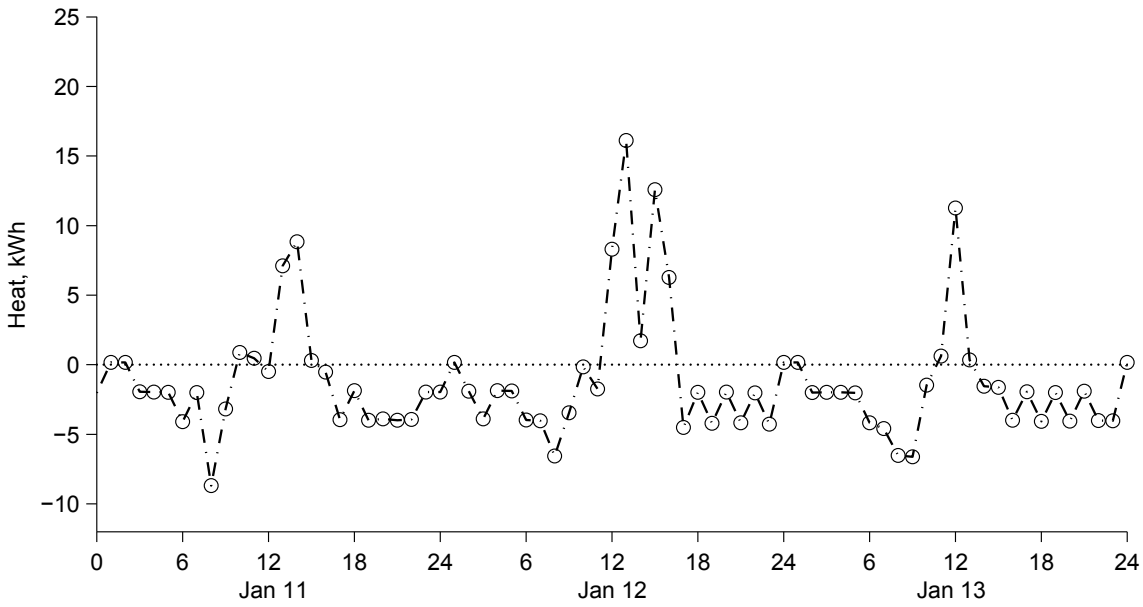

Fig. 5.18 Heat storage of ice storage tank from Jan. 11 to Jan. 13

Storage temperature

I. Water storage tank

Fig. 5.19 presents the temperature of nodes ($N1 \dots N5$) in the water storage tank. Most of the temperatures fell in between 42.9 ℃ and 49.3 ℃. The largest temperature drop occurred in January 12 down to 36.7 ℃. The hourly results showed the node $N5$ had the steadiest temperatures among all the nodes. The node $N1$ had the most dynamic change of temperature, which was due to the charging and discharging operation of the immersion heat exchanger $HX1$. The temperature variation of each node during this period was: node $N5$ in 2 ℃, node $N4$ in 3 ℃, node $N3$ in 4.2 ℃, node $N2$ in 4.4 ℃, and node $N1$ in 12.6 ℃. Thermal stratification existed locally at some time, for instance, among the nodes $N2$, $N3$, $N4$, and $N5$ from 18:00 on January 12 to 6:00 on January 13.

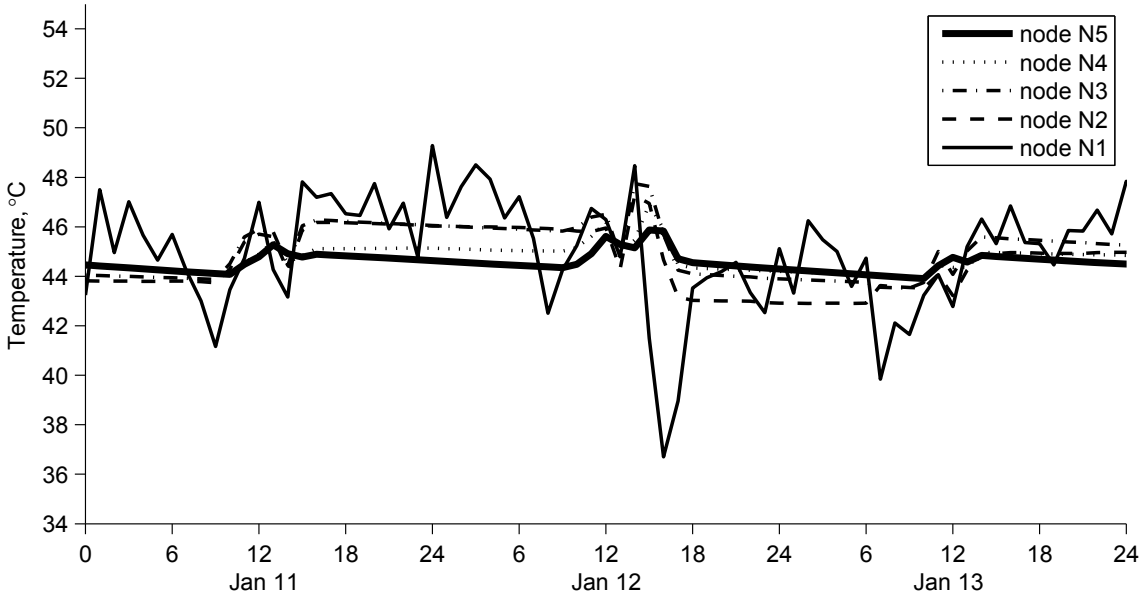

Fig. 5.19 Node temperature of water storage tank from Jan. 11 to Jan. 13

II. Ice storage tank

Fig. 5.20 presents the temperature of the water-layer of ice storage tank. The water temperature remained almost constant at 0.1 ℃. Related to the water-lay temperature, the mass fraction of ice in the ice storage tank is presented on Fig. 5.21. The mass fraction of ice was 0.45 at the beginning of January 11, reached 0.53 at the end of January 13. The results showed the coexistence of two phases of water in the ice storage tank during this period. The ice storage tank had the maximum ice mass fraction of 0.7 in this simulated case. At the end of January 13, the ice storage capacity of ice storage tank was used up to 75.7%.

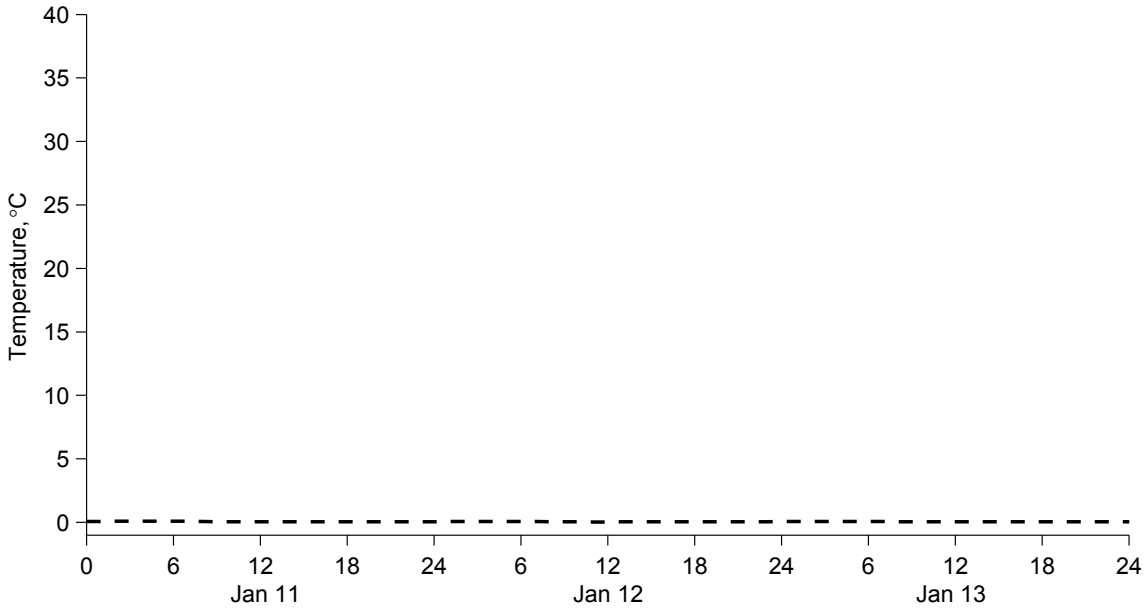

Fig. 5.20 Water-layer temperature of ice storage tank from Jan. 11 to Jan. 13

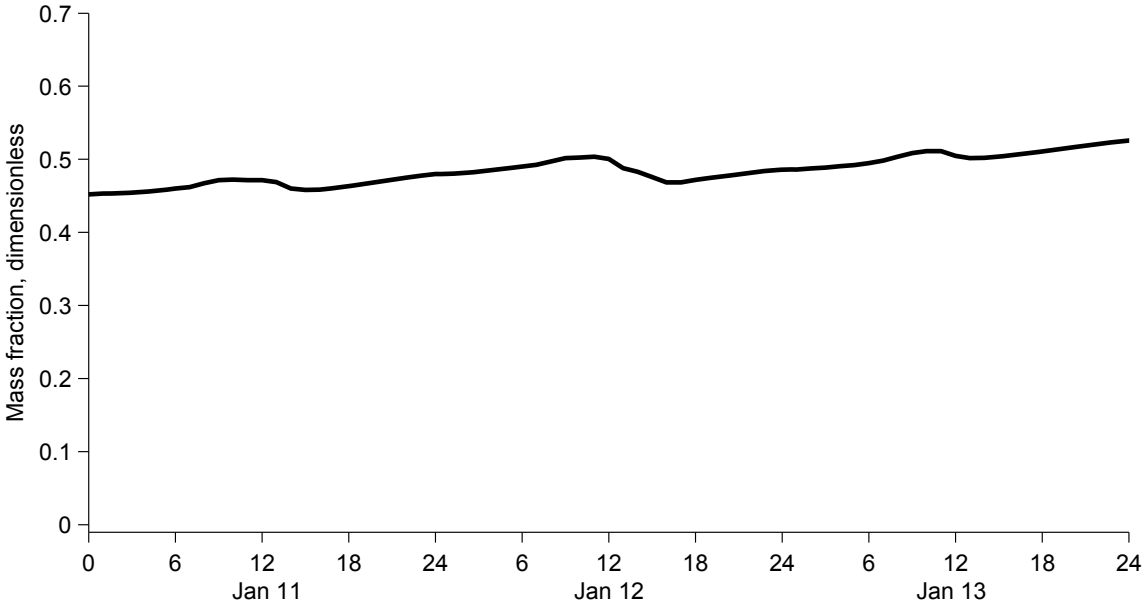

Fig. 5.21 Ice mass fraction of ice storage tank from Jan. 11 to Jan. 13

Electricity use

Fig. 5.22 presents the total electricity consumption of the combisystem during the three day in heating season. The electricity was used to operating the heat pump,

and the circulating pumps $P1$, $P2$, and $P3$. The heat pump used 121 kWh of electricity, the largest amount in the overall. The circulating pumps $P1$, $P2$, and $P3$ used electricity of 0.15 kWh, 0.218 kWh, and 0.237 kWh, respectively.

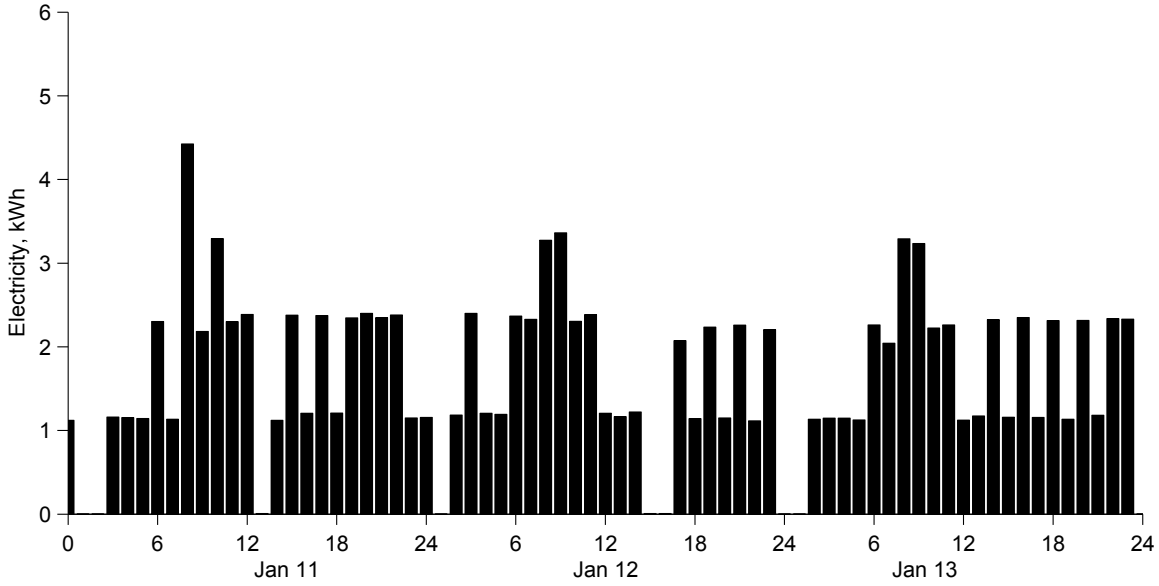

Fig. 5.22 Electricity consumption of solar combisystem from Jan. 11 to Jan. 13

5.4. Response for space heating

As space heating demand for the indoor space, the radiant floor was provided heat from two heat sources, the heat pump and the water storage tank. This section presents the management of the two heat sources to respond the radiant floor and meet the space heating demand, which is the operation of circulation loop $L3$.

Table 5.5 presents the space heating demand and the heat supply to radiant floor. The results showed the space heating demands were satisfied completely, among the heat pump supplied 30.4% and the water storage tank supplied 69.6%. The results

were due to the use of water storage tank was controlled to respond the radiant floor needs for heat at the higher priority (4.9.3). The advantage of the strategy was the space heating demand was matched by operating the circulating pump $P3$ to transfer the demanded amount of heat to the radiant floor. Unlikely, the heat pump (with constant water flows at the evaporator and condenser) lacked of flexibility, in terms of heat output amount. Not using this strategy, the operation would tend to overheat the space, or overheat the water storage tank and further cause the combisystem shut down.

Table 5.5 Results of space heating demand and heat supply to radiant floor

	Space heating demand, kWh	Heat supply, kWh		
		By heat pump	From water storage tank	Overall
October	171.68	23.05	148.63	171.68
November	976.15	220.76	755.39	976.15
December	1,991.79	653.39	1,338.39	1,991.79
January	2,331.04	875.18	1,455.86	2,331.04
February	1,721.11	539.30	1,181.82	1,721.11
March	949.38	187.15	762.24	949.38
April	182.27	29.18	153.09	182.27
Season	8,323	2,528	5,795	8,323
	-	30.4%	69.6%	100%

5.5. Operation of heat pump with ice storage tank

Heat pump performance

Table 5.6 presents the heat pump operation results, including the energy flows and the operation COP over the heating season. Among the heat pump output of 9326 kWh, the water storage tank received 73% (6,799 kWh), more than the radiant floor. The seasonal average COP was 3.19.

Table 5.6 Monthly results of heat pump operation

	Energy input, kWh		Heat output from condenser, kWh			
	Electricity	Heat at evaporator	To radiant floor	To water storage tank	Overall	COP, dimensionless
October	64.64	187.65	23.05	229.24	252.29	3.93
November	367.64	801.98	220.76	948.86	1,169.62	3.19
December	714.98	1,455.79	653.39	1,517.37	2,170.77	3.04
January	854.89	1,611.14	875.18	1,590.85	2,466.04	2.89
February	564.02	1,201.15	539.30	1,225.87	1,765.17	3.13
March	264.50	804.02	187.15	881.38	1,068.52	4.06
April	99.43	334.77	29.18	405.02	434.20	4.41
Year	2,930	6,397	2,528	6,799	9,327	3.19

Fig. 5.23 presents the daily mean COP of heat pump throughout an entire heating season. The daily mean temperature of water entering the evaporator is presented in Fig. 5.24, in Fig. 5.25 presents the daily mean temperature of water entering the condenser. Results shown with the three figures suggested the impact made on the heat pump COP from the inlet temperature at the evaporator side.

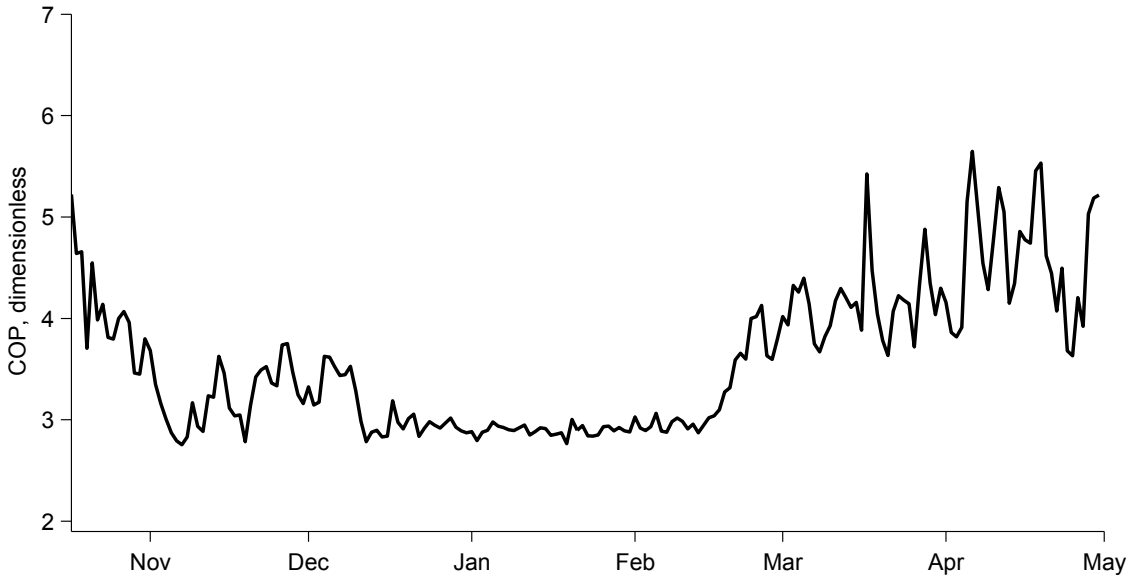

Fig. 5.23 Heat pump COP in heating season, daily mean

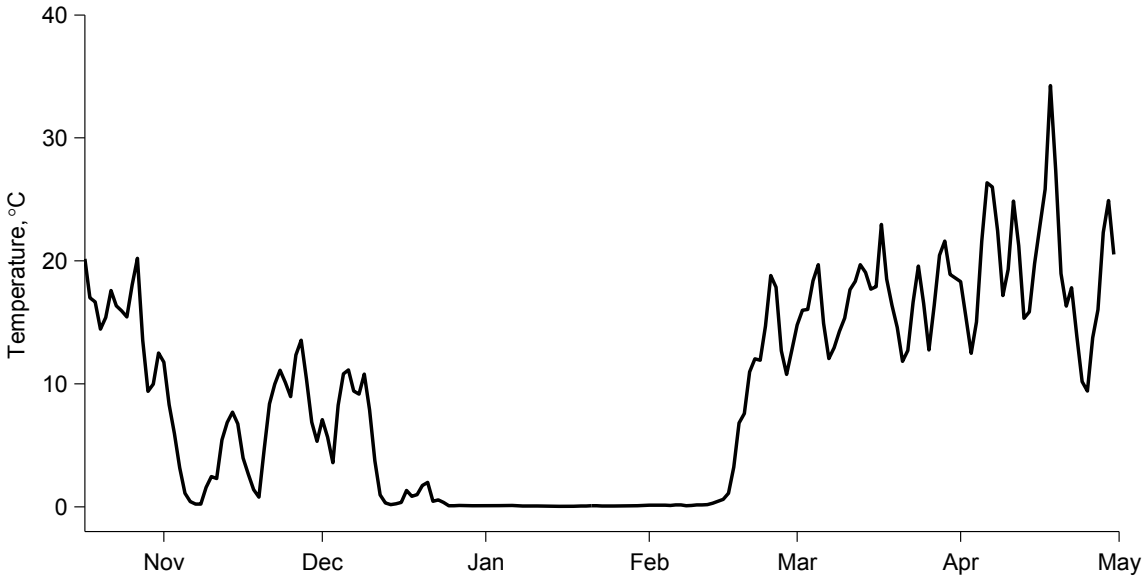

Fig. 5.24 Temperature of water entering heat pump evaporator, daily mean

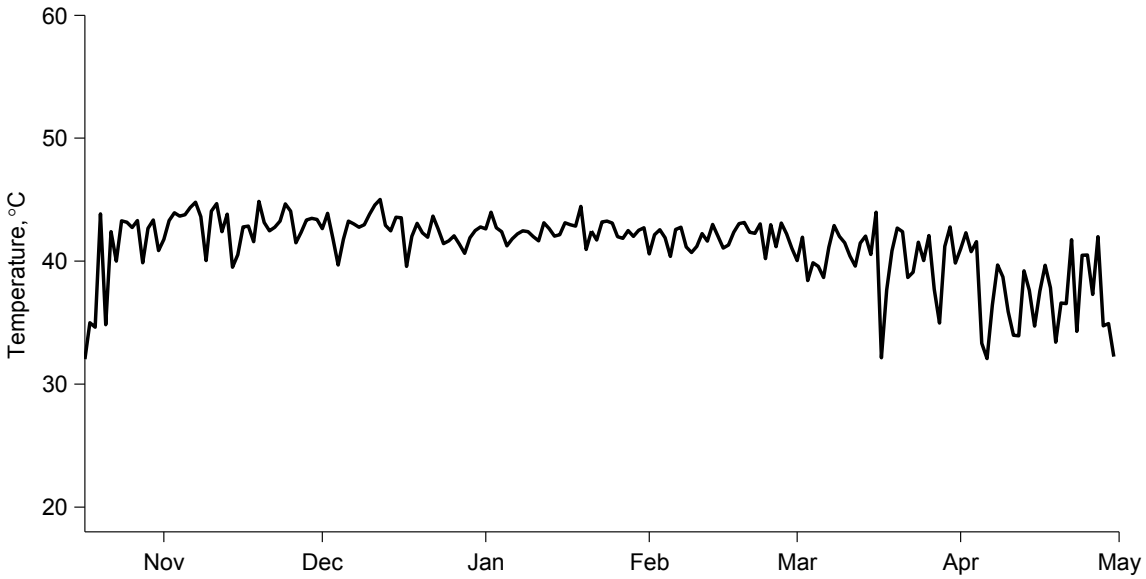

Fig. 5.25 Temperature of water entering heat pump condenser, daily mean

State of water in ice storage tank

Fig. 5.26 presents the mass fraction of ice in the ice storage tank. The ice appeared in November, presenting a stable existence since early December. Throughout one month of accumulation, the mass fraction of ice climbed up to the peak of 0.69 at

the late January. The ice melted away by mid-February. After then and till the end of the heating season, the ice storage tank contained only liquid water.

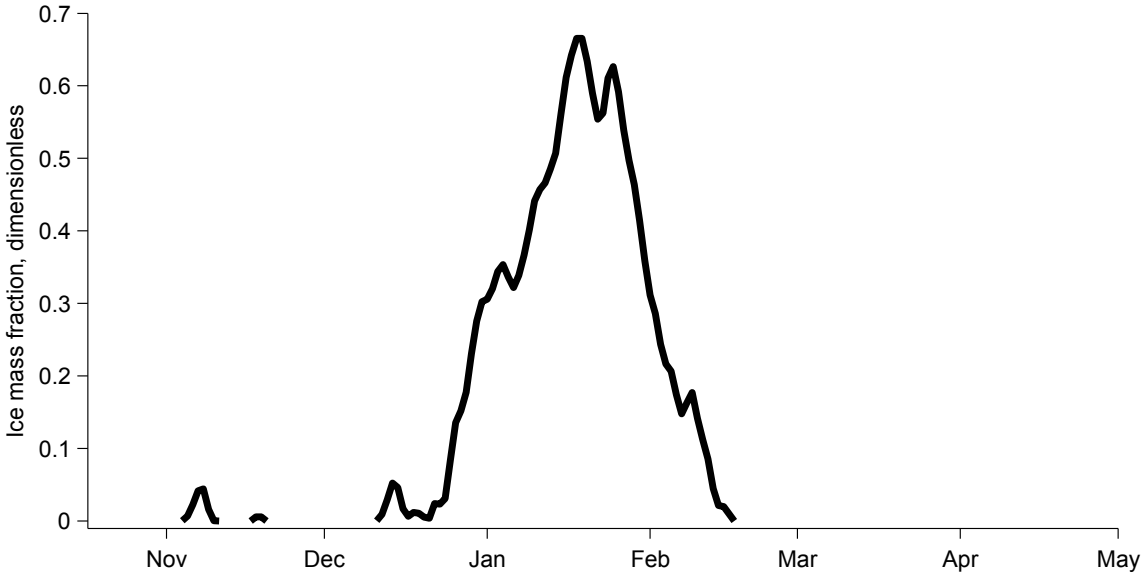

Fig. 5.26 Ice mass fraction of ice storage tank in heating season, daily mean

5.6. Operation of solar collector with thermal storage

Solar heat was an exclusive heat source to the combisystem. Table 5.7 presents the energy flows regarding the operation of solar thermal collectors, as well as the thermal efficiency of solar thermal collectors. During the time when the solar thermal collectors were *on* operation, the annual incident solar energy was 25,067 kWh, the annual solar heat collection was 14,121 kWh, while 10,946 kWh of solar heat failed to be collected and lost to the outdoor environment. The operation of solar thermal collectors had an annual average thermal efficiency of 0.51.

Table 5.7 Monthly results of solar collector operation

	Incident solar radiation, kWh	Solar heat collection, kWh			Heat loss to outdoor environment, kWh	Thermal efficiency of solar collector, dimensionless
		In water storage tank	In ice storage tank	Overall		
January	2,823.18	232.74	1,475.10	1,707.84	1,115.34	0.58
February	3,680.97	289.61	1,933.30	2,222.92	1,458.05	0.57
March	4,714.15	272.66	2,535.08	2,807.75	1,906.41	0.54
April	4,015.50	119.03	2,392.72	2,511.75	1,503.75	0.57
May	1,200.62	433.03	0.00	433.03	767.59	0.31
June	948.72	342.73	0.00	342.73	605.99	0.31
July	725.36	298.52	0.00	298.52	426.83	0.36
August	758.99	274.45	0.00	274.45	484.53	0.31
September	875.64	350.41	0.00	350.41	525.23	0.35
October	1,783.80	217.84	801.05	1,018.88	764.91	0.51
November	1,530.94	99.18	875.26	974.43	556.51	0.62
December	2,008.93	173.25	1,004.75	1,178.00	830.94	0.55
Year	25,067	3,103	11,017	14,121	10,946	0.51

Distribution of solar heat collection

Among the annual solar heat collection (14,121 kWh), the water storage tank received 3,103 kWh of heat throughout an entire year, counted for 22%. The ice storage tank received 11,017 kWh of heat during the heating season (from May 1 to October 16), counted for 78%. The operation of ice storage tank handled the majority of solar heat storage.

Among the annual heat stored in the water storage tank (3,103 kWh), the water storage tank stored 1,870 kWh of heat in the heating season. In addition to the 11,017 kWh of heat stored in the ice storage tank in the heating season, the overall solar heat storage during the heating season was 12,887 kWh, counted for 87% of the annual solar heat collection. The rest 23% of solar heat collection was made during the non-heating season, which was all charged to the water storage tank.

Thermal efficiency of solar collector operation

The two storage tanks, with different levels of operation temperature, made different impact on the performance of solar thermal collector. Table 5.8 presents the thermal efficiency of solar thermal collector by storage tanks, to show the impact made by the entering temperature of collector working fluid.

Table 5.8 Monthly results of thermal efficiency of solar thermal collector

Units: dimensionless

	With water storage tank	With ice storage tank
January	0.30	0.66
February	0.34	0.62
March	0.33	0.58
April	0.31	0.59
May	0.31	-
June	0.31	-
July	0.36	-
August	0.31	-
September	0.35	-
October	0.32	0.59
November	0.26	0.69
December	0.28	0.63
Year	0.32	0.62

Operated with the water storage tank, the solar thermal collector had the annual mean thermal efficiency of 0.32. Operated with the ice storage tank, the solar collector thermal efficiency ranged from 0.58 in March to 0.69 in November, leading the annual mean thermal efficiency of 0.63. The thermal efficiency of solar thermal collector rose about two times when against a cold thermal storage, compared to with a warm thermal storage.

5.7. Operation of water storage tank

Temperature

The water storage tank was modeled as a stratified thermal storage tank. Table 5.9 presents the temperatures of five nodes ($N1$ to 5) in the water storage tank, along with the hot water draw-off temperature. The temperature profile is presented on Fig. 5.27. The results showed that the nodes $N3$, $N4$ & $N5$ have higher monthly average temperatures from May to November than other months.

Table 5.9 Monthly results of water storage tank node temperatures

	Node temperature, ℃						Hot water draw-off temperature, ℃
	N1	N2	N3	N4	N5	Mean	
January	45.3	44.9	45.3	45.1	44.7	45.1	44.8
February	45.2	44.8	45.4	45.3	45.0	45.1	45.1
March	43.8	44.8	46.1	45.9	45.4	45.2	45.5
April	41.7	44.1	45.8	45.9	45.4	44.6	45.5
May	31.3	46.0	57.6	59.7	59.5	50.9	59.6
June	34.5	47.9	58.7	60.3	59.9	52.3	60.0
July	37.8	49.7	59.1	60.6	60.2	53.5	60.2
August	39.7	51.1	59.7	60.7	60.0	54.3	60.2
September	35.9	48.1	58.0	60.2	60.0	52.4	60.0
October	39.0	45.6	51.9	53.5	53.4	48.7	53.3
November	46.3	45.1	45.2	45.0	44.6	45.2	44.6
December	45.6	44.7	44.9	44.8	44.5	44.9	44.5
Year	40.5	46.4	51.5	52.3	51.9	48.5	51.4

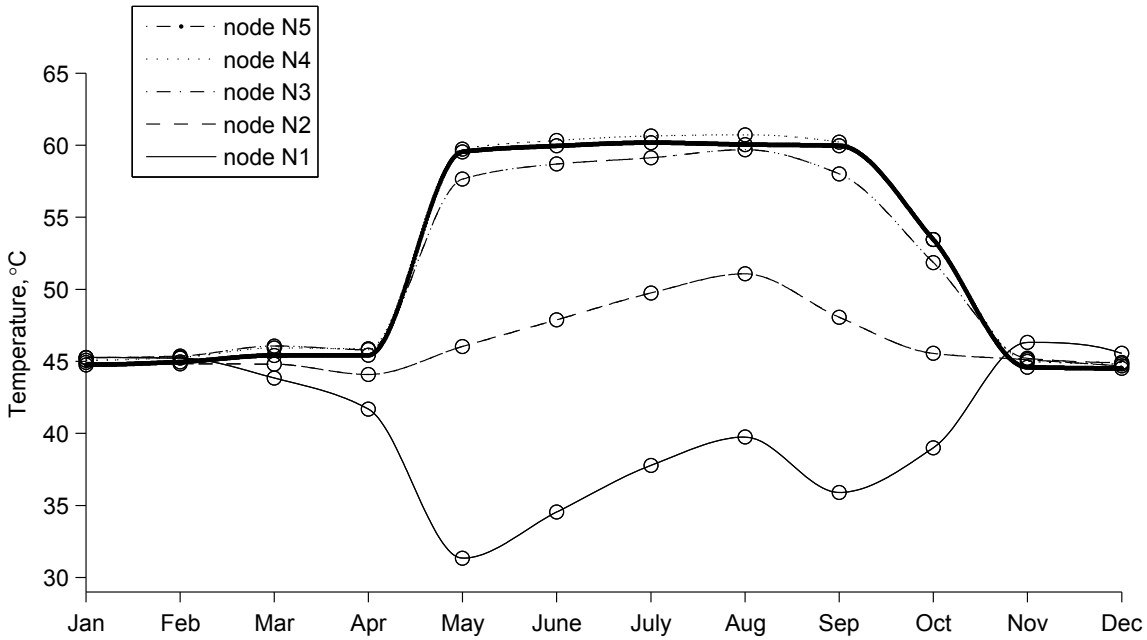

Fig. 5.27 Node temperature of Water storage tank, monthly mean

Heat input and output

The temperature distribution in the water storage tank was the outcome of the heat transfer that the storage tank underwent. Table 5.10 presents the heat flows of the water storage tank operation. The annual heat input was 9,902 kWh. The annual heat output was 9,236 kWh. Due to the temperature difference with the surroundings, the storage tank lost 667 kWh of heat throughout an entire year.

Table 5.10 Monthly results of heat flows of water storage tank

	Heat input, kWh			Heat output, kWh			Heat transfer with surroundings, kWh	Heat storage, kWh
	From solar collector	By heat pump	Overall	To space	For hot water	Overall		
January	232.74	1,590.85	1,823.59	1,455.86	309.10	1,764.96	-51.21	7.43
February	289.61	1,225.87	1,515.49	1,181.82	293.02	1,474.84	-46.33	-5.68
March	272.66	881.38	1,154.04	762.24	346.55	1,108.79	-51.17	-5.91
April	119.03	405.02	524.05	153.09	322.63	475.73	-48.11	0.21
May	433.03	0.00	433.03	0.00	351.81	351.81	-59.46	21.76
June	342.73	0.00	342.73	0.00	279.79	279.79	-60.36	2.58
July	298.52	0.00	298.52	0.00	233.21	233.21	-64.96	0.35
August	274.45	0.00	274.45	0.00	208.46	208.46	-66.50	-0.51
September	350.41	0.00	350.41	0.00	284.46	284.46	-60.91	5.03
October	217.84	229.24	447.08	148.63	260.18	408.81	-56.82	-18.56
November	99.18	948.86	1,048.04	755.39	248.14	1,003.53	-49.98	-5.47
December	173.25	1,517.37	1,690.62	1,338.39	303.09	1,641.48	-50.88	-1.74
Year	3,103	6,799	9,902	5,795	3,440	9,236	-667	-0.51

5.8. Heat transit via thermal storage

The heat transit is referred to the overall transfer of heat through heat charging and heat discharging. The two thermal storage tanks of combisystem bridged the time gap of heat between the available and in needy. Fig. 5.28 presents the heat charges and discharges of the water storage tank over the year. The annual gross of heat transit of the water storage tank is calculated as a sum of the heat charged to the water storage tank and the heat discharged from the water storage tank; the amount was 19,138 kWh. Fig. 5.29 presents the heat charges and discharges of the ice storage tank over the year. The annual gross of heat transit of the ice storage tank is calculated as a sum of the heat charged to the ice storage tank and the heat discharged from the ice storage tank; the amount was 17,414 kWh.

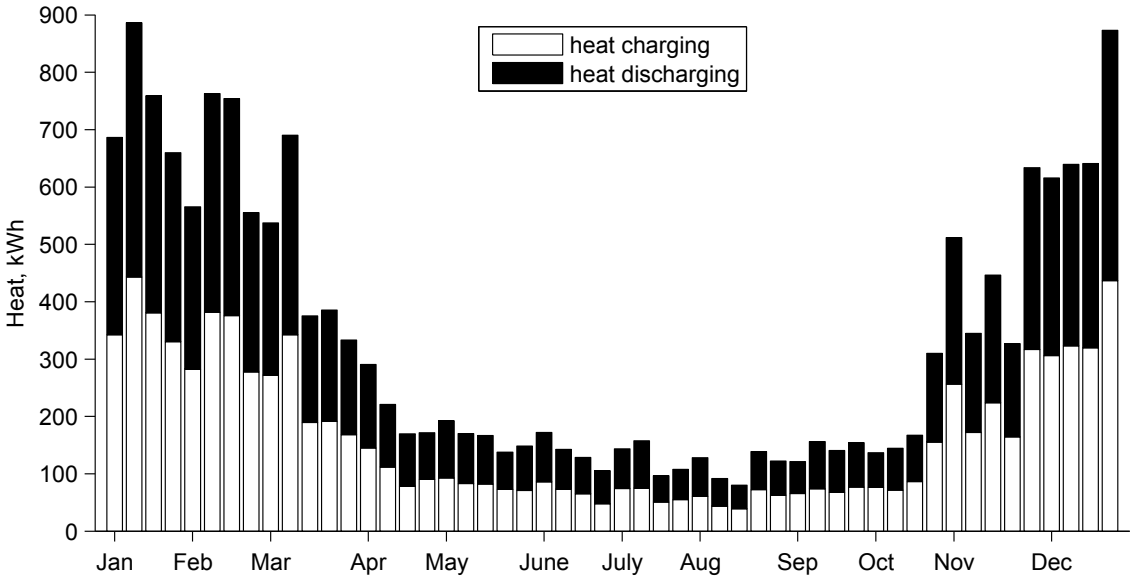

Fig. 5.28 Heat transit via water storage tank, by week

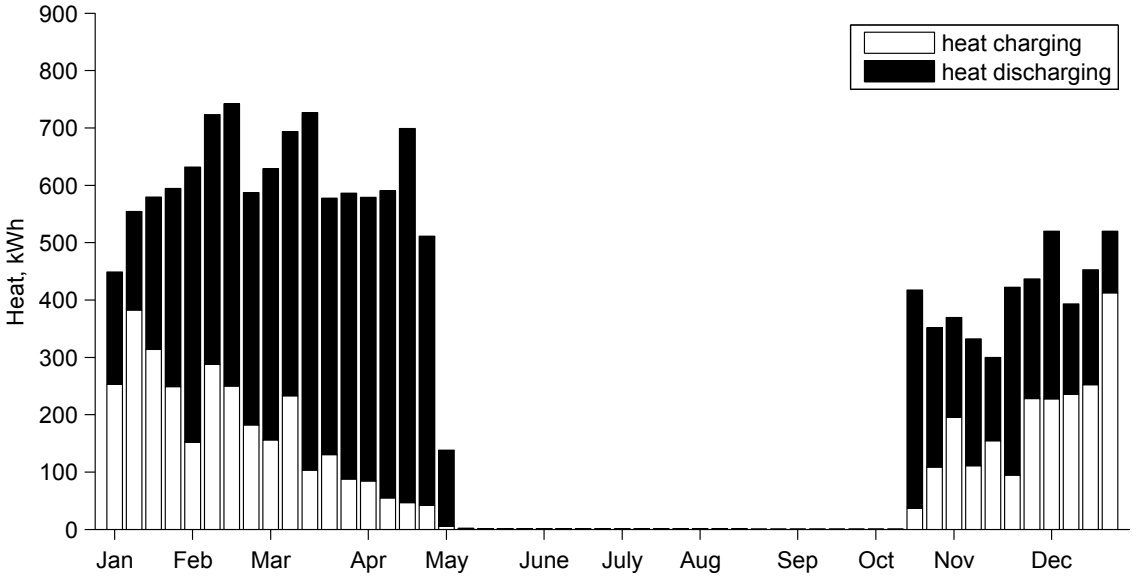

Fig. 5.29 Heat transit via ice storage tank, by week

The annual gross of heat transit via the ice storage tank was 1,724 kWh less than the water storage tank. Counting the two storage tanks together, the overall heat transit was 36,552 kWh. Among this amount, the water storage tank has been in charge of

52.4%, the ice storage tank 47.6%. The results showed the significant performance of the water storage tank in the simulated combisystem annual operation.

5.9. Exergy performance of solar combisystem

Combisystem exergetic COP

The exergetic COP is calculated as the ratio of the exergy of heating load (507 kWh) to the auxiliary electricity consumption (2,956 kWh). The combisystem had an annual exergetic COP of 0.17.

Solar exergy fraction compared to reference system

Table 5.11 presents the exergy used by the specified reference system (i.e., electric heating system), and the exergy collection of the combisystem solar thermal collectors.

Table 5.11 Reference system exergy use vs. combisystem solar exergy collection of solar combisystem

	Reference system			Solar combisystem	
	Electrical exergy use of baseboard heater, kWh	Electrical exergy use of water heater, kWh	Total exergy use, kWh	Collected solar exergy, kWh	Solar exergy fraction, dimensionless
January	2,331.04	277.51	2,608.55	49.85	0.02
February	1,721.11	262.53	1,983.64	95.67	0.05
March	949.38	306.54	1,255.92	226.53	0.18
April	182.27	283.44	465.72	209.86	0.45
May	0.00	213.88	213.88	76.27	0.36
June	0.00	156.79	156.79	61.23	0.39
July	0.00	117.67	117.67	53.70	0.46
August	0.00	100.80	100.80	49.49	0.49
September	0.00	145.52	145.52	62.63	0.43
October	171.68	171.73	343.41	91.19	0.27
November	976.15	218.15	1,194.30	41.64	0.03
December	1,991.79	271.83	2,263.62	49.53	0.02
Year	8,323	2,526	10,850	1,068	0.10

Over the entire year, the solar collectors collected 1,068 kWh of thermal energy. Compared to 10,850 kWh of exergy of heating load by the reference system, the combisystem had a solar exergy fraction of 0.10. The maximum solar exergy fraction appeared in August as of 0.49. The minimum solar exergy fraction of 0.02 appeared in January and December.

Solar exergy contribution

Among 26,421 kWh of exergy, sum of the annual incident solar exergy (23,465 kWh) and the annual electrical exergy, the annual incident solar exergy contribution was 88.8%.

Among 4,024 kWh of exergy, sum of the annual solar exergy collection (1,068 kWh) and the annual electricity consumption, the annual collected solar exergy contribution was 26.5%.

Exergy efficiency

Table 5.12 presents the exergy destruction estimated by monthly and annual operation of the combisystem. The combisystem operation over the year destroyed 15,657 kWh of exergy out of the total 26,421 kWh of exergy supply including the incident solar exergy and electricity. Less exergy were destroyed during May through October than the other months. Among the component equipment, the most amount of exergy was destroyed by operating the solar thermal collector, accounted for 77.6%. Other contributions were: the heat pump 11.2%, the radiant floor 4.3%, the water

storage tank 3.8%, the ice storage tank 2.9%, and the circulating pumps 0.2%. The estimated exergetic efficiency is presented in Table 5.13.

Table 5.12 Monthly results of exergy destroyed by solar combisystem operation

Units:kWh

	Solar combisystem	Solar collectors	Heat pump	Pumps	Auxiliary heater	Ice storage tank	Water storage tank	Radiant floor
January	2,390.27	1,548.87	512.22	4.85	0	21.93	111.51	190.87
February	2,590.32	1,985.22	335.54	4.04	0	35.82	94.76	134.94
March	2,845.44	2,401.82	160.30	3.29	0	140.03	68.58	71.42
April	2,420.35	2,141.41	62.53	2.78	0	172.75	27.54	13.34
May	361.54	329.09	-	0.78	0	2.51E-02	31.65	-
June	285.56	259.60	-	0.67	0	1.23E-02	25.28	-
July	247.54	225.75	-	0.47	0	6.43E-03	21.31	-
August	227.53	207.43	-	0.55	0	3.22E-03	19.55	-
September	289.35	265.39	-	0.51	0	1.58E-03	23.44	-
October	992.11	862.60	38.84	1.44	0	49.06	27.04	13.12
November	1,246.33	870.53	216.00	2.75	0	22.11	54.18	80.76
December	1,760.89	1,053.20	423.84	4.08	0	20.00	95.58	164.18
Year	15,657	12,151	1,749	26	0	462	600	669
	100%	77.6%	11.2%	0.2%	0.0%	2.9%	3.8%	4.3%

Table 5.13 Annual results of exergetic efficiency of solar combisystem operation

Solar combisystem	Solar thermal collectors	Heat pump	Ice storage tank	Water storage tank	Radiant floor
40.7%	9.3%	42.6%	19.0%	61.0%	17.8%

If the exergy destroyed during the solar thermal collector operation is excluded from the analysis, the exergy destroyed was summed to 3,506 kWh and the corresponding exergy efficiency was 12.9% (among 4,024 kWh).

6. Conclusions

This thesis has presented the development of a solar combisystem computer model, implemented in EES program. The work presented in the thesis includes: (i) A methodology for the development of a solar combisystem computer model; (ii) The mathematical models of the solar combisystem model components; (iii) The features of a EES-based computer model of a solar combisystem being developed; (iv) A simulated solar combisystem operation case results; and (v) The analysis of the simulated solar combisystem operating conditions based on the Second Law of thermodynamics.

- The model development basis was the Second Law of thermodynamics, which was chosen for the ability to represent the energy and the quality of the energy related to the solar combisystem operation.
- The mathematical model of the solar combisystem was developed in component approach as of modular type, which left the opportunity for the developed modules to be integrated for models of diverse HVAC systems.
- The mathematical model of solar combisystem was implemented in the EES program, which was chosen for its equation-based scheme, as well as the built-in functions for calculating the thermodynamic properties of working fluids.
- The complete computer model of solar combisystem is suitable for modeling the selected solar combisystem operation as a function of the space heating demand, domestic hot water consumption, outdoor dry-bulb air temperature, and solar

radiation, and subject to the operating control along with the simulation time step assigned by the user.

Operation features

The energy-consuming equipment of the solar combisystem includes the solar thermal collector, circulating pumps, heat pump, and auxiliary heater. The solar thermal collector and the heat pump are the primary energy-consuming components, their energy consumptions are determined not only by the heating requirements and climate condition, but also affected by the entering state of heat transfer fluid. The states at the equipment inlets rely on the operation of thermal storage tanks under the operating control performed on the complete solar combisystem.

- The simulated solar combisystem provided 3,440 kWh of heat for the annual domestic hot water use of a typical one-storey detached house, and met the residential space heating demand of 8,323 kWh throughout a heating season of 196 days with the outdoor temperature the lowest at -28.1 ℃ in Montreal Canada.
- The draw-off temperature of the domestic hot water was 51.4 ℃ in annual average. The supply temperature of the radiant floor was 37.7 ℃ in seasonal average, while the return temperature being controlled at constant 20 ℃.
- Satisfying the annual heating needs of 11,764 kWh in total, the solar combisystem received 14,121 kWh of solar heat from the solar thermal collectors, consumed 2,956 kWh of electricity to run a water-to-water heat

pump and three circulation pumps whereas without starting up the auxiliary electric heater.

- The water storage tank (warm thermal storage) had an annual average temperature of 48.5 ℃.
- The ice storage tank (cold thermal storage) had an annual average temperature of 13.7 ℃.

Energy performance

- The solar combisystem operation represents:
    a. An annual system COP of 3.98;
    b. An annual solar energy fraction of 1.3 compared to an electric heating system;
    c. An annual incident solar energy contribution of 89.5% and an annual collected solar energy contribution of 82.7%;
    d. An annual system energy efficiency of 42.0% regarding the incident solar heat during the collectors *on* operation as the thermal energy input, and of 68.9% regarding the solar heat collection as the thermal energy input.
- The solar thermal collector operation represents:
    a. An annual average thermal efficiency of 0.51;
    b. An annual average thermal efficiency of 0.62 operated against the cold thermal storage;
    c. An annual average thermal efficiency of 0.32 operated against the warm thermal storage.

- The heat pump had a seasonal average COP of 3.19.

Exergy performance

- The solar combisystem destroyed 15,657 kWh of exergy over the annual operation and represents:
    a. An annual exergetic COP of 0.17;
    b. An annual solar exergy fraction of 0.10 compared to an electric heating system;
    c. An annual incident solar exergy contribution of 88.8% and an annual collected solar exergy contribution of 26.5%;
    d. An annual system exergy efficiency of 40.7% regarding the incident solar exergy during the collectors *on* operation as the thermal exergy input, and of 12.9% regarding the solar exergy collection as the thermal exergy input.
- The annual average exergy efficiency was:
    a. 61.0% for the water storage tank;
    b. 19.0% for the ice storage tank;
    c. 9.3% for the solar thermal collectors;
    d. 42.55% for the heat pump;
    e. 17.82% for the radiant floor.

6.1. Future work

I. Model validation

To improve the developed solar combisystem model, validation of the component models and the whole solar combisystem model can be carried out, if installation or experimental setup is available.

II. Analysis of sensitivity

An interesting issue found during the model simulation is that the solar combisystem component capacities, the system operating control, and the combisystem heating performance are closely related. To investigate the three aspects the impact added by one onto the other will provide valuable information for the system application, and favor the solar combisystem operation towards better performance.

III. Solar combi-plus, high solar combi-plus, and optimization

The results showed the drawback of oversizing of the solar combisystem for the simulated case, without cooling load in the non-heating season. A case with solar cooling can be simulated using the developed model with certain modification to investigate a solar combi-plus system operation, to see if able to achieve the performance as a high solar combi-plus system does, and further conduct optimization study. The studied solar combisystem seemed has the potential because the

configuration has both sensible thermal storage and latent thermal storage, plus the configuration is not only complex but also flexible.

IV. Second Law model Library of HVAC components

Similar model development can be done onto other HVAC components for a Second Law model library of simulation programs.

References

Agudelo, A., & Cortés, C. (2010). Thermal Radiation and the Second Law. *Energy*, *35*(2), 679–691.

Aguilar, C., White, D. J., & Ryan, D. L. (2005). CBEEDAC 2005-RP-02 Domestic Water Heating and Water Heater Energy Consumption in Canada. *CBEEDAC Canadian Building Energy End-Use Data and Analysis Centre*. Retrieved May 26, 2011, from http://sedc-coalition.eu/wp-content/uploads/2011/07/CREEDAC-Canadian-Residential-Hot-Water-Apr-2005.pdf

Akpinar, E. K., & Koçyiğit, F. (2010). Energy and Exergy Analysis of a New Flat-Plate Solar Air Heater Having Different Obstacles on Absorber Plates. *Applied Energy*, *87*(11), 3438–3450.

Akyuz, E., Coskun, C., Oktay, Z., & Dincer, I. (2012). A Novel Approach for Estimation of Photovoltaic Exergy Efficiency. *Energy*, *44*(1), 1–8.

Aljundi, I. H. (2009). Energy and Exergy Analysis of a Steam Power Plant in Jordan. *Applied Thermal Engineering*, *29*(2-3), 324–328.

Allard, Y., Kummert, M., Bernier, M., & Moreau, A. (2011). Intermodel Comparison and Experimental Validation of Electrical Water Heater Models in TRNSYS. In *Proceedings of Building Simulation 2011* (pp. 688–695). Conference of International Building Performance Simulation Association, 14-16 November 2011, Sydney, Australia. IBPSA.

Al-Najem, N. M., & El-Refaee, M. M. (1997). A Numerical Study for the Prediction of Turbulent Mixing Factor in Thermal Storage Tanks. *Applied Thermal Engineering*, *17*(12), 1173–1181.

Alta, D., Bilgili, E., Ertekin, C., & Yaldiz, O. (2010). Experimental Investigation of Three Different Solar Air Heaters: Energy and Exergy Analyses. *Applied Energy*, *87*(10), 2953–2973.

Anon. (1977). Heat Pumps: Their Chances Today. *Power*, *121*, 80–83.

Ao, Y., Gunnewiek, L., & Rosen, M. A. (2008). Critical Review of Exergy-Based Indicators for the Environmental Impact of Emissions. *International Journal of Green Energy*, *5*(1-2), 87–104.

Apache Openoffice. (2013). Apache OpenOffice Calc. The Apache Software Foundation.

ASHRAE. (1994). HVAC 1 Toolkit: A Toolkit for Primary HVAC System Energy Calculation. American Society of Heating, Refrigerating and Air-Conditioning Engineers.

ASHRAE. (2004). *ASHRAE Standard 55-2004 Thermal Environmental Conditions for Human Occupancy*. Atlanta, GA: American Society of Heating, Refrigerating and Air-Conditioning Engineers.

ASHRAE. (2007). Service Water Heating. In *ASHRAE Handbook. HVAC Applications* (pp. 49.1–29). Atlanta, Ga.: American Society of Heating, Refrigerating and Air-Conditioning Engineers.

ASHRAE. (2009a). Energy Estimating and Modeling Methods. In *ASHREA Handbook. Fundamentals* (pp. 19.1–38). Atlanta, Ga.: American Society of Heating, Refrigerating and Air-Conditioning Engineers.

ASHRAE. (2009b). Thermal Storage. In *ASHREA Handbook. Fundamentals* (pp. 34.1–33). Atlanta, Ga.: American Society of Heating, Refrigerating and Air-Conditioning Engineers.

ASHRAE. (2009c). Heat, Air, and Moisture Control in Building Assemblies— Material Properties. In *ASHREA Handbook. Fundamentals* (pp. 26.1–22). Atlanta, Ga.: American Society of Heating, Refrigerating and Air-Conditioning Engineers.

ASHRAE. (2011). *Fundamentals of HVAC Control Systems* (p. 354). Atlanta, GA: American Society of Heating, Refrigerating and Air-Conditioning Engineers.

ASHRAE TC7.4. (2013). ASHRAE TC7.4 Exergy Analysis For Sustainable Buildings. *ASHRAE Technical Committee 7.4*. Retrieved November 17, 2013, from http://tc74.ashraetcs.org/

Badescu, V. (2002). First and Second Law Analysis of a Solar Assisted Heat Pump Based Heating System. *Energy Conversion and Management*, *43*(18), 2539–2552.

Bahnfleth, W. P., & Song, J. (2005). Constant Flow Rate Charging Characteristics of a Full-Scale Stratified Chilled Water Storage Tank with Double-Ring Slotted Pipe Diffusers. *Applied Thermal Engineering*, *25*(17-18), 3067–3082.

Baker, J. (2008). New Technology and Possible Advances in Energy Storage. *Energy Policy*, *36*(12), 4368–4373.

Bakirci, K., & Yuksel, B. (2011). Experimental Thermal Performance of a Solar Source Heat-Pump System for Residential Heating in Cold Climate Region. *Applied Thermal Engineering*, *31*(8-9), 1508–1518.

Balaras, C. A., Dascalaki, E. G., Tsekouras, P., & Aidonis, A. (2010). High Solar Combi Systems in Europe. *ASHRAE Transactions*, *116*, 408–415.

Behschnitt, S. A. (1996). *A Comparison of Water-Ethalnol, Pure Water and Ice as Storage Media for Building Thermal Storage Applications*. Master Thesis. University of Wisconsin-Madison, Madison, USA.

Bejan, A., Kearney, D. W., & Kreith, F. (1981). Second Law Analysis and Synthesis of Solar Collector Systems. *Solar Energy Engineering*, *103*, 23–28.

Bjurstrom, H., & Carlsson, B. (1985). An Exergy Analysis of Sensible and Latent Heat Storage. *Heat Recovery Systems*, *5*(3), 233–250.

BLAST Support Office. (1991). *Blast User Reference*. Urbana-Champaign, Illinois: BLAST Support Office, Department of Mechanical and Industrial Engineering, University of Illinois.

Bong, T. Y. (1983). Toward an Efficient Operation of a Series Solar Heat Pump System. *ASHRAE Transactions*, *89*(2A), 617–627.

Brandemeuhl, M. (1993). HVAC 2 Toolkit: A Toolkit for Secondary HVAC System Energy Calculations. American Society of Heating, Refrigerating, and Air-Conditioning Engineers.

Brandemuehl, M. J., & Gabel, S. (1994). Development of a Toolkit for Secondary HVAC Sytem Energy Calculations. *ASHRAE Transactions*, *100*(1), 21–32.

Buhl, W. F., Erdem, A. E., Winkelmann, F. C., & Sowell, E. F. (1993). Recent Improvements in SPARK: Strong Component Decomposition, Multivalued Objects, and Graphical Interface. In *Proceedings of Building Simulation'93*. Conference of International Building Performance Simulation Association, 16-18 August 1993, Adelaide, Australia. IBPSA.

Building Technologies Office. (2013). *EnergyPlus Engineering Reference* (p. 1348). University of Illinois, Ernest Orlando Lawrence Berkeley National Laboratory.

California Energy Commission. (2005). CEC-500-2005-161 Hot Water Distribution System Research – Phase I Final Report. *California Energy Commission Public Interest Energy Research (PIER) Program*. Retrieved December 05, 2012, from http://www.google.ca/url?sa=t&rct=j&q=&esrc=s&source=web&cd=1&cad=rja&ved=0CCsQFjAA&url=http%3A%2F%2Fwww.cuwcc.org%2FWorkArea%2Fdownloadasset.aspx%3Fid%3D2178&ei=xhqPUujnJcm0qgG-gYGgDQ&usg=AFQjCNG43xcoHfeQMujHzHAL3hnw4WuUBg&bvm=bv.56988011,d.aWM

Cengel, Y. A., & Boles, M. A. (2002). *Thermodynamics: An Engineering Approach* (4th ed., p. 821). New York: McGraw-Hill.

Chandrashekar, M., Le, N. T., Sullivan, H. F., & Hollands, K. G. T. (1982). A Comparative Study of Solar Assisted Heat Pump Systems for Canadian Locations. *Solar Energy*, *28*, 217–226.

Chow, T. T. (2010). A Review on Photovoltaic/Thermal Hybrid Solar Technology. *Applied Energy*, *87*(2), 365–379.

Church, K. (2008). Cascadia: An Exergetic Approach to Neighbourhood Design. ECBCS Annex 49. Retrieved April 30, 2012, from http://www.annex49.com/tools/02_Cascadia.zip

Consolar. (2012). Solus II Highest Energy Savings on Hot Water and Heating. *Greenshop Group*. Retrieved June 15, 2011, from http://www.consolar.de/fileadmin/Consolar/user/downloads_EN/PI/PI_EN-SOLUS_II-WEB.pdf

Crawley, D. B., Lawrie, L. K., Winkelmann, F. C., Buhl, W. F., Huang, Y. J., Pedersen, C. O., … Glazer, J. (2001). EnergyPlus: Creating a New-Generation Building Energy Simulation Program. *Energy and Buildings*, *33*, 319–331.

Cruickshank, C. A., & Harrison, S. J. (2010). Heat Loss Characteristics for a Typical Solar Domestic Hot Water Storage. *Energy and Buildings*, *42*(10), 1703–1710.

Cruickshank, C. A., & Harrison, S. J. (2011). Thermal Response of a Series- and Parallel-Connected Solar Energy Storage to Multi-Day Charge Sequences. *Solar Energy*, *85*(1), 180–187.

Day, A. R., & Karayiannis, T. G. (1994). Solar-Assisted Heat Pump Research and Development. *Building Services Engineering Research and Technology*, *15*(2), 71–80.

Dewulf, J., Van Langenhove, H., Muys, B., Bruers, S., Bakshi, B. R., Grubb, G. F., … Sciubba, E. (2008). Critical Review Exergy: Its Potential and Limitations in Environmental Science and Technology. *Environmental Science & Technology*, *42*(7), 2221–2232.

Dincer, I. (2002). On Thermal Energy Storage Systems and Applications in Buildings. *Energy and Buildings*, *34*, 377–388.

Dincer, I., & Rosen, M. A. (2005). Thermodynamic Aspects of Renewables and Sustainable Development. *Renewable and Sustainable Energy Reviews*, *9*(2), 169–189.

Dincer, I., & Rosen, M. A. (2011). *Thermal Energy Storage* (2nd ed., p. 599). Chichester, U.K.: Wiley.

Duffie, J. A., & Beckman, W. A. (2006). *Solar Engineering of Thermal Processes* (3rd ed., p. 908). Hoboken, N.J.: Wiley.

Dumas, M., & Marcoux, C. (2004). Variation Annuelle de la Température de L'eau dans le Réseau d'aqueduc de Montréal. *ASHRAE Montréal*. Retrieved October 27, 2006, from http://www.ashrae-mtl.org/text/a_ashrae.html

Durmayaz, A., & Yavuz, H. (2001). Exergy Analysis of a Pressurized-Water Reactor. *Applied Energy*, *69*, 39–57.

ECBCS A37. (2003). IEA ECBCS Annex 37 Low Exergy Systems for Heating and Cooling. *IEA Energy in Buildings and Communities Programme*. Retrieved March 03, 2012, from http://www.ecbcs.org/annexes/annex37.htm

ECBCS A49. (2010). IEA ECBCS Annex 49 Low Exergy Systems for High Performance Buildings and Communities. *IEA Energy in Buildings and Communities Programme*. Retrieved August 06, 2012, from http://www.ecbcs.org/annexes/annex49.htm

Edgerton, R. H. (1980). Second Law and Radiation. *Energy*, *5*, 693–707.

Ehyaei, M. A., Mozafari, A., Ahmadi, A., Esmaili, P., Shayesteh, M., Sarkhosh, M., & Dincer, I. (2010). Potential Use of Cold Thermal Energy Storage Systems for Better Efficiency and Cost Effectiveness. *Energy and Buildings*, *42*(12), 2296–2303.

Ellehauge, K. (2003). Solar Combisystems Final Report: Key Issues in Solar Thermal (Solar Thermal Technology Promotion). *European Altener Programme*. Retrieved March 17, 2011, from http://www.google.ca/url?sa=t&rct=j&q=&esrc=s&source=web&cd=1&cad=rja&ved=0CCsQFjAA&url=http://www.elle-kilde.dk/altener-combi/dwload/combisystems-final_2003-05-20.pdf&ei=txyPUr_xMoWgqAGckIDQDQ&usg=AFQjCNHIl4WRxb2Dd1Ri40mwdLUkrYdSaQ&bvm=bv.56988011,d.aWM

EU HighCombi. (2011). High Combi Project. *European Union HIGH COMBI Project*. Retrieved November 17, 2013, from http://www.highcombi.eu/

Ezan, M. A., Erek, A., & Dincer, I. (2011). Energy and Exergy Analyses of an Ice-on-Coil Thermal Energy Storage System. *Energy*, *36*(11), 6375–6386.

Fan, J., & Furbo, S. (2012a). Thermal Stratification in a Hot Water Tank Established by Heat Loss from the Tank. *Solar Energy*, *86*(11), 3460–3469.

Fan, J., & Furbo, S. (2012b). Buoyancy Driven Flow in a Hot Water Tank due to Standby Heat Loss. *Solar Energy*, *86*(11), 3438–3449.

Freeman, T. L., Mitchell, J. W., & Audit, T. E. (1979). Performance of Combined Solar-Heat Pump Systems. *Solar Energy*, *22*, 125–135.

FSEC. (2010). FSEC Standard 101-10 Operation of the Solar Thermal Collector Certification Program. *Florida Solar Energy Center*. Retrieved October 28, 2011, from http://www.fsec.ucf.edu/en/publications/pdf/standards/FSECstd_101-10.pdf

Furbo, S., Andersen, E., Thür, A., Shah, L. J., & Andersen, K. D. (2005). Performance Improvement by Discharge from Different Levels in Solar Storage Tanks. *Solar Energy*, *79*(5), 431–439.

Furbo, S., Vejen, N. K., & Shah, L. J. (2005). Thermal Performance of a Large Low Flow Solar Heating System with a Highly Thermally Stratified Tank. *Journal of Solar Energy Engineering*, *127*(1), 15.

Gaggioli, R. A. (2010). Teaching Elementary Thermodynamics and Energy Conversion: Opinions. *Energy*, *35*(2), 1047–1056.

GeoSmart. (2012). Premium H. *GeoSmart Energy*. Retrieved March 05, 2013, from http://geosmartenergy.com/geothermal-energy/geothermal-products/hydronic-system.html

Glembin, J., & Rockendorf, G. (2012). Simulation and Evaluation of Stratified Discharging and Charging Devices in Combined Solar Thermal Systems. *Solar Energy*, *86*(1), 407–420.

Haller, M. Y., Cruickshank, C. A., Streicher, W., Harrison, S. J., Andersen, E., & Furbo, S. (2009). Methods to Determine Stratification Efficiency of Thermal Energy Storage Processes– Review and Theoretical Comparison. *Solar Energy*, *83*(10), 1847–1860.

Haller, M. Y., Streicher, W., Andersen, E., & Furbo, S. (2008). Comparative Analysis of Thermal Energy Storage Stratification Efficiency— a New Method Combines Advantages of Previous Approaches. In *Proceedings of EffStock 2009*. 11th International Conference on Thermal Energy Storage for Efficiency and Sustainability, 14-17 June 2009, Stockholm, Sweden.

Harris, G. G. M. (1957). The Heat Pump, Its Relation to Solar Energy and Heat Storage. *Electrical News and Engineering*, *66*(1), 60–63.

Hasnain, S. M. (1998). Review on Sustainable Thermal Energy Storage Technologies, Part II: Cool Thermal Storage. *Energy Conversion and Management*, *39*(11), 1139–1153.

Hastings, S. R., & Wall, M. (2007). *Sustainable Solar Housing*. London; Sterling, VA: Earthscan.

Hugo, A. (2008). *Computer Simulation and Life Cycle Analysis of a Seasonal Thermal Storage System in a Residential Building*. Master Thesis. Concordia University, Montreal, Canada.

Hugo, A., Zmeureanu, R., & Rivard, H. (2010). Solar Combisystem with Seasonal Thermal Storage. *Journal of Building Performance Simulation*, *3*(4), 255–268.

IEA HPC. (2012). Heat Pump Technology. *IEA Heat Pump Programme*. Retrieved October 05, 2012, from http://www.heatpumpcentre.org/en/aboutheatpumps/heatpumptechnology/Sidor/default.aspx

IEA-SHC T44/A38. (2011). Solar and Heat Pump Systems Industry Newsletter. *IEA-SHC Task 44/ Annex 38*. Retrieved February 08, 2012, from http://www.heatpumpcentre.org/en/projects/ongoingprojects/annex38/Documents/2011-01_Newsletter_Final (2).pdf

IEE SolarCombi+. (2010). Solar Combi+ Project. *Intelligent Energy Europe SolarCombi+ Project*. Retrieved January 07, 2012, from http://www.solarcombiplus.eu/index_en.htm

Ievers, S., & Lin, W. (2009). Numerical Simulation of Three-Dimensional Flow Dynamics in a Hot Water Storage Tank. *Applied Energy*, *86*(12), 2604–2614.

IPCC WGI. (2013). Working Group I Contribution to the IPCC Fifth Assessment Report, Climate Change 2013: The Physical Science Basis Summary for Policymakers. *IPCC Working Group I*. Retrieved September 27, 2013, from http://www.climatechange2013.org/images/uploads/WGIAR5-SPM_Approved27Sep2013.pdf

Ismail, K. A. R., Leal, J. F. B., & Zanardi, M. A. (1997). Models of Liquid Storage Tanks. *Energy*, *22*(8), 805–815.

Itard, L. (2003). H.e.n.k., A Software Tool for the Integrated Design of Buildings and Installations in the Early Design Stage. In *Proceedings of Building Simulation 2003* (pp. 555–562). 8th International IBPSA Conference, 11-14 August 2003, Eindhoven, Netherlands. IBPSA.

Itard, L. (2005). Implementation of Exergy— Calculations in an Existing Software State Tool for Exergy-Flow Calculations in the Early Design Stage. In *Proceedings of Building Simulation 2005* (pp. 459–466). 9th International IBPSA Conference, 15-18 August 2005, Montreal, Canada. IBPSA.

Jeter, S. M. (1981). Maximum Conversion Efficiency for the Utilization of Direct Solar Radiation. *Solar Energy*, *26*, 231–236.

JJH/LBNL. (2013). DOE-2 Based Building Energy Use and Cost Analysis Software. *EnerLogic and James J. Hirsch & Associates*. Retrieved November 25, 2013, from http://doe2.com/

Jordan, U., & Furbo, S. (2005). Thermal Stratification in Small Solar Domestic Storage Tanks Caused by Draw-offs. *Solar Energy*, *78*(2), 291–300.

Jordan, U., & Vajen, K. (2001). *Realistic Domestic Hot-Water Profiles in Different Time Scales*. IEA SHC Task 26: Solar Combisystems.

Karagiorgas, M., Galatis, K., Tsagouri, M., Tsoutsos, T., & Botzios-Valaskakis, A. (2010). Solar Assisted Heat Pump on Air Collectors: A Simulation Tool. *Solar Energy*, *84*(1), 66–78.

Kennedy, M. C., & O'Hagan, A. (2001). Bayesian Calibration of Computer Models. *Journal of the Royal Statistical Society: Series B (Statistical Methodology)*, *63*(3), 425–464.

Klein, S. A. (2006). TRNSYS: Transient Systems Simulation Program.

Klein, S. A. (2012). Engineering Equation Solver Academic Commercial v.9.215-3D. F-Chart Software.

Kleinbach, E. M. (1990). *Performance Study of One-Dimensional Models for Stratified Thermal Storage Tank*. Master Thesis. University of Wisconsin-Madison, Madison, USA.

Kleinbach, E. M., Beckman, W. A., & Klein, S. A. (1993). Performance Study of One-Dimensional Models for Stratified Thermal Storage Tanks. *Solar energy*, *50*, 155–166.

Koroneos, C., & Tsarouhis, M. (2012). Exergy Analysis and Life Cycle Assessment of Solar Heating and Cooling Systems in the Building Environment. *Journal of Cleaner Production*, *32*, 52–60.

Kreith, F., & Bohn, M. S. (2001). *Principles of Heat Transfer* (6th ed.). Australia: Brooks/Cole Pub.

Kugle, S., Green, S., Haji-Sheikh, A., & Lou, D. Y. S. (1984). Performance of Solar Assisted Heat Pump Sytems in Residential Applications. *Solar Energy*, *32*(2), 169–179.

Kush, E. A. (1980). Performance of Heat Pumps at Elevated Evaporating Temperatures with Application to Solar Input. *Journal of Solar Energy Engineering*, *102*, 203–210.

Laughlin, R. B. (2011). *Powering the Future: How We Will (Eventually) Solve the Energy Crisis and Fuel the Civilization of Tomorrow* (p. 224). New York: Basic Books.

Leckner, M. (2008). *Life Cycle Energy and Cost Analysis of a Net Zero Energy House (NZEH) Using a Solar Combisystem*. Master Thesis. Concordia University, Montreal, Canada.

Leckner, M., & Zmeureanu, R. (2011). Life Cycle Cost and Energy Analysis of a Net Zero Energy House with Solar Combisystem. *Applied Energy*, *88*(1), 232–241.

Lemmon, E. W., Huber, M. L., & Mclinden, M. O. (2013). NIST Reference Fluid Thermodynamic and Transport Properties— REFPROP v.9.1 User's Guide. *National Institute of Standards and Technology*.

Loehrke, R. I., Gari, H. N., Sharp, M. K., & Haberstroh, R. D. (1978). A Passive Technique for Enhancing Thermal Stratification in Liquid Storage Tanks. *ASME*, (78-HT-50).

Lund, P. D. (2005). Sizing and Applicability Considerations of Solar Combisystems. *Solar Energy*, *78*(1), 59–71.

Maciejewski, P. K. (1996). Evidence of a Convective Instability Allowing Warm Water to Freeze in Less Time than Cold Water. *Journal of Heat Transfer*, *118*, 65–72.

Mathworks. (2011). MATLAB R2011b 7.13.0.564. The Mathworks.

Metz, W. D. (1977). Solar Thermal Energy: Bringing the Pieces Together. *Science*, *197*(4304), 650–651.

Microsoft. (2013). Microsoft Excel. Microsoft Corporation.

Molinari, M. (2011). S.E.P.E.: An Exergy Analysis and Optimization Tool. *ECBCS Annex 49*. Retrieved February 11, 2012, from http://www.annex49.com/tools/03_SEPE.zip

Moran, M. J., & Shapiro, H. N. (1999). *Fundamentals of Engineering Thermodynamics* (4th ed., p. 918). New York : Wiley.

Moreno-Rodríguez, A., González-Gil, A., Izquierdo, M., & Garcia-Hernando, N. (2012). Theoretical Model and Experimental Validation of a Direct-Expansion Solar Assisted Heat Pump for Domestic Hot Water Applications. *Energy*, *45*(1), 704–715.

Myers, G. E. (1992). Equilibrium via Element Potentials and Computers. Winter Annual Meeting of the American Society of Mechanical Engineers, 8-13 November 1992, Anaheim, USA. ASME.

Nelson, J. E. B., Balakrishnan, A. R., & Murthy, S. S. (1998). Transient Analysis of Energy Storage in a Thermally Stratified Water Tank. *International Journal of Energy Research*, *22*, 867–883.

Nelson, J. E. B., Balakrishnan, A. R., & Murthy, S. S. (1999a). Parametric Studies on Thermally Stratified Chilled Water Storage Systems. *Applied Thermal Engineering*, *19*, 89–115.

Nelson, J. E. B., Balakrishnan, A. R., & Murthy, S. S. (1999b). Experiments on Stratified Chilled-Water Tanks. *International Journal of Refrigeration*, *22*, 216–234.

Ng Cheng Hin, J. (2013). *Life Cycle Optimization of a Residential Solar Combisystem for Minimum Cost, Energy Use and Exergy Destroyed*. Master Thesis. Concordia University, Montreal, Canada.

Ng Cheng Hin, J., Zmeureanu, R., & Rosen, M. A. (2013). Exergy Analysis of a Residential Thermal Storage System. In *Proceedings of CCTC 2013*. 3rd Climate Change Technology Conference, 27-29 May 2013, Montreal, Canada. EIC.

NRCan-OEE. (2012). Total End-Use Sector— Energy Use Analysis. *Natural Resources Canada Office of Energy Efficiency*. Retrieved October 09, 2012, from http://oee.nrcan.gc.ca/corporate/statistics/neud/dpa/tablesanalysis2/aaa_ca_1_e_4.cfm?attr=0

Olesen, B. W. (1977). Thermal Comfort Requirements for Floors Occupied by People with Bare Feet. *ASHRAE Transactions*, *83*, 41–57.

Oppel, F. J., Ghajar, A. J., & Moretti, P. M. (1986). Computer Simulation of Stratified Heat Storage. *Applied Energy*, *23*, 205–224.

Palacios, E., Admiraal, D. M., Marcos, J. D., & Izquierdo, M. (2012). Experimental Analysis of Solar Thermal Storage in a Water Tank with Open Side Inlets. *Applied Energy*, *89*(1), 401–412.

Panek, J., & Johnson, S. (1994). *FERMILAB-TM-1874 Cryogenic Process Simulation*. Fermi National Accelerator Laboratory. Retrieved from http://lss.fnal.gov/archive/test-tm/1000/fermilab-tm-1874.pdf

Panthalookaran, V., Heidemann, W., & Müller-Steinhagen, H. (2007). A New Method of Characterization for Stratified Thermal Energy Stores. *Solar Energy*, *81*(8), 1043–1054.

Papillon, P., Nielsen, J. E., Cholin, X., Letz, T., Thür, A., Kuhness, G., … Drueck, H. (2010). Solar Combisystems Promotion and Standardisation Final Report. *Intelligent Energy Europe COMBISOL Project*. CombiSol. Retrieved October 10, 2012, from http://eaci-projects.eu/iee/fileshow.jsp?att_id=16647&place=pa&url=http://CombiSol Publishable Report[1].pdf&prid=1491

Park, C., Clark, D. R., & Kelly, G. E. (1985). An Overview of HVACSIM+, A Dynamic Building/HVAC/Control Systems Simulation Program. In *Proceedings of the 1st Annual Building Energy Simulation Conference*. 21-22 August 1985, Seattle, WA.

Parrott, J. E. (1978). Theoretical Upper Limit to the Conversion Efficiency of Solar Energy. *Solar Energy*, *21*(3), 227–229.

Petela, R. (1964). Exergy of Heat Radiation. *Journal of Heat Transfer*, *86*, 187–192.

Petela, R. (2005). Exergy Analysis of the Solar Cylindrical-Parabolic Cooker. *Solar Energy*, *79*(3), 221–233.

Petela, R. (2010). *Engineering Thermodynamics of Thermal Radiation: For Solar Power Utilization* (p. 399). New York: McGraw Hill.

Raffenel, Y., Fabrizio, E., Virgone, J., Blanco, E., & Filippi, M. (2009). Integrated Solar Heating Systems: From Initial Sizing Procedure to Dynamic Simulation. *Solar Energy*, *83*(5), 657–663.

Rhee, J., Campbell, A., Mariadass, A., & Morhous, B. (2010). Temperature Stratification from Thermal Diodes in Solar Hot Water Storage Tank. *Solar Energy*, *84*(3), 507–511.

Rosen, M. A. (2001a). The Exergy of Stratified Thermal Energy Storages. *Solar Energy*, *71*(3), 173–185.

Rosen, M. A. (2001b). Energy- and Exergy-Based Comparison of Coal-Fired and Nuclear Steam Power Plants. *Exergy, An International Journal*, *1*(3), 180–192.

Rosen, M. A., & Dincer, I. (2001). Exergy as the Confluence of Energy, Environment and Sustainable Development. *Exergy, An International Journal*, *1*(1), 3–13.

Rosen, M. A., Dincer, I., & Kanoglu, M. (2008). Role of Exergy in Increasing Efficiency and Sustainability and Reducing Environmental Impact. *Energy Policy*, *36*(1), 128–137.

Rosen, M. A., Leong, W. H., & Le, M. N. (2001). Modelling and Analysis of Building Systems that Integrate Cogeneration and District Heating and Cooling. In

Proceeding of eSim 2001 Conference (pp. 187–194). 13-14 June 2001, Ottawa, Canada. IBPSA-Canada.

Rosen, M. A., Pedinelli, N., & Dincer, I. (1999). Energy and Exergy Analysis of Cold Thermal Storage Systems. *International Journal of Energy Research*, *1038*(February), 1029–1038.

Rosen, M. A., Tang, R., & Dincer, I. (2004). Effect of Stratification on Energy and Exergy Capacities in Thermal Storage Systems. *International Journal of Energy Research*, *28*(2), 177–193.

Sargent, R. G. (2011). Verification and Validation of Simulation Models. In *Proceedings of the 2011 Winter Simulation Conference* (pp. 183–198). Institute of Electrical and Electronics Engineers, 11-14 December 2011, Phoenix, Arizona, USA.

Schmidt, D. (2004). Design of Low Exergy Buildings— Method and a Pre-Design Tool. *International Journal of Low Energy and Sustainable Buildings*, *3*, 1–47.

Shah, L. J., & Furbo, S. (2003). Entrance Effects in Solar Storage Tanks. *Solar Energy*, *75*(4), 337–348.

SHC T26. (2012). IEA SHC Task 26 Solar Combisystems. *IEA Solar Heating and Cooling Programme*. Retrieved October 09, 2012, from http://www.iea-shc.org/task26/

SHC T44A38. (2011). IEA-SHC Task 44/ Annex 38 Solar and Heat Pump Systems Industry Newsletter First Issue. *IEA Solar Heating and Cooling Programme & IEA Heat Pump Programme*. Retrieved January 07, 2012, from http://www.heatpumpcentre.org/en/projects/ongoingprojects/annex38/Documents/2011-01_Newsletter_Final (2).pdf

Shenoy, A. (2004). *Simulation, Modeling and Analysis of a Water to Air Heat Pump*. Master Thesis. Oklahoma State University, Stillwater, USA.

Shin, M.-S., Kim, H.-S., Jang, D.-S., Lee, S.-N., Lee, Y.-S., & Yoon, H.-G. (2004). Numerical and Experimental Study on the Design of a Stratified Thermal Storage System. *Applied Thermal Engineering*, *24*(1), 17–27.

Singh, S., Chander, S., & Saini, J. S. (2012). Exergy Based Analysis of Solar Air Heater Having Discrete V-Down Rib Roughness on Absorber Plate. *Energy*, *37*(1), 749–758.

Soni, J., & Gupta, R. C. (2012). Exergy Analysis of Vapour Compression Refrigeration System with Using R- 407C and R-410A. *International Journal of Engineering Research & Technology*, *1*(7), 1–12.

Sowell, E. F., & Moshier, M. A. (1995). HVAC Component Model Libraries for Equation-Based Solvers. In *Proceedings of Building Simulation '95* (pp. 189–196). 4th Conference of International Building Simulation Association, 1995, Madison, USA. IBPSA.

Spur, R., Fiala, D., Nevrala, D., & Probert, D. (2006). Performances of Modern Domestic Hot-Water Stores. *Applied Energy*, *83*(8), 893–910.

SRCC. (2013). Certification Info— Solar Collector Certification Program. *Solar Rating & Certification Corporation*. Retrieved March 10, 2012, from http://www.solar-rating.org/certification/collector.html

StatPoint. (2012). Statgraphics Centurion XVI.I. StatPoint Techonologies.

Staus, G. A. (1997). Solving Equations with EES. *Journal of Science and Technology*, *7*(2), 4–6.

Stojanović, B., & Akander, J. (2010). Build-up and Long-Term Performance Test of a Full-Scale Solar-Assisted Heat Pump System for Residential Heating in Nordic Climatic Conditions. *Applied Thermal Engineering*, *30*(2-3), 188–195.

SunEarth. (2012). EC-24 Solar Collector Certification and Rating. *Solar Rating & Certification Corporation*. Retrieved July 21, 2012, from https://securedb.fsec.ucf.edu/srcc/coll_detail?srcc_id=2006024A

Sunwell. (2012). Deepchill Variable-State Ice Machines & Systems. *Sunwell Technologies.* Retrieved March 05, 2013, from http://www.sunwell.com/systems.htm

Suzuki, A. (1988). A Fundamental Equation for Exergy Balance on Solar Collectors. *Journal of Solar Energy Engineering*, *110*(2), 102–106.

Tamasauskas, J., Poirier, M., Zmeureanu, R., & Sunyé, R. (2012). Modeling and Optimization of a Solar Assisted Heat Pump Using Ice Slurry as a Latent Storage Material. *Solar Energy*, *86*(11), 3316–3325.

Tang, C. C. (2005). *Modeling Packaged Heat Pump in a Quasi-Steady State Energy Simulation Program*. Master Thesis. Oklahoma State University, Stillwater, USA.

Terrell, R. E. (1979). Performance and Analysis of a "Series" Heat Pump-Assisted Solar Heated Residence in Madison, Wisconsin. *Solar Energy*, *23*(5), 451–453.

Torío, H. (2010). Pre-Design Tool: Tool for Buildings Exergy Analysis. *ECBCS Annex 49*. Retrieved February 11, 2012, from http://www.annex49.com/tools/01_Annex_Pre_Design_Tool.zip

Torío, H., Angelotti, A., & Schmidt, D. (2009). Exergy Analysis of Renewable Energy-Based Climatisation Systems for Buildings: A Critical View. *Energy and Buildings*, *41*(3), 248–271. Retrieved from http://linkinghub.elsevier.com/retrieve/pii/S0378778808002211

Turner, J. S. (1973). *Buoyancy Effects in Fluids* (p. 367). Cambridge [Eng.]: University Press.

Verkhivker, G. P., & Kosoy, B. V. (2001). On the Exergy Analysis of Power Plants. *Energy Conversion and Management*, *42*(18), 2053–2059.

Visser, H., & Van Dijk, H. A. L. (1991). *Test Procedures for Short Term Thermal Stores*. (H. Visser & H.A.L.Van Dijk, Eds.)*Kluwer Academic Publishers*. Dordrecht: Kluwer Academic Publishers.

Volk, M. (2005). *Pump Characteristics and Applications* (2nd ed., p. 533). Boca Raton [Fla.]: Taylor & Francis.

Wei, Z. (2006). *Analysis of Energy, Exergy and Greenhouse Gas Emissions for Variable Air Volume Systems in an Office Building*. Master Thesis. Concordia University, Montreal, Canada.

Wei, Z., & Zmeureanu, R. (2009). Exergy Analysis of Variable Air Volume Systems for an Office Building. *Energy Conversion and Management*, *50*(2), 387–392.

Wilo. (2012). Wilo Online Catalogue. *Wilo Canda*. Retrieved March 11, 2013, from http://productfinder.wilo.com/en/DE/productrange/0000000d0000476f00050023/fc_range_description

Wu, X. (2004). *Second Law Analysis of Residential Heating Systems*. Master Thesis. Concordia University, Montreal, Canada.

Zheng, X. (2006). *Exergy Analysis of Water Loop Heat Pump System in an Office Building*. Master Thesis. Concordia University, Montreal, Canada.

Zmeureanu, R., & Wu, X. (2007). Energy and Exergy Performance of Residential Heating Systems with Separate Mechanical Ventilation. *Energy*, *32*(3), 187–195.

Zmeureanu, R., & Zheng, X. (2008). Second Law Analysis of the Water Loop Heat Pump System for Office Buildings. In *Proceedings of World Renewable Energy Congress X*. 19-25 July 2008, Glasgow, UK.

Appendices

Appendix A

Application constraints of Eq. (4.3)

To reveal the potential of the situations (1) η^{Coll}< 0 and (2) η^{Coll}> 1, a theoretical approach of finding solutions to quadratic is presented below. Abnormal results would occur, if

$$\begin{aligned} a_0 + a_1 \frac{T_{in,w}^{Coll} - T_{oa}}{G} + a_2 \frac{\left(T_{in,w}^{Coll} - T_{oa}\right)^2}{G} < 0 \qquad (i) \\ a_0 + a_1 \frac{T_{in,w}^{Coll} - T_{oa}}{G} + a_2 \frac{\left(T_{in,w}^{Coll} - T_{oa}\right)^2}{G} > 1 \qquad (ii) \end{aligned} \tag{1}$$

which could be further transformed as (denoting T_{oa} to T_a, $T_{in,w}^{Coll}$ to T_{in})

$$\begin{aligned} \frac{a_2}{G} {T_a}^2 - \left(\frac{2a_2}{G} T_{in} + \frac{a_1}{G}\right) T_a + \left(\frac{a_2}{G} {T_{in}}^2 + \frac{a_1}{G} T_{in} + a_0\right) < 0 \qquad (i) \\ \frac{a_2}{G} {T_a}^2 - \left(\frac{2a_2}{G} T_{in} + \frac{a_1}{G}\right) T_a + \left(\frac{a_2}{G} {T_{in}}^2 + \frac{a_1}{G} T_{in} + a_0 - 1\right) > 0 \qquad (ii) \end{aligned} \tag{2}$$

or

$$\begin{aligned} Y_0 < 0 \qquad (i) \\ Y_1 > 0 \qquad (ii) \end{aligned} \tag{3}$$

where,

$$\begin{aligned} Y_0 = \frac{a_2}{G} {T_a}^2 - \left(\frac{2a_2}{G} T_{in} + \frac{a_1}{G}\right) T_a + \left(\frac{a_2}{G} {T_{in}}^2 + \frac{a_1}{G} T_{in} + a_0\right) \qquad (i) \\ Y_1 = \frac{a_2}{G} {T_a}^2 - \left(\frac{2a_2}{G} T_{in} + \frac{a_1}{G}\right) T_a + \left(\frac{a_2}{G} {T_{in}}^2 + \frac{a_1}{G} T_{in} + a_0 - 1\right) \qquad (ii) \end{aligned} \tag{4}$$

fits in a general quadratic form of

$$\begin{matrix} Y_0 = A{T_a}^2 + BT_a + C_0 & (i) \\ Y_1 = A{T_a}^2 + BT_a + C_1 & (ii) \end{matrix} \quad (5)$$

which bears the discriminant

$$\Delta = \begin{cases} B^2 - 4AC_0 & (i) \\ B^2 - 4AC_1 & (ii) \end{cases} \quad (6)$$

with

$$A = \frac{a_2}{G}, \quad (7)$$

$$B = -\left(\frac{2a_2}{G}T_{in} + \frac{a_1}{G}\right), \quad (8)$$

$$\begin{matrix} C_0 = \frac{a_2}{G}{T_{in}}^2 + \frac{a_1}{G}T_{in} + a_0 & (i) \\ C_1 = \frac{a_2}{G}{T_{in}}^2 + \frac{a_1}{G}T_{in} + a_0 - 1 & (ii) \end{matrix} \quad (9)$$

When $\Delta \geq 0$, quadratic function Y_0 and Y_1 has two distinct roots

$$T_{a_{1,2}} = \frac{-B \pm \sqrt{\Delta}}{2A}. \quad (10)$$

Quadratic functions in Eqn. (4) are illustrated in Fig. 1 using the case solar collector coefficients, where $a_2 < 0$, $A < 0$ and, therefore, the curves open upward. If quadratic discriminant $\Delta > 0$, two distinct roots exist as the plotted situation. Eqn. (3) (i) is true when $T_a < T_{a_1}$, or $T_a > T_{a_2}$; Eqn. (3) (ii) is true when $T_{a_1} < T_a < T_{a_2}$. Under the application of the solar collector operation, only T_{a_1} is meaningful, since one can calculate T_{a_2} at a much value than that of the outdoor air may reach in reality, such as 200 °C. The weighted curves that overlaying upon Y_0 and Y_1 highlight where $Y_0 < 0$ and $Y_1 > 0$, respectively. Similar situation for $\Delta = 0$, but two distinct roots becoming one. If $\Delta < 0$, the roots do not exist, the quadratic curves fall below the axis T_a. Therefore, Eqn.

(3) (i) always holds but not (ii). Among the situations explicated, whenever Eqn. (3) true justifies the invalid application of thermal efficiency of solar collector, which should always lie in a range of 0≤ η^{Coll}≤ 1.

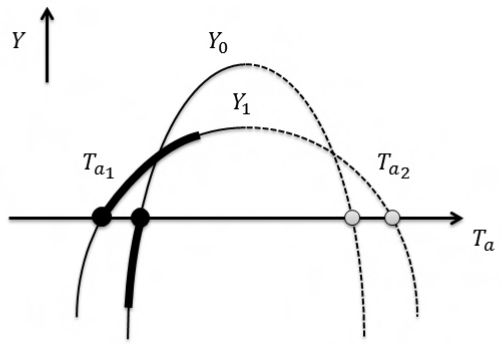

Fig. 1 Solutions to quadratic in applications of solar thermal efficiency

The application constrains of solar thermal collector product used in the case study were examined in the quadratic approach. Fig. 2 shows the upper and lower bounds of the outdoor air temperature with respect to the solar insolation from 0 W/m^2 to 1200 W/m^2 while various entering temperatures, T_{in}, between 0.01 ℃ to 70 ℃. For instance, the valid application of thermal efficiency should be with the outdoor temperature ranging in -20 ℃< T_a< 40 ℃ when the entering temperature at 20 ℃ and the solar insolation density at 200 W/m^2.

Abiding by the lower bounds ensures thermal efficiency of solar thermal collector η^{Coll}> 0, *by the upper bounds ensures* η^{Coll}< 1. Along the vertical axis downward, the bounds of outdoor temperature drop and lower bounds go along with lower entering temperatures. Along the horizontal axis to the left side, the outdoor temperature is

constrained tighter within narrow ranges as the solar insolation decreasing. But, constraints are relieved providing the solar insolation higher than 425 W/m^2.

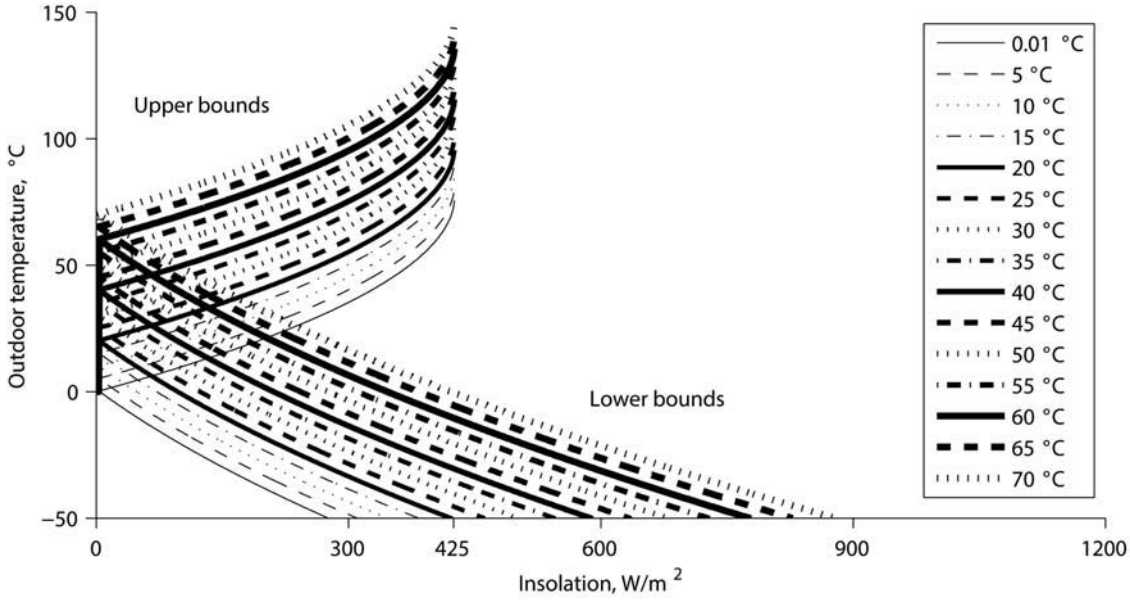

Fig. 2 Upper and lower bounds of outdoor temperature of case solar thermal efficiency

Appendix B

Input and output of the component models

The solar thermal collector model:

	Symbols	Descriptions	Units
Inputs	a_0	Coefficient of solar collector thermal efficiency	dimensionless
	a_1	Coefficient of solar collector thermal efficiency	W/(m^2·℃)
	a_2	Coefficient of solar collector thermal efficiency	W/(m^2·℃^{2})
	A_{panel}^{Coll}	Gross area of single solar thermal collector panel	m^2
	n^{Coll}	Number of solar thermal collector panel	dimensionless
	$\dot{V}_{unit}^{Coll}$	Volume flow rate per unit collector area	m^3/(s·m^2)
	$\dot{G}$	Power density of insolation upon tilted collector panel surface, time variable	W/m^2
	T_{oa}	Outdoor air temperature, time variable	℃
	$T_{in,w}^{Coll}$	Temperature of water entering solar thermal collector, associated variable	℃
Outputs	$T_{out,w}^{Coll}$	Temperature of water leaving solar thermal collector	℃
	$\dot{m}_w^{Coll}$	Mass flow rate of water through solar thermal collector	kg/s
	$\dot{V}_w^{Coll}$	Volume flow rate of water through solar thermal collector	m^3/s
	$\dot{Q}^{Coll}$	Solar heat absorption rate of solar thermal collector	W

The heat pump model:

	Symbols	Descriptions	Units
Inputs	$\dot{V}_{base}^{Evap}$	Volume flow rate of water through evaporator under baseline condition, input parameter	m^3/s
	$\dot{V}_{base}^{Cond}$	Volume flow rate of water through condenser under baseline condition, input parameter	m^3/s
	$\dot{W}_{base}^{HP}$	Electric power of heat pump under baseline condition, input parameter	W
	$\dot{Q}_{base}^{Cond}$	Heat output rate at condenser under baseline condition, input parameter	W
	$b_0, b_1, \dots b_4$	Coefficients of heat pup electric power, input parameter	-
	$d_0, d_1, \dots d_4$	Coefficients of heat transfer rate at condenser, input parameter	-
	$\dot{V}_{w}^{Evap}$	Volume flow rate of water through evaporator, input parameter	m^3/s
	$\dot{V}_{w}^{Cond}$	Volume flow rate of water through condenser, input parameter	m^3/s
	$T_{in,w}^{Evap}$	Temperature of water entering evaporator, associated variable	℃
	$T_{in,w}^{Cond}$	Temperature of water entering condenser, associated variable	℃
	$T_{mean,w}^{Evap}$	Mean temperature of water through evaporator, input parameter	℃
	$T_{mean,w}^{Cond}$	Mean temperature of water through condenser, input parameter	℃
	ΔT_{suprh}	Superheat temperature difference, input parameter	℃
	P_c	Pressure of condensation, input parameter	Pa
	P_e	Pressure of vaporization, input parameter	Pa
	$\dot{Q}_{demd}^{RF}$	Space heating demand onto radiant floor, input time variable	W
Outputs	$T_{out,wf}^{Evap}$	Temperature of liquid water leaving evaporator	℃
	$T_{out,w}^{Cond}$	Temperature of water leaving condenser	℃
	$\dot{m}_{w}^{Evap}$	Mass flow rate of water through evaporator	kg/s
	$\dot{m}_{wf}^{Evap}$	Mass flow rate of liquid water leaving evaporator	kg/s
	$\dot{m}_{wi}^{Evap}$	Mass flow rate of solid water (ice) leaving evaporator	kg/s
	$\dot{m}_{w}^{Cond}$	Mass flow rate of water through condenser	kg/s
	$\dot{V}_{w}^{Evap}$	Volume flow rate of water through evaporator	m^3/s
	$\dot{V}_{w}^{Cond}$	Volume flow rate of water through condenser	m^3/s
	$\dot{W}^{HP}$	Electric power of heat pump	W
	$\dot{Q}^{Cond}$	Heat output rate at condenser	W
	$\dot{Q}^{HP4RF}$	Heat output rate from heat pump to radiant floor	W
	$\dot{Q}^{HP4WT}$	Heat output rate from heat pump to water storage tank	W

The ice storage tank model:

	Symbols	Descriptions	Units
Inputs	L^{IT}	Length of rectangular storage tank	m
	W^{IT}	Width of rectangular storage tank	m
	H^{IT}	Height of rectangular storage tank	m
	U_{insu}^{IT}	Thermal transmittance of insulation attached to ice storage tank	W/(m^2·℃)
	T_{max}^{W}	Maximum temperature of water-layer	℃
	γ_{max}	Maximum ice mass fraction in ice storage tank	dimensionless
	Δt	Time step	s
	T_{ia}	Indoor air temperature	℃
	$\dot{m}_{w}^{ITS}$	Mass flow rate of water entering from ice storage tank heat source, associated variable	kg/s
	$\dot{m}_{wi}^{ITL}$	Mass flow rate of solid water from ice storage tank heat sink, associated variable	kg/s
	$\dot{m}_{wf}^{ITL}$	Mass flow rate of liquid water entering from ice storage tank heat sink, associated variable	kg/s
	$T_{in,w}^{ITS}$	Temperature of water entering from ice storage tank heat source, associated variable	℃
	$T_{in,wf}^{ITL}$	Temperature of water entering from ice storage tank heat sink, associated variable	℃
	$c_{p_{in,w}}^{ITS}$	Constant pressure specific heat of water entering from ice storage tank heat source, associated variable	J/(kg·℃)
	$c_{p_{in,wf}}^{ITL}$	Constant pressure specific heat of liquid water entering from ice storage tank heat sink, associated variable	J/(kg·℃)
Outputs	T_{w}^{W}	Temperature of water-layer	℃

The water storage tank model:

	Symbols	Descriptions	Units
Inputs	H^{WT}	Height of water storage tank	m
	D^{WT}	Diameter of cylinder water storage tank	m
	δ_{shell}^{WT}	Thickness of water storage tank shell	m
	k_{shell}^{WT}	Thermal conductivity of water storage tank shell	W/(m·°C)
	U_{insu}^{WT}	Thermal transmittance of insulation attached to water storage tank	W/(m^2·°C)
	Δt	Time step	s
	T_{ia}	Indoor air temperature	°C
	$\dot{V}_w^{DHW}$	Volume flow rate of domestic hot water drawn, input variable	m^3/s
	T_w^{Main}	Temperature of water from city main, input variable	°C
	$\dot{Q}^{WTS1}$	Heat charging rate of immersion heat exchanger $HX1$, associated variable	W
	$\dot{Q}^{WTS2}$	Heat charging rate of immersion heat exchanger $HX2$, associated variable	W
	$\dot{Q}_{demd}^{RF}$	Space heating demand onto radiant floor, input variable	W
Outputs	T_w^{Ni}	Temperature of water-node Ni	°C
	$T_{out,w}^{WTL1}$	Temperature of water leaving immersion heat exchanger $HX1$	°C
	$\dot{Q}^{WTL1}$	Heat discharging rate of immersion heat exchanger $HX1$	W
	$\dot{Q}^{WTL2}$	Heat output rate of water storage tank for domestic water heating	W
	$\dot{Q}^{WTL}$	Heat output rate of water storage tank for heating	W
	$\dot{Q}^{WT4RF}$	Heat transfer rate from water storage tank to radiant floor	W

The radiant floor mode:

	Symbols	Descriptions	Units
Inputs	$\dot{Q}^{WT4RF}$	Heat transfer rate from water storage tank to radiant floor, associated variable	W
	$\dot{Q}^{HP4RF}$	Heat transfer rate from heat pump to radiant floor, associated variable	W
	$T_{out,w}^{WTL1}$	Temperature of water leaving immersion heat exchanger $HX1$, associated variable	°C
	$T_{out,w}^{Cond}$	Temperature of water leaving heat pump condenser, associated variable	°C
Outputs	$\dot{m}_w^{RF}$	Mass flow rate of water through radiant floor	kg/s
	$\dot{Q}^{RF}$	Heat input rate to radiant floor	W

The circulating pump model:

	Symbols	Descriptions	Units
Inputs	c_0	Coefficient of electric power input to circulating pump	W
	c_1	Coefficient of electric power input to circulating pump	W·s/m^3
	c_2	Coefficient of electric power input to circulating pump	W·s^2/m^6
	c_3	Coefficient of electric power input to circulating pump	W·s^3/m^9
	c_4	Coefficient of electric power input to circulating pump	W·s^4/m^{12}
	c_5	Coefficient of electric power input to circulating pump	W·s^5/m^{15}
	c_6	Coefficient of electric power input to circulating pump	W·s^6/m^{18}
	c_7	Coefficient of electric power input to circulating pump	W·s^7/m^{21}
	c_8	Coefficient of electric power input to circulating pump	W·s^8/m^{24}
	$\dot{V}_{max}^{Pump}$	Maximum volume flow rate of water through circulating pump	m^3/s
	$\dot{V}_w^{Pump1}$	Volume flow rate of circulating pump $P1$, associated variable	m^3/s
	$\dot{V}_w^{Pump2}$	Volume flow rate of circulating pump $P2$, associated variable	m^3/s
	$\dot{V}_w^{Pump3}$	Volume flow rate of circulating pump $P3$, associated variable	m^3/s
Outputs	$\dot{W}^{Pump1}$	Electric power input to circulating pump $P1$	W
	$\dot{W}^{Pump2}$	Electric power input to circulating pump $P2$	W
	$\dot{W}^{Pump3}$	Electric power input to circulating pump $P3$	W
	$\dot{W}_{supp}^{Pump}$	Overall power input on circulating pumps	W

The control system model:

	Symbols	Descriptions	Units
Inputs	$\dot{G}$	Power density of insolation upon tilted collector panel surface, input variable	W/m^2
	$\dot{Q}_{demd}^{RF}$	Space heating demand onto radiant floor, input variable	W
	$\dot{V}_w^{DHW}$	Volume flow rate of domestic hot water drawn, time variable	m^3/s
	γ	Ice mass fraction of ice storage tank, associated variable	dimensionless
	γ_{max}	Maximum ice mass fraction in ice storage tank, input parameter	dimensionless
	T_w^W	Ice storage tank water-layer temperature, associated variable	℃
	T_{set}^{WT}	Temperature set for water storage tank, input parameter	℃
	T_{var}^{WT}	Variation allowed respecting to setting temperature of water storage tank, input parameter	℃
	T_w^{N1}	Temperature of water-node $N1$, associated variable	℃
	T_w^{N3}	Temperature of water-node $N3$, associated variable	℃
	T_w^{N5}	Temperature of water-node $N5$, associated variable	℃
	$T_{out,w}^{WTL1}$	Temperature of water leaving immersion heat exchanger $HX1$, associated variable	℃
	$T_{out,w}^{Cond}$	Temperature of water leaving condenser	℃
	T_{com}^{RF}	Comfort temperature of radiant floor, input parameter	℃
Outputs	θ^{Coll}	Controlled variable for operating circulating pump $P1$	dimensionless
	$\theta^{Coll4IT}$	Controlled variable for three-way valve $V1$, respecting the operation between solar thermal collector and ice storage tank	dimensionless
	$\theta^{Coll4WT}$	Controlled variable for three-way valve $V1$, respecting the operation between solar thermal collector and water storage tank	dimensionless
	θ^{HP}	Controlled variable for operating heat pump	dimensionless
	θ^{HP4WT}	Controlled variable for three-way valve $V2$, respecting the operation between heat pump and water storage tank	dimensionless
	θ^{HP4RF}	Controlled variable for three-way valve $V2$, respecting the operation between heat pump and radiant floor	dimensionless
	θ^{WT4RF}	Controlled variable for bypass valve $V3$, respecting the operation between water storage tank and radiant floor	dimensionless
	θ^{Aux}	Controlled variable for operating auxiliary heater	dimensionless

Appendix C

Empire EC-24 SRCC OG-100 certification

SOLAR COLLECTOR CERTIFICATION AND RATING

SRCC OG-100

CERTIFIED SOLAR COLLECTOR

SUPPLIER:	**SunEarth, Inc.** 8425 Almeria Avenue Fontana, CA 92335 USA
MODEL:	Empire EC-24
COLLECTOR TYPE:	Glazed Flat-Plate
CERTIFICATION#:	2006024A
Original Certification Date:	18-DEC-07

COLLECTOR THERMAL PERFORMANCE RATING

Kilowatt-hours Per Panel Per Day				Thousands of BTU Per Panel Per Day			
CATEGORY (Ti-Ta)	CLEAR DAY (6.3 kWh / m^2.day)	MILDLY CLOUDY (4.7 kWh / m^2.day)	CLOUDY DAY (3.1 kWh / m^2.day)	CATEGORY (Ti-Ta)	CLEAR DAY (2000 Btu / ft^2.day)	MILDLY CLOUDY (1500 Btu / ft^2.day)	CLOUDY DAY (1000 Btu / ft^2.day)
A (-5 ℃)	9.6	7.3	4.9	A (-9 ℉)	32.9	24.7	16.7
B (5 ℃)	8.9	6.5	4.1	B (9 ℉)	30.3	22.2	14.1
C (20 ℃)	7.6	5.3	3.0	C (36 ℉)	26.0	18.0	10.1
D (50 ℃)	4.9	2.8	0.8	D (90 ℉)	16.8	9.6	2.9
E (80 ℃)	2.3	0.6	0.0	E (144 ℉)	7.9	2.1	0.0

A- Pool Heating (Warm Climate) **B-** Pool Heating (Cool Climate) **C-** Water Heating (Warm Climate) **D-** Water Heating (Cool Climate) **E-** Air Conditioning

COLLECTOR SPECIFICATIONS

Gross Area: 2.298 m^2 24.74 ft^2
Dry Weight: 36.1 kg 80. lb
Test Pressure: 1103. KPa 160. psig
Net Aperture Area: 2.03 m^2 21.86 ft^2
Fluid Capacity: 2.7 liter 0.7 gal

COLLECTOR MATERIALS

Frame: Aluminum Extrusion
Cover (Outer): Low Iron Tempered Glass
Cover (Inner): None

Pressure Drop

Flow		ΔP	
ml/s	gpm	Pa	in H_2O
20.00	0.32	25.10	0.10
50.00	0.79	117.6	0.5
80.00	1.27	276.20	1.11

Absorber Material: Tube - Copper / Plate - Copper
Absorber Coating: Black Chrome
Insulation Side: Polyisocyanurate
Insulation Back: Polyisocyanurate & Fiberglass

TECHNICAL INFORMATION

Efficiency Equation [NOTE: Based on gross area and (P)=Ti-Ta]

				Y INTERCEPT	SLOPE
SI Units:	η= 0.728	-2.98830 (P)/I	-0.01930 $(P)^2/I$	0.735	-4.041 $W/m^2.℃$
IP Units:	η= 0.728	-0.52639 (P)/I	-0.00189 $(P)^2/I$	0.735	-0.712 $Btu/hr.ft^2.℉$

Incident Angle Modifier [(S)=1/cosθ - 1, 0°<θ<=60°]

$K\tau\alpha$ = 1	-0.296 (S)	0.019 $(S)^2$	
$K\tau\alpha$ = 1	-0.28 (S)	Linear Fit	

Test Fluid: Water
Test Flow Rate: 20.1 ml /s.m^2 0.0295 gpm/ft^2

REMARKS:

June, 2012
Certification must be renewed annually, For current status contact:
SOLAR RATING & CERTIFICATION CORPORATION
400 High Point Drive, Suite 400 ♦ Cocoa, Florida 32926 ♦ (321) 213-6037 ♦ Fax (321) 821-0910

Source: SunEarth (2012)

Appendix D

Regarding coefficients identification with StatGraphics for GeoSmart HS050

I. The plot of $\frac{\dot{W}^{HP}}{3390}$ for Eqn. (4.19) regression

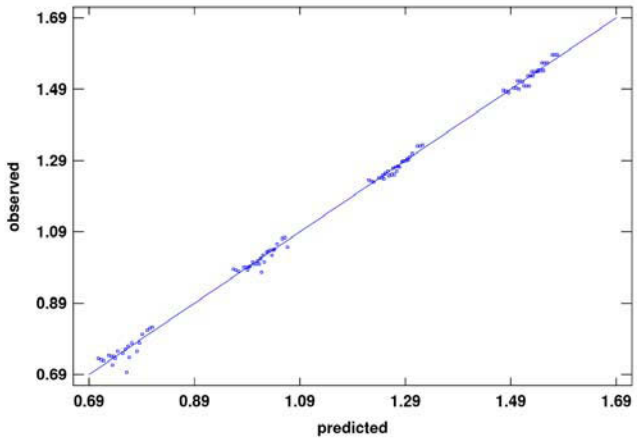

R-Squared = 99.7768 percent

Standard Error of Est. = 0.0136088

The R-Squared statistic indicates that the model as fitted explains 99.7768% of the variability in $\frac{\dot{W}^{HP}}{3390}$. The standard error of the estimate shows the standard deviation of the residuals to be 0.0136088.

II. The plot of $\frac{\dot{Q}^{Cond}}{21072}$ for Eqn. (4.20) regression

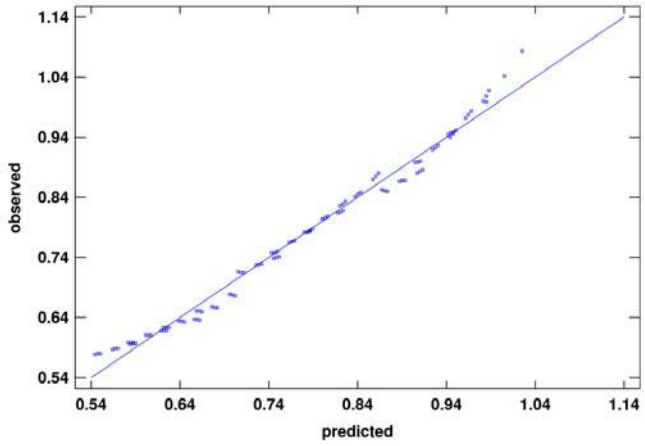

R-Squared = 98.6571 percent

Standard Error of Est. = 0.0158837

The R-Squared statistic indicates that the model as fitted explains 98.6571% of the variability in $\frac{\dot{Q}^{Cond}}{21072}$. The standard error of the estimate shows the standard deviation of the residuals to be 0.0158837.

III. GeoSmart HS050 performance data

HS050 - Performance Data cont.

Heating Capacity

Source		Load Flow-8 GPM							Load Flow-11.5 GPM						Load Flow-15 GPM					
EST °F	Flow GPM	ELT °F	LLT °F	HC MBTUH	Power kW	HE MBTUH	COP	LST °F	LLT °F	HC MBTUH	Power kW	HE MBTUH	COP	LST °F	LLT °F	HC MBTUH	Power kW	HE MBTUH	COP	LST °F
25	11.5	60	Operation not recommended																	
		80																		
		100																		
		120																		
	15	60	71.3	43.9	2.50	35.4	5.15	20.1	67.9	44.0	2.50	35.4	5.16	20.1	66.0	44.0	2.49	35.5	5.18	20.1
		80	91.0	42.6	3.41	31.0	3.66	20.7	87.6	42.6	3.37	31.1	3.71	20.7	85.9	42.6	3.33	31.3	3.75	20.7
		100	110.6	41.3	4.32	26.6	2.80	21.3	107.4	41.3	4.25	26.8	2.85	21.3	105.7	41.3	4.17	27.0	2.90	21.3
		120	130.3	40.0	5.23	22.2	2.24	22.0	127.2	40.0	5.12	22.5	2.29	21.9	125.5	39.9	5.01	22.8	2.33	21.9
30	8	60	71.8	45.7	2.36	37.6	5.67	20.3	69.0	45.8	2.43	37.5	5.53	20.3	66.3	45.8	2.49	37.3	5.39	20.4
		80	91.4	44.4	3.31	33.1	3.92	21.5	88.8	44.4	3.33	33.0	3.91	21.5	86.1	44.4	3.34	33.0	3.89	21.5
		100	111.1	43.0	4.27	28.5	2.96	22.7	108.5	43.0	4.23	28.6	2.98	22.6	105.9	43.0	4.19	28.7	3.01	22.6
		120	130.7	41.7	5.22	23.9	2.34	23.8	128.2	41.7	5.13	24.1	2.38	23.8	125.7	41.6	5.04	24.4	2.42	23.7
	11.5	60	72.2	47.2	2.50	38.6	5.53	22.4	69.3	47.2	2.49	38.7	5.56	22.4	66.5	47.3	2.48	38.8	5.59	22.4
		80	91.7	45.5	3.41	33.9	3.92	23.4	89.0	45.6	3.37	34.1	3.96	23.3	86.3	45.6	3.33	34.2	4.01	23.3
		100	111.3	43.9	4.31	29.2	2.98	24.3	108.7	43.9	4.25	29.4	3.03	24.2	106.0	43.9	4.18	29.6	3.08	24.2
		120	130.9	42.3	5.22	24.5	2.37	25.2	128.4	42.3	5.13	24.8	2.42	25.1	125.8	42.2	5.03	25.0	2.46	25.1
	15	60	72.5	48.6	2.64	39.6	5.39	24.6	69.6	48.7	2.56	40.0	5.59	24.5	66.7	48.8	2.47	40.4	5.79	24.5
		80	92.0	46.7	3.50	34.8	3.91	25.2	89.2	46.8	3.41	35.1	4.02	25.2	86.4	46.8	3.32	35.5	4.13	25.1
		100	111.5	44.8	4.36	29.9	3.01	25.9	108.9	44.8	4.27	30.2	3.08	25.8	106.2	44.8	4.17	30.6	3.15	25.8
		120	131.1	42.9	5.22	25.1	2.41	26.6	128.5	42.9	5.12	25.4	2.45	26.5	125.9	42.8	5.02	25.7	2.50	26.5
50	8	60	75.1	58.8	2.56	50.0	6.65	37.1	71.6	58.6	2.54	50.0	6.72	37.1	68.0	58.5	2.52	49.9	6.80	37.1
		80	94.5	56.3	3.47	44.4	4.71	38.5	91.1	56.2	3.42	44.6	4.80	38.5	87.7	56.2	3.36	44.7	4.88	38.5
		100	113.9	53.9	4.39	38.9	3.58	40.0	110.6	53.8	4.30	39.2	3.66	39.9	107.4	53.8	4.21	39.4	3.74	39.8
		120	133.2	51.4	5.30	33.3	2.83	41.4	130.2	51.4	5.18	33.7	2.91	41.3	127.1	51.5	5.06	34.2	2.98	41.2
	11.5	60	75.7	61.0	2.64	52.0	6.78	39.8	72.0	60.8	2.58	52.0	6.91	39.9	68.3	60.5	2.51	51.9	7.06	39.9
		80	95.0	58.1	3.53	46.1	4.83	41.0	91.5	57.9	3.44	46.2	4.93	41.0	87.9	57.8	3.36	46.3	5.04	41.0
		100	114.2	55.2	4.41	40.2	3.67	42.1	110.9	55.1	4.31	40.4	3.75	42.1	107.6	55.0	4.21	40.6	3.83	42.0
		120	133.5	52.4	5.30	34.3	2.89	43.3	130.3	52.3	5.18	34.6	2.96	43.2	127.2	52.3	5.06	35.0	3.03	43.1
	15	60	76.3	63.3	2.72	54.0	6.79	42.6	72.4	62.9	2.61	54.0	7.03	42.6	68.6	62.5	2.51	53.9	7.27	42.6
		80	95.4	59.9	3.58	47.7	4.89	43.4	91.8	59.6	3.47	47.8	5.03	43.4	88.2	59.4	3.36	47.9	5.17	43.4
		100	114.6	56.6	4.44	41.5	3.72	44.3	111.2	56.4	4.32	41.7	3.82	44.3	107.7	56.2	4.20	41.9	3.91	44.2
		120	133.7	53.3	5.30	35.2	2.94	45.2	130.5	53.2	5.18	35.5	3.01	45.1	127.3	53.1	5.05	35.8	3.07	45.1
70	8	60	78.5	71.8	2.76	62.4	7.62	53.9	74.1	71.5	2.65	62.5	7.92	53.9	69.8	71.2	2.54	62.5	8.21	53.9
		80	97.6	68.2	3.63	55.8	5.50	55.6	93.5	68.1	3.51	56.1	5.69	55.5	89.3	67.9	3.39	56.3	5.87	55.5
		100	116.7	64.7	4.51	49.3	4.20	57.3	112.8	64.6	4.37	49.7	4.34	57.2	108.9	64.6	4.23	50.2	4.47	57.1
		120	135.7	61.1	5.38	42.7	3.33	59.0	132.1	61.2	5.23	43.4	3.43	58.8	128.4	61.3	5.08	44.0	3.54	58.7
	11.5	60	79.3	74.9	2.78	65.4	7.90	57.3	74.7	74.3	2.66	65.2	8.18	57.3	70.1	73.7	2.55	65.0	8.48	57.3
		80	98.2	70.7	3.64	58.3	5.69	58.6	93.9	70.3	3.52	58.3	5.86	58.6	89.6	69.9	3.39	58.3	6.04	58.6
		100	117.2	66.6	4.51	51.2	4.32	60.0	113.1	66.3	4.37	51.4	4.44	59.9	109.1	66.1	4.24	51.6	4.57	59.9
		120	136.1	62.4	5.38	44.0	3.40	61.4	132.3	62.4	5.23	44.5	3.49	61.3	128.6	62.3	5.08	45.0	3.59	61.2
	15	60	80.1	77.9	2.79	68.4	8.18	60.6	75.3	77.1	2.67	67.9	8.47	60.7	70.5	76.2	2.55	67.5	8.76	60.7
		80	98.9	73.2	3.65	60.7	5.87	61.7	94.4	72.5	3.52	60.5	6.04	61.7	89.9	71.9	3.39	60.3	6.21	61.7
		100	117.6	68.4	4.52	53.0	4.44	62.7	113.5	68.0	4.38	53.1	4.56	62.7	109.3	67.6	4.24	53.1	4.68	62.7
		120	136.4	63.7	5.38	45.3	3.47	63.8	132.6	63.5	5.23	45.7	3.56	63.7	128.7	63.3	5.08	46.0	3.65	63.7
90	8	60	81.9	84.9	2.85	75.2	8.73	70.6	76.5	82.8	3.51	70.8	7.21	71.7	71.1	80.7	4.16	66.5	5.68	72.9
		80	100.6	80.1	3.71	67.4	6.32	72.6	95.6	78.7	4.09	64.8	5.70	73.3	90.6	77.4	4.47	62.2	5.08	74.0
		100	119.4	75.2	4.58	59.6	4.82	74.6	114.8	74.7	4.68	58.7	4.68	74.9	110.2	74.1	4.77	57.8	4.55	75.1
		120	Operation not recommended																	
	11.5	60	82.3	86.6	2.86	76.9	8.89	74.9	76.8	84.1	3.12	73.5	7.91	75.6	71.2	81.6	3.38	70.1	7.08	76.4
		80	101.1	81.8	3.72	69.0	6.43	76.5	95.9	80.2	3.84	67.1	6.12	76.9	90.8	78.6	3.95	65.1	5.83	77.3
		100	119.8	76.9	4.59	61.2	4.91	78.0	115.1	76.2	4.56	60.7	4.90	78.1	110.4	75.5	4.52	60.1	4.90	78.3
		120	Operation not recommended																	
	15	60	82.8	88.3	2.86	78.5	9.05	79.2	77.0	85.4	2.73	76.1	9.19	79.5	71.3	82.5	2.59	73.7	9.33	79.9
		80	101.5	83.4	3.73	70.7	6.55	80.3	96.2	81.6	3.58	69.3	6.68	80.5	91.0	79.7	3.43	68.0	6.81	80.7
		100	120.2	78.6	4.61	62.8	5.00	81.4	115.4	77.7	4.44	62.6	5.14	81.4	110.6	76.9	4.26	62.3	5.28	81.4
		120	Operation not recommended																	

8/19/09

Source: GeoSmart (2012)

Appendix E

Wilo-Star 16F performance curve

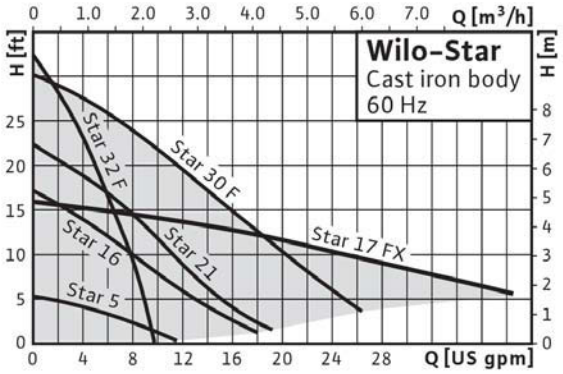

Source: Wilo (2012)